

POLITECNICO DI MILANO

Scuola di Ingegneria dei Processi Industriali

Corso di Laurea Magistrale in Ingegneria Chimica

Dipartimento di Chimica, Materiali e Ingegneria Chimica “Giulio
Natta”



Tesi di Laurea Magistrale

**Poly(L-Lactide) production for Biomedical applications:
Modeling and simulation of the polymerization process and
experimental characterization of the final product**

Relatore: Prof. Flavio Manenti

Correllatore: Prof. Rubens Maciel Filho

Candidati:

Davide Refinetti
Matr. n. 783007

Alessia Sonzogni
Matr. n. 784687

Anno Accademico 2012/2013

Abstract

Ring-opening polymerization (ROP) of L,L-lactide carried out in bulk melt in the presence of stannous octoate as catalyst and 1-dodecanol as co catalyst has been studied through experiments and modeling. The experiments have been carried out firstly in ampoules (micro-experiments) at various temperature conditions with the aim to define the parameters of kinetic model. A comprehensive kinetic model involving reversible catalyst activation, reversible propagation, reversible chain transfer reaction, intermolecular trans esterification and non radical random chain scission has been studied. The corresponding material and population balances have been solved using the *method of the moments*. The ODE (Ordinary Differential Equation) system obtained was implemented in C++ environment and solved using *BzzMath*[®] numerical library. Furthermore a complete Batch reactor model has been developed and PID temperature control and adaptive temperature control have been implemented in order to reach the desired target of the process (polymer molecular weight and monomer conversion). Typical model outputs, such as monomer conversion, average molecular weights, polydispersity index, have been validated with experimental data. A remarkably good agreement has been obtained between model and experimental evidences.

The reaction was carried out in a isothermal reactor (macro-experiments) at various reaction conditions: temperature from 140°C to 200°C , monomer to catalyst ratios and cocatalyst to catalyst ratios in order to investigate the influence of this parameters on the properties of the final polymer (Mw, Tm, Tg, crystallinity, etc...). PLA produced was analyzed with different analytical methods: GPC, DSC, TGA, FT-IR, RDX, MEV. Finally in vitro experiments were performed in order to evaluate the biocompatibility of the synthesized polymer.

Sommario

Il lavoro ha previsto la realizzazione e la modellazione di polimerizzazione in massa dell'L-lattide mediante aperture di anello (ROP) in presenza di Stannous Octoate come catalizzatore e 1-dodecanolo come co-catalizzatore. Gli esperimenti sono stati condotti inizialmente in ampolle (micro-scala) a differenti temperature (tra 140 e 200° C). È stato analizzato un modello cinetico che considera: reazioni reversibili di attivazione del catalizzatore, reazione reversibile di propagazione, reazione reversibile di trasferimento di catena, transesterificazioni molecolari e reazioni random non radicaliche di scissione di catena. I bilanci materiali ed i bilanci di popolazione di catena, sono stati risolti utilizzando il metodo dei momenti. Il sistema ODE (Ordinary Differential Equation) ottenuto è stato implementato in ambiente C++ ed è stato risolto mediante l'utilizzo della libreria numerica *BzzMath*[®]. È stato sviluppato un modello completo di reattore Batch su cui sono stati implementati un controllore PID di temperatura ed un controllore adattativo di temperatura al fine di raggiungere le specifiche di processo desiderate (in termini di peso molecolare finale del polimero ottenuto e conversione del monomero). Le grandezze ottenute dal modello: peso molecolare, conversione e polidispersità sono stati convalidati utilizzando i valori ottenuti dai dati sperimentali. Infine, la reazione è stata condotta in un reattore isoterma (macro-scala) a differenti condizioni di reazione: temperatura da 140 a 200°C e a differenti rapporti monomero su catalizzatore e cocatalizzatore su catalizzatore, con l'obiettivo di valutare l'influenza delle condizioni di reazione sulle proprietà finali del polimero prodotto (M_w , T_m , T_g , cristallinità, ecc...). Il PLA sintetizzato è stato analizzato mediante differenti tecniche analitiche : GPC, DSC, TGA, FT-IR, RDX, MEV. Concludendo sono stati condotti esperimenti in vitro in modo da valutare la biocompatibilità del polimero sintetizzato.

Index

CHAPTER 1 Introduction	1
1.1 Production of PLA based biomaterials.....	1
1.1.1 PLA Stereoisomers and Lactic acid production.....	1
1.1.2 PLA for biomedical applications.....	2
1.2 PLA Synthesis.....	3
1.2.1 Direct Polycondensation.....	4
1.2.2 Azeotropic dehydrative condensation.....	7
1.2.3 Enzymatic Polymerization.....	8
1.2.4 Ring opening polymerization of Lactide.....	8
1.3 Outline of The Thesis.....	14
CHAPTER 2 ROP of L-Lactide: kinetic study	16
2.1 Introduction.....	16
2.2 Kinetic Scheme analysis.....	18
2.2.1 Living behavior of ROP of L-Lactide.....	19
2.2.2 Transesterification reactions.....	20
2.2.3 Non Radical Random Chain Scission.....	22
2.3 Experimental Section.....	25
2.3.1 Materials.....	25
2.3.2 Experimental Procedure.....	25
2.3.2.1 Ampoules sealing Procedure.....	25
2.3.2.2 Reaction Procedure.....	27
2.3.2.3 Polymer extraction.....	28
2.3.3 Characterization Methods.....	29
2.3.3.1 Conversion.....	29
2.3.3.2 Size Exclusion Chromatography Analysis (GPC).....	29
2.4 Model Development.....	31
2.4.1 Method of the moments.....	36
2.5 Parameters Estimation.....	43
2.6 Results and discussions.....	46
CHAPTER 3 Batch Reactor modeling	55
3.1 Introduction.....	55

3.2 Isothermal model.....	57
3.2.1 ROH/C effect.....	57
3.2.2 M/C effect.....	59
3.2.3 A/C Effect.....	60
3.2.4 Temperature Effect.....	61
3.3 Adiabatic model.....	63
3.4 Open loop model.....	69
3.4.1 Overall heat transfer coefficient evaluation.....	70
3.4.1.1 PLA Rheological characterization.....	74
3.4.2 Simulation results.....	79
CHAPTER 4 Temperature Control.....	81
4.1 Introduction.....	81
4.2 Optimal temperature trajectory detection.....	82
4.3 PI Temperature Control.....	85
4.3 Adaptive Temperature Control.....	87
CHAPTER 5 Influence of reaction conditions on PLA polymerization.....	95
5.1 Introduction.....	95
5.2 Experimental Section.....	95
5.2.1 Materials.....	95
5.2.2 Experimental Procedure.....	96
5.3 Experiments at different temperatures.....	97
5.3.1 Characterization Methods.....	97
5.3.1.1 GPC analysis.....	97
5.3.1.2 Density.....	99
5.4 Experiments at different M/C and ROH/C ratios.....	101
5.4.1 Characterization Methods.....	102
5.4.1.1 GPC analysis.....	102
5.4.1.2 Density.....	104
CHAPTER 6 PLA characterization analyses.....	106
6.1 Introduction.....	106
6.2 Thermal analysis.....	106
6.2.1 DSC - Differential scanning calorimetry.....	106
6.2.1.1 Introduction.....	106

6.2.1.2 Instrumentation	107
6.2.1.3 Experimental Results for experiments at Constant Temperature	109
6.2.1.4 Experimental Results for experiments at Constant Ratios.....	111
6.2.2 TGA - Thermogravimetric analysis.....	115
6.2.2.1 Introduction.....	115
6.2.2.2 Instrumentation	115
6.2.2.3 Experimental Results for experiments at Constant Temperature	116
6.2.2.4 Experimental Results for experiments at Constant Ratios.....	118
6.3 Spectroscopic Analysis.....	120
6.3.1 FT-IR - Fourier transform infrared spectroscopy	120
6.3.1.1 Introduction.....	120
6.3.1.2 Instrumentation	122
6.3.1.3 Experimental Results for experiments at Constant Temperature	124
6.3.1.4 Experimental Results for experiments at Constant Ratio	125
6.3.2 RDX – X-Ray Diffraction	128
6.3.2.1 Introduction.....	128
6.3.2.2 Instrumentation	129
6.3.2.3 Experimental Results for experiments at Constant Temperature	131
6.3.2.4 Experimental Results for experiments at Constant Ratio	132
6.4 Microscopic analysis	135
6.4.1 SEM/ EDS - Scanning Electron Microscopy/Energy dispersive x-ray detector	135
6.4.1.1 Introduction.....	135
6.4.1.2 Instrumentation	136
6.4.1.3 Results and Discussions.....	138
6.5 In vitro experiments.....	138
6.5.1 Introduction	138
6.5.2 Material and methods- Adipose cells – mesenchymal tissue	138
CHAPTER 7 Conclusions and Outlook	144
7.1 Conclusions and Outlook	144
References	146

CHAPTER 1

Introduction

1.1 Production of PLA based biomaterials

1.1.1 PLA Stereoisomers and Lactic acid production

Poly(Lactic Acid) or Poly(Lactide) (PLA) belongs to the family of aliphatic polyesters commonly made of α -hydroxyl acids (as Lactic acid or Glycolic acid) and is considered biodegradable and compostable. PLA is a thermoplastic, high-strength, high-modulus polymer that can be made from annually renewable resources to yield articles for use in either the industrial packaging field or in the biocompatible-bioabsorbable medical device market. PLA can be easily processed on standard plastics equipment to yield molded parts, film or fibers[4].

Lactic acid is a chiral molecule as it presents a stereocenter in the carboxylic carbon. For this reason this molecule can exist in two optically active forms (enantiomers) which differ in the way of deviating polarized light. These two enantiomers are called L-Lactic acid and D-Lactic acid.

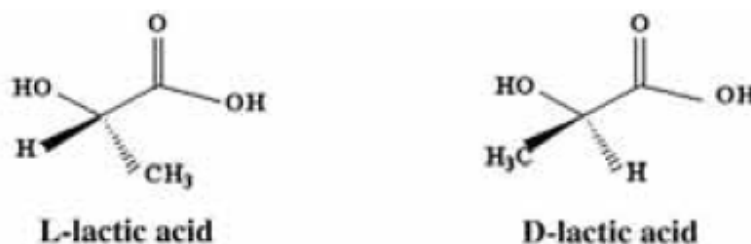


Fig. 1.1[1] Lactic acid stereoisomers

Since Lactic acid is a chiral molecule PLA has three stereoisomers: Poly(L-Lactic acid) (PLLA), Poly(D-Lactic acid) (PDLA) and Poly(DL-Lactic acid) (PDLLA).

The amount of L or D-stereoisomer in the polymeric chains influences physical and chemical properties of the material.

Lactic acid polymers	Glass Transition Temperature T_g [°C]	Melting Temperature T_m [°C]	Density (g/cm ³)	Elastic Modulus (GPa)	Ultimate Tensile Strength [Mpa]	Degradation Time [month]
PLLA	55-80	173-178	1.290	2.7	31	>24
PDLLA	43-53	120-170	1.25	1.9	-	12-16
PDLA	40-50	120-150	1.248	-	-	-

Table 1.1 Lactic acid polymers properties[1]

Isotactic and optically active PLLA and PDLA are crystalline, whereas relatively atactic and optically inactive PDLLA (result of the polymerization of the racemic mixture formed by 50% L-stereoisomer and 50% D-stereoisomer [2]) is amorphous. Lactic acid has two main production routes:

- chemical synthesis;
- fermentation.

Chemical synthesis of Lactic acid is carried out by hydrolysis of lactonitrile. This synthesis way leads to the production of a racemic mixture (optically inactive) of L and D-Lactic acid. Fermentation of carbohydrates represents a more interesting route of Lactic acid production. The interest in fermentative production of Lactic acid has increased due to prospects of developing environmental friendly processes using renewable resources as raw materials instead of fossil-based feedstock. Furthermore fermentation-derived Lactic acid presents several advantages compared to chemical synthesis. Fermentation process can lead to the production of an optically pure L-Lactic acid or D-Lactic acid by selecting a proper bacterial strain (Lactobacilli) and presents low process temperature, low energy consumption and low cost substrates (fermentable substrates like sugars or starch)[1],[3]. About 90% of the total Lactic acid produced worldwide is made by bacterial fermentation while the remaining portion is made by hydrolysis of lactonitrile.

1.1.2 PLA for biomedical applications

Over the last century, biocompatible materials such as metals, ceramics and polymers have been extensively used for surgical implantation. Metals and ceramics have contributed to major advances in the medical field, particularly in orthopedic tissue replacement. However, metals and ceramics are not biodegradable and their

processability is very limited. Polymer materials have received increasing attention and been widely used for tissue engineering because of easy control over biodegradability and processability. Bioabsorbable polymers are optimal candidates for developing therapeutic devices such as temporary prostheses, three-dimensional porous structures as scaffolds for tissue engineering and drug delivery systems[1]. Synthetic biodegradable poly-lactones such as PLA, Poly(Glycolic acid) (PGA) and Poly(Caprolactone) (PCL) as well as their copolymers are now commonly used in biomedical devices because of their excellent biocompatibility. Poly(L-Lactic acid) (PLLA) is widely used in biomedical applications due to its biodegradability, biocompatibility, thermal plasticity and suitable mechanical properties. Bioabsorbable fixation devices have been extensively used as dissolvable suture meshes and recently, by orthopedic surgeons. Its main application includes surgical sutures, implants for bone fixation, drug delivery devices and materials for tissue engineering. In tissue engineering, cells can grow in a PLLA scaffold that is inserted at the site of organ defect. When inserted in vivo, it is able to degrade simply by hydrolysis of the ester bonds without any use of enzymes or catalysts, thus a second surgical removal of implant is unnecessary. PLA is obtained from lactic acid and converted back to the latter one when hydrolytically degraded[1].

PLLA has gained great attention because of its excellent biocompatibility and mechanical properties. Furthermore the hydrolysis of PLLA leads to the formation of L-Lactic acid which can be metabolized by cellular activity in glucose (so energy) and, due to its small size can permeate through the lipid membrane[3]. On the other hand the high crystallinity degree of PLLA (around 37% as maximum value) leads to long degradation time (due to diffusive limitations of water in crystal domains which slow down the hydrolysis process) and causes inflammatory reactions in the body[1]. In order to overcome this problem PLA can be used as a material combination of L-Lactic acid and D,L-Lactic acid monomers, being the latter rapidly degraded without formation of crystalline fragments during the process. An alternative choice which can be used in order to reduce the degradation time of PLLA is to produce a copolymer of Lactic acid and Glycolic acid (hydroxyethanoic acid). This copolymer (PLGA) reduces degradation time of PLLA, being Glycolic acid rapidly degraded by hydrolysis, and, on the other hand, enhances mechanical properties of pure PGA thanks to the presence of L-Lactic acid.

1.2 PLA Synthesis

PLA can be prepared by different polymerization process from lactic acid including: polycondensation, ring opening polymerization and by direct methods like azeotropic dehydration and enzymatic polymerization. Currently direct polymerization

(polycondensation) and ring opening polymerization (ROP) are the most used production techniques[1]. Figure 1.2 [4] shows the main routes for PLA synthesis.

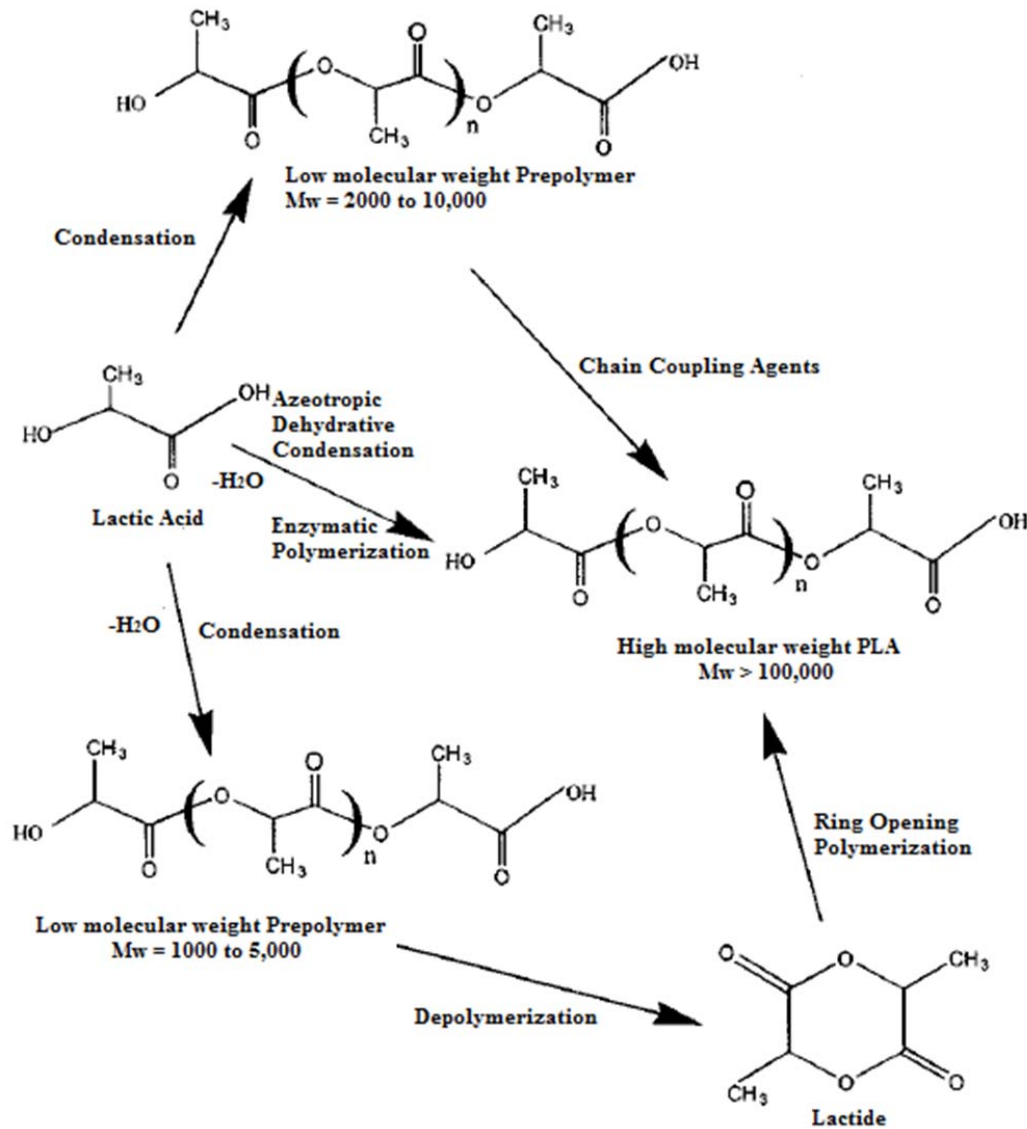


Fig. 1.2 Synthesis methods for high molecular weight PLA

1.2.1 Direct Polycondensation

The existence of both hydroxyl and carboxyl group in Lactic acid enables it to be converted into polyester via polycondensation reaction[1]. However the final product is a low-molecular-weight, glassy, brittle polymer which is useless for any applications[4] (either in biomedical devices or in food packaging). This is due to the fact that polycondensation processes involved esterification reactions which are equilibrium

reactions. In order to move the equilibrium of this reaction towards products (enhancing monomer conversion and polymer molecular weight) high vacuum must be applied to remove the produced water. Furthermore intra-molecular transesterifications of growing chains, also called back-biting reactions, lead to the formation of ring molecules as byproducts. The main product of these side reactions is the cyclic dimer of Lactic acid called Lactide.

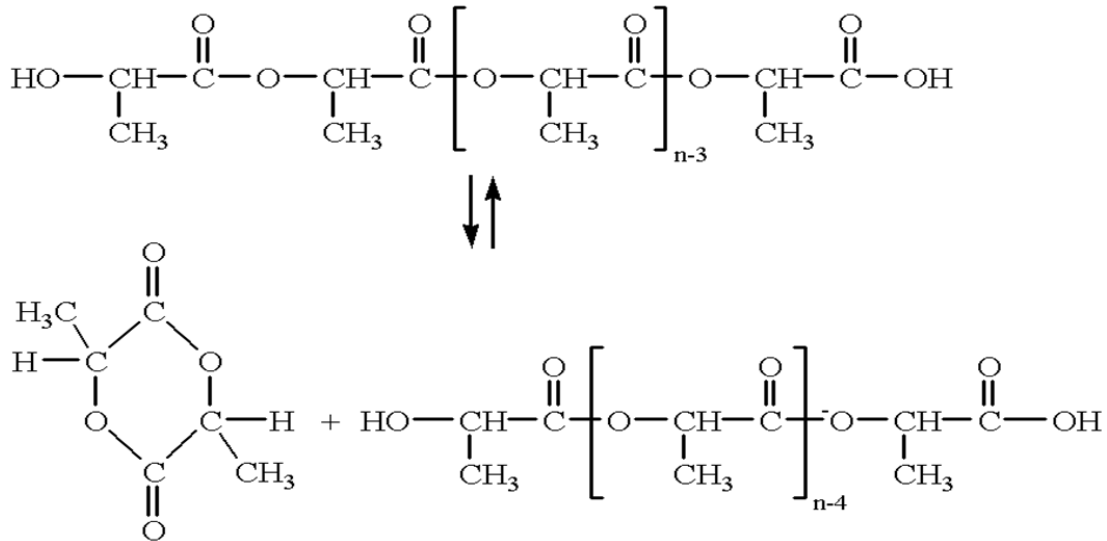


Fig. 1.3 Back-biting reactions

As these reactions are equilibrium reactions a way to reduce the formation of these byproducts is to recover, condensate and reflux to the reactor Lactides in order to reach equilibrium conditions. Obviously the presence of back-biting reactions negatively influences the final properties of the synthesized polymer because they decrease the average length of the polymer chains and affect PLA purity. Polycondensation is the least-expensive route to produce PLA, but it's difficult in a solvent free system (bulk polymerization) to obtain high molecular weight polymers unless coupling agents, esterification-promoting adjuvants or chain-extending agents are added to the reaction media. This adds complexity and costs to polycondensation process[4]. Chain-coupling agents can preferentially react with either carboxyl or hydroxyl group leading to different kinetics of chain coupling. Condensed PLA can be modified to produce either all carboxyl or hydroxyl groups. Hydroxyl-terminated PLA can be obtained by adding to the reaction mixture small amounts of multifunctional hydroxyl compounds such as 2-butene-1,4diol, glycerol or 1,4-butanediol which lead to preferential hydroxyl-end groups[4].

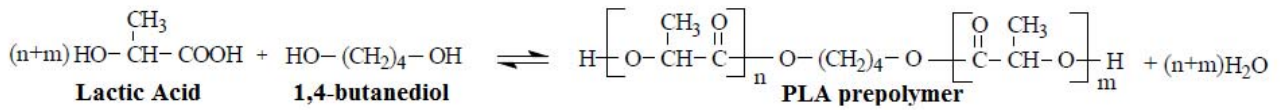
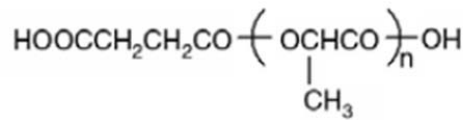
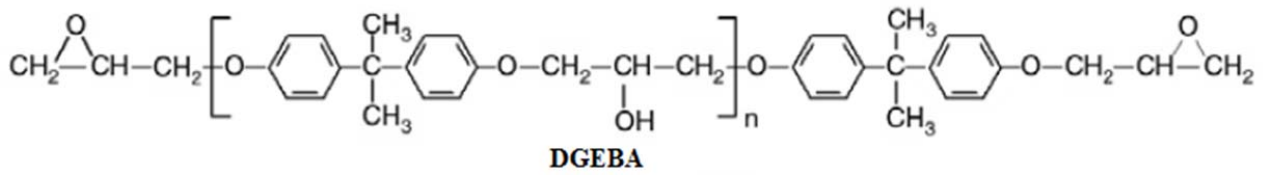
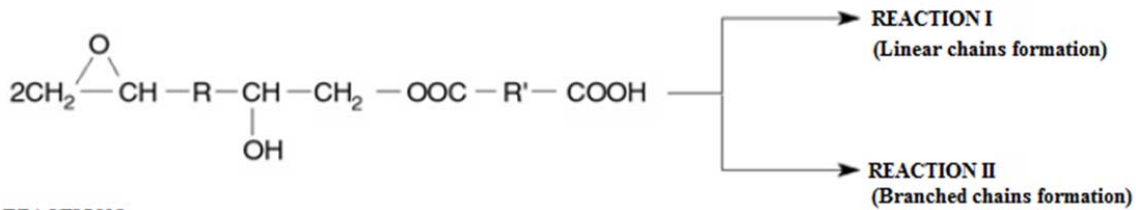
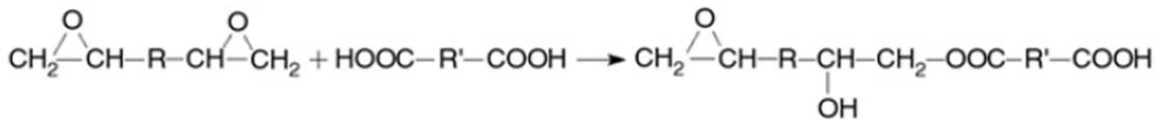


Fig. 1.4[5] Chain coupling with 1,4-butanediol: production of hydroxyl-terminated PLA

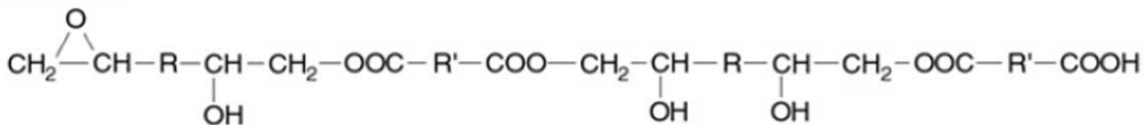
Also postcondensation reactions can be used in order to obtain either an hydroxyl or a carboxyl-terminated PLA. For example by using a monofunctional epoxide such as butyl glycidyl ether all carboxyl groups of the polymer chains can be converted in hydroxyl groups[4]. The same concept can be applied in order to obtain carboxyl-terminated PLA. By adding multifunctional carboxyl acids such as maleic, succinic, adipic or itaconic acid to the reaction mixture all-terminated-carboxyl PLA is produced during polycondensation. Furthermore PLA can also be postprocessed with acid anhydrides such as maleic or succinic to convert hydroxyl to carboxyl-end groups[4]. Various esterification-promoting adjuvants and chain-extending agents have been reported that can be used to increase molecular weight of PLA condensation products[7]. Some examples of esterification-promoting adjuvants are bis(trichloromethyl) carbonate, dicyclohexylcarbodiimide and carbonyl diimidazole. These adjuvants lead to reaction byproducts that must be either neutralized or removed. bis(trichloromethyl) carbonate leads to the formation of hydrochloric acid, which can degrades the polymer. Dicyclohexylcarbodiimide forms unreacted and insoluble dicyclohexylurea, which can be filtered in the final purification steps. The advantages of esterification-promoting adjuvants are that the final product is highly purified and free from residual metals, catalyst and low-molecular-weight oligomers. The disadvantages are higher costs due to the increased number of reaction steps, the use of dangerous or flammable solvents, inability to form copolymers containing different functional groups, and the additional purification and separation steps of non-recoverable byproducts[4]. The use of chain-extending agents overcomes many of the disadvantages associated with esterification-promoting adjuvants. Reactions involving chain-extending agents are more economically feasible, as they can be carried out in the reaction mixture with lower amounts required and separation steps of them aren't needed. Improved mechanical properties associated with the chain-extending agent are also found, and the flexibility to manufacture copolymers with different functional groups is greatly expanded. The disadvantages are that the final polymer may still contain unreacted chain-extending-agents, residual metal or polymer impurities. Furthermore extending agents are not biodegradable or bioabsorbable, so they can't be used if PLA is used to made biomedical devices. Some examples of chain-extending agents are isocyanates, acid chlorides, anhydrides, epoxides, thiirane and oxazoline. Figure 5 shows the reaction scheme followed by dyglycidil ether of bisphenol A (DGEBA), as chain-extending agent for the production of a copolymer PLA/DGEBA with high molecular weight[6].



Carboxyl-terminated PLA



REACTION I



REACTION II

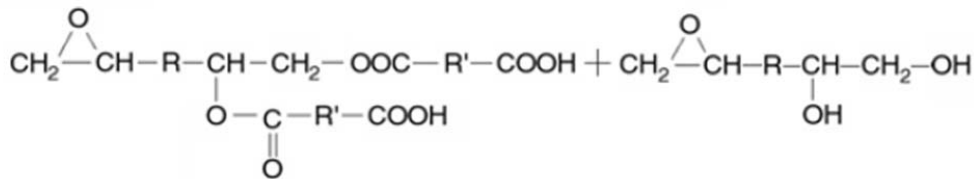


Fig. 1.5 Reaction mechanism of dicarboxylated PLLA reacting with DGEBA

1.2.2 Azeotropic dehydrative condensation

Mitsui Toatsu Chemicals commercialized a process in which Lactic acid and catalyst are azeotropically dehydrated in a refluxing, high-boiling, aprotic solvent under reduced pressure to obtain high-molecular weight PLA (weight-average molecular weight reached greater than 300,000 [Da]) avoiding the use of chain extenders or coupling agents. The main drawbacks of this synthesis route are the presence of residual catalyst

in the polymer and the use of a solvent. A general procedure for this route consists of reduced pressure distillation of lactic acid for 2 to 3 hours at 130[°C] to remove the majority of the condensation water. Catalyst and diphenyl ether are added; then a tube packed with 3[Å] molecular sieves is attached to the reaction vessel. The refluxing solvent is returned to the vessel by way of the molecular sieves for an additional 30–40 hours at 130[°C]. The polymer can then be isolated as it is or dissolved and precipitated for further purification. This polymerization technique leads to high molecular weight polymers, but with considerable catalyst impurities due to the high amounts of it needed in order to achieve acceptable reaction rates[4]. This residual catalyst can cause many problems during further processing, such as unwanted degradation, uncontrolled or irreproducible hydrolysis rates, or, in the case of biomedical applications, catalyst toxicity and differences in releasing properties of drug delivery systems[4]. Kim and Woo obtained PLA with a viscosity-average molecular weight of about 33,000 through the azeotropic dehydration at 138 °C for 48-72 h using a m-xylene as high-boiling, aprotic solvent[9].

1.2.3 Enzymatic Polymerization

Enzymatic synthesis is an environmentally friendly method that can be carried out under mild conditions and can provide adequate control of the polymerization process [1]. Chanfreau et al. [8], reported the enzymatic synthesis of Poly(L-Lactide) using a ionic liquid (1-hexyl-3-ethylimidazoliumhexafluorophosphate [HMIM][PF6]) mediated by the enzyme lipase B from *Candida antarctica* (Novozyme 435). The highest PLLA yield (63%) was attained at 90 °C with an average molecular weight of 37,800 g/mol [8].

1.2.4 Ring opening polymerization of Lactide

PLA polycondensation processes lead to low molecular weight polymers due to the production of water during polymerization. For this reason high vacuum is needed in the process in order to increase final molecular weight of the polymer. Furthermore coupling agents, chain extenders or high boiling solvent (for azeotropic dehydrative condensation) are needed in order to produce high molecular weight polymer. The presence of these compounds gives complexity to the polymerization process and affects PLA final purity. As the added agents or solvent can influence biocompatibility and bioabsorbability of PLA these synthesis ways are not adequate for the production of polymers used as biomedical devices.

An alternative way which avoids formation of water in the polymerization process is ring opening polymerization (ROP) of Lactide. Lactide is the cyclic dimer of Lactic acid. As Lactic acid is a chiral molecule also Lactide can exist in several enantiomeric forms: L-Lactide, D-Lactide, meso-Lactide.

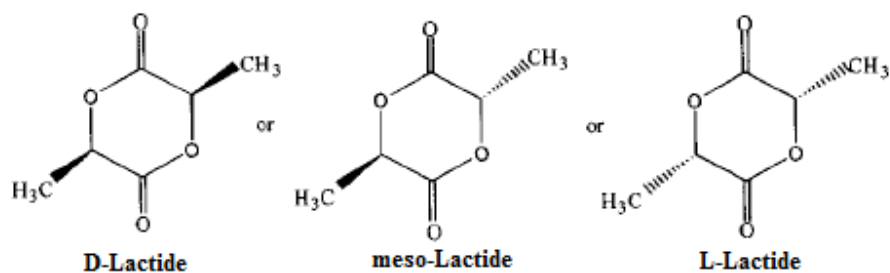


Fig. 1.6 Lactide enantiomers

D-Lactide and L-Lactide can also form a 1:1 racemic stereocomplex called D,L-Lactide. The ring opening polymerization of Lactide was first demonstrated by Carothers in 1932[12], but high molecular weights were not obtained until improved Lactide purification techniques were developed by DuPont in 1954[13].

The absence of hydroxyl groups in the molecule avoid formation of water during propagation process. Propagation reaction of ROP are transesterification reactions between monomer (Lactide) and hydroxyl groups contained in polymer chains. These reactions are equilibrium reactions and they are represented by the reverse reaction referred to back-biting reaction (Fig. 1.3). As can be seen there's no formation of byproducts in the propagation reaction, so high molecular weight polymer can be obtained without using external compounds such as chain extenders, coupling agents or high boiling solvents and avoiding high level of vacuum. ROP can be carried out in bulk, so except for monomer and catalyst the final polymer presents an high purity and its characteristics of biocompatibility and bioabsorbability are not affected by undesired compounds.

Depending on the chosen catalyst Lactide can undergoes ROP following different mechanisms: anionic, cationic or coordination-insertion[1].

It has been found trifluoromethanesulfonic acid (triflic acid) and methyl trifluoromethanesulfonic acid (methyl triflate) are the only cationic initiators for ROP[10,11]. The chain growth proceeds by cleavage of the alkyl-oxygen bond. Propagation mechanism begins with positively charged Lactide ring being cleaved at the alkyl-oxygen bond by an S_N2 attack by the triflate anion. The triflate end-group reacts with a second molecule of Lactide again in an S_N2 fashion to yield a charged Lactide that is opened. Then the triflate anion opens again the charged Lactide, and polymerization proceeds [13]. Cationic polymerization of Lactide is shown in Fig. 1.7[4].

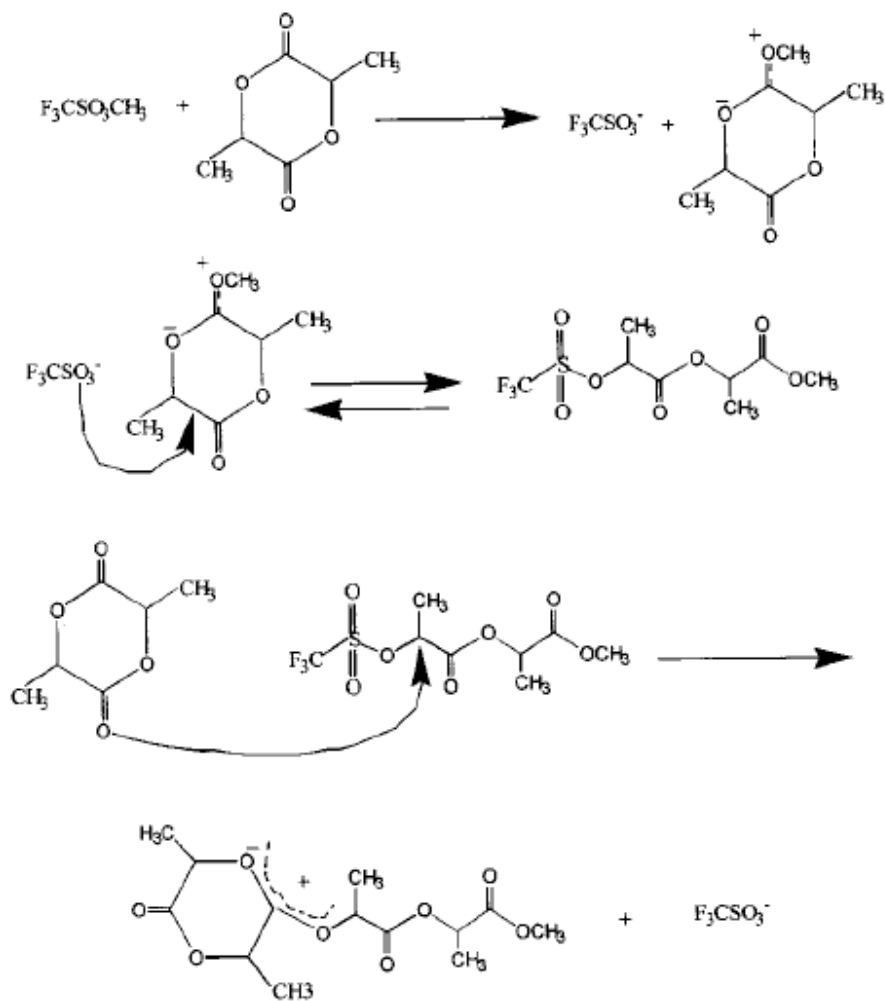


Fig. 1.7 Cationic ROP mechanism for PLA with methyl triflate as catalyst

Anionic lactide polymerizations proceed by the nucleophilic reaction of the anion with the carbonyl and the subsequent acyl-oxygen cleavage. This produces an alkoxide end-group, which continues to propagate. The anionic polymerization mechanism is shown in Fig. 1.8[4].

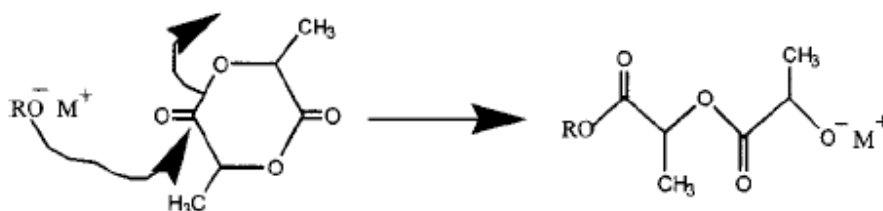


Fig. 1.8 Anionic ROP mechanism for PLA with metal alkoxides

Jedlinski et al. [14,15] have shown that the use of primary alkoxides such as potassium methoxide can lead to well-defined polymers with negligible racemization, termination

or transesterification (producing polymers with a narrow chain length distribution). Racemization of less than 5% was seen, starting with 99.9% pure L-Lactide [14,15]. An extensive study of various anionic initiators for Lactide polymerization was conducted. Kricheldorf et al.[16,17] found that initiators of higher nucleophilicity are needed to initiate Lactides. Weaker bases, such as potassium benzoate, potassium phenoxide, or zinc stearate, do not initiate at low temperatures, but will initiate at high temperatures (120°C). The high-temperature initiations occur in bulk but with considerable racemization and other side reactions, which hinder propagation [16,18]. Initiators such as n-, sec-, or tert-butyl lithium and potassium tert-butoxide rapidly initiate the polymerization at low temperatures, but they also lead to side reactions, such as deprotonation of the lactide monomer [19,20]. This deprotonation causes inconsistent polymerization, racemization, and, when done by the active chain end, termination, which thereby limits the molecular weights. There are toxicity concerns with the use of lithium initiators, whereas the use of potassium or sodium metal ions leads to polymers that are less toxic and are considered biocompatible.

The anionic and cationic initiations as described above are usually done in solvent systems and, due to their high reactivities, are susceptible to racemization and transesterification. Furthermore the presence of a solvent in the polymerization system affects PLA final purity.

Bulk melt polymerization process is preferred if the final goal of the process is the production of PLA for biomedical devices. In this case less reactive and non-toxic catalysts are used, such as metal carboxylates, oxides or alkoxides with no need of using solvents during polymerization. Lactide in presence of these catalysts undergoes ROP through a coordination-insertion mechanism of the ring in the growing chain. PLA is easily polymerized in presence of tin, zinc, aluminum and other heavy metal catalysts. Tin(II) and zinc show the best performances as catalysts as they lead to high molecular weight PLA with high level of purity (almost complete monomer conversion). This is due to the presence of their covalent metal-oxygen bonds and free *p* or *d* orbitals[16,21]. Kricheldorf and Serra [22] screened 24 different oxides, carbonates, and carboxylates in the bulk polymerization of Lactide at 120, 150, and 180°C [17]. It was found that the most effective catalysts with respect to yield, molecular weight, and racemization were tin(II) oxide or octoate, lead(II) oxide, antimony octoate and bismuth octoate. The best results were obtained with tin oxide and octoate at 120–150°C with conversions higher than 90% and less than 1% racemization. Few carbonates gave acceptable polymerizations, and all had considerable racemization. The alkali metal carboxylates, such as sodium and calcium, were similar to the carbonates [15].

Previous research has led to the wide use of tin compounds, namely tin(II) bis-2-ethylhexanoic acid (tin or stannous octoate) as a catalyst in PLA synthesis. This is mainly due to its solubility in many lactones, low toxicity, FDA approval, high catalytic activity, and ability to give high-molecular-weight polymers with low

racemization[23,24,25]. PLA production by ROP with tin(II) octoate is discussed in more detail in Chapter 2.

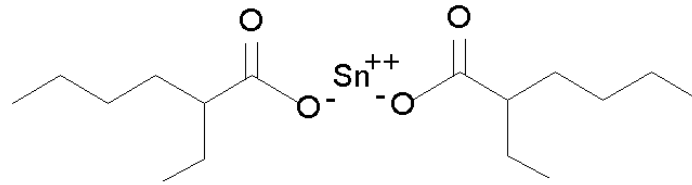
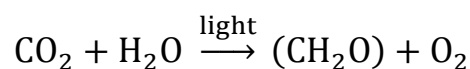


Fig. 1.9 tin(II) bis-2-ethylhexanoic acid

In 1988 a project to develop PLA was launched by Cargill Inc. The project goal was to establish new product and value opportunities for starch processed by the company. Dr. Pat Gruber was the initiator and project champion. Along with a small group of scientists, Dr. Gruber developed key processes for conversion of Lactic acid into Lactide and processes and technologies for purification and polymerization/devolatilization of Lactide. In 1994 the company built a 5000 metric tons per year PLA facility in Savage, Minnesota to prove and further develop Lactic acid to PLA technology on a semi-works scale and to launch the development of a commercial market for PLA. In early 1995 Cargill realized it needed a partner with a strong presence in the polymer market. Cargill assembled a list of partner attributes and Dow emerged as the best candidate. In November 1997 Cargill Dow LLC was founded as a 50/50 joint venture between Cargill Inc. and The Dow Chemical Company to pursue the commercialization of PLA polymers under the trade name NatureWorks™.

A stand-alone company today, Cargill Dow, is building a global platform of sustainable and versatile polymers and chemicals entirely made from renewable resources[2]. In November 2001, NatureWorks LLC started the production of Ingeo® (ingenious materials from plants not oil) PLA resins in its 140,000 ton-per-year manufacturing facility in Blair, Nebraska, USA. One year later, NatureWorks started producing Lactic acid in its 180,000 ton-per-year manufacturing facility located next to the polymer plant. Today, these two plants are the only large-scale commercial production facilities for PLA worldwide[26].

The whole PLA production process developed by Cargill Dow is shown in Fig. 1.10 (Lactic acid production) and Fig. 1.11[26] (PLA production). The life cycle of Ingeo® PLA starts with corn production. CO₂ and water from atmosphere are converted in carbohydrates by corn plants during the photosynthesis process. Photosynthesis process can be schematized with the following reaction:



Where (CH₂O) represents a carbohydrate, such as sucrose and starch. Therefore, all carbon, hydrogen, and oxygen found in the starch molecule or in the final PLA molecule is originated from water and CO₂ photo-converted by corn plants. This leads to the production of a polymer 100% made from renewable sources. After the separation of starch from the other components present in corn (fats, proteins, fibers, ash and water), enzymatic hydrolysis is carried on starch in order to convert it in a fermentable substrate: dextrose. Dextrose is sent to a fermentation reactor where a proper bacterial strain (*Lactobacilli*) converts it in Lactic acid. Other nutrients (nitrogen based nutrients) are added to the fermentation broth in order to increase bacterial growth. These bacteria have a narrow pH window in which they show an optimal activity that is almost at neutral pH values. As the fermentation product is an acid, a base must be added to the fermentation system in order to maintain neutral values of pH and avoid the inhibition of Lactic acid on bacterial growth. Ca(OH)₂ is added to the system and the product is recovered as calcium lactate. In order to recover the desired product (Lactic acid) an acidulation step is carried out by adding sulfuric acid to the fermentation product. This step leads to the formation of CaSO₄ (Gypsum) which is removed from crude Lactic acid with a rotary filter drum. Crude Lactic acid is separated from heavy components present in the mixture (such as unconverted dextrose, nutrients etc.) by evaporation. These heavy tails are recycled to the fermentation system while Lactic acid is further purified and sent to the polymerization section.

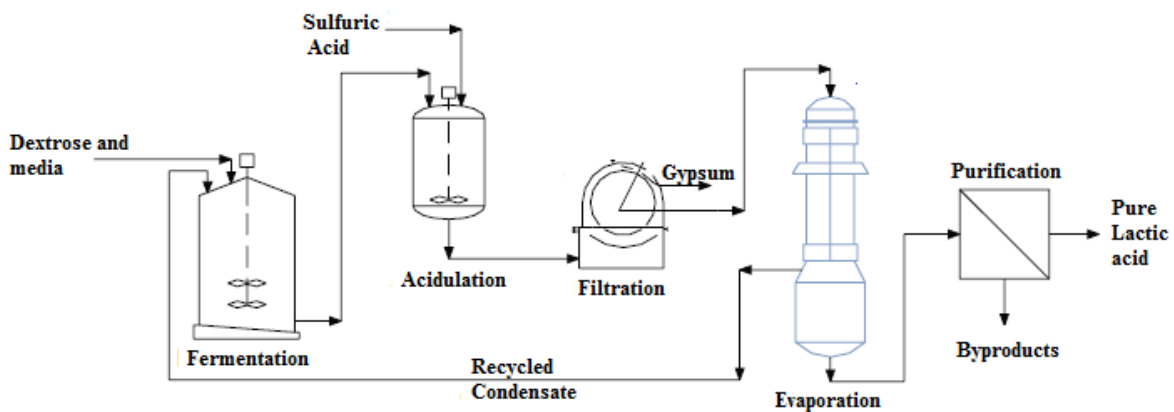


Fig. 1.10 NatureWorks™ Lactic acid production process

Ingeo® PLA is produced through the ROP of Lactide in a continuous polymerization process. In the first step aqueous Lactic acid is purified from water in a vacuum distillation column. The reboiler of the column is a polymerization reactor in which low molecular weight PLA (prepolymer) is produced through polycondensation of Lactic acid. Next, the prepolymer is catalytically converted into the cyclic dimer, Lactide, and separated by vaporization. Lactide mixture is then purified from water by distillation.

Finally, high molecular weight PLA is produced through catalytic ROP of Lactide. Both prepolymerization and polymerization step does not require the use of a solvent which means that polymerization is carried out through bulk melt polymerization processes. At each step unconverted reactants, such as Lactic acid (in the prepolymerization step) or Lactide (in the polymerization step), are recovered and recycled. Finally high molecular weight PLA melt is crystallized and dried to obtain Ingeo® PLA pellets.

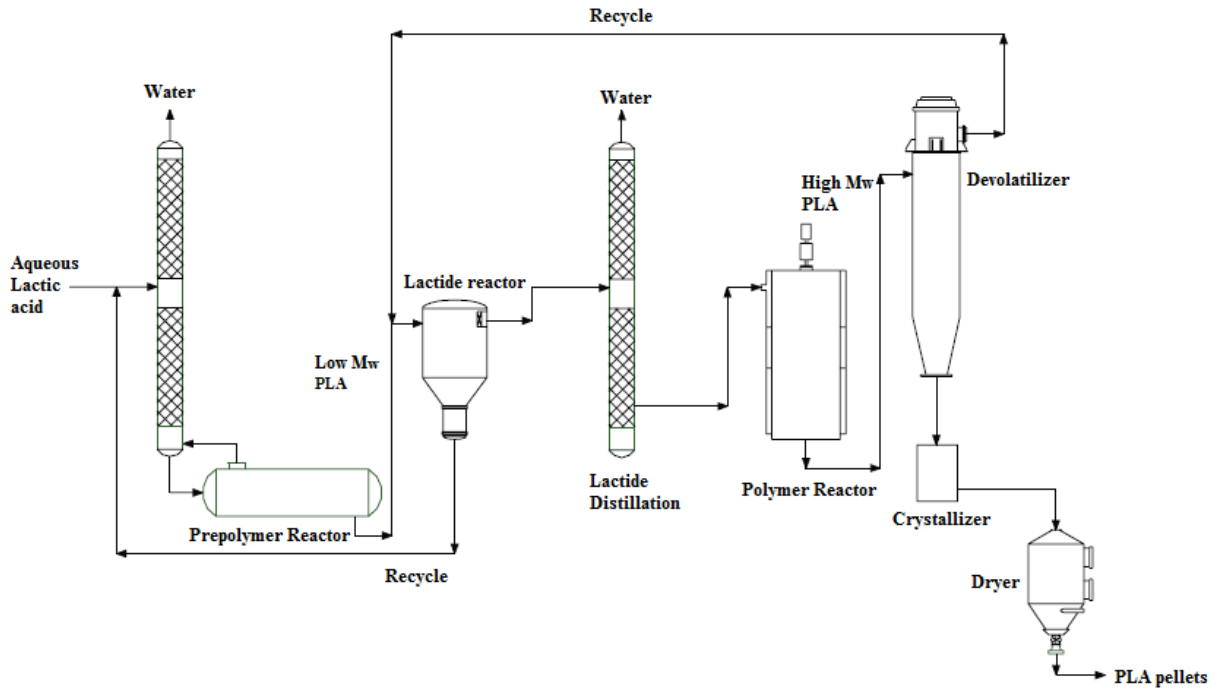


Fig. 1.11 NatureWorks™ Lactide formation and PLA polymerization process

1.3 Outline of The Thesis

This thesis was developed in collaboration with *LOPCA* (Laboratório de otimização e controle avançado de processo), *DEMBio* (Departamento de Engenharia de Materiais e Bioprocessos), *Biofabris* (Instituto de Biofabricação) at the department of Chemical Engineering of *UNICAMP* (Universidade Estadual de Campinas, Campinas - São Paulo, Brasil). The final part was carried out in collaboration with *FCM* (Faculdade de Ciências Médicas) at the department of medicine of *UNICAMP*.

The main goals of this thesis are:

- Synthesizing PLLA through ROP of L-Lactide;
- Developing a mathematical model for the simulation of ROP of L-Lactide in Batch reactor through bulk melt polymerization process;

- Characterizing physical properties and biocompatibility behavior of the synthesized polymer.

As this product must find application in biomedical area as material for bone fixation or for scaffolds PLLA was chosen as the best enantiomeric form of PLA in terms of mechanical properties. A weight average molecular weight of 100,000[Da] was fixed as target for the final polymer, because this value was the minimum one found in literature to satisfy mechanical requirements as scaffolds[28].

In the first part (Chapter 2) of this thesis, a detailed kinetic mechanism of ROP of L-Lactide taken from the literature[29], is described. Experiments on ROP of L-lactide in bulk melt were carried out from 140°C to 200°C in order to validate this model. The kinetic scheme used in this work involves reversible activation, reversible propagation, reversible chain transfer, reversible transesterifications and non-radical chain scission reactions. The kinetic scheme was modeled using a statistical method based on chain population balances: the method of the moments. Then the model was implemented using C++ as programming language and solved using *BzzMath*©[27] numerical libraries.

GPC analysis was used in order to obtain the dynamic evolution of weight average molecular weight, and number average molecular weight, while monomer conversion was measured by gravimetric analysis. These data were used to find kinetic constants of the model used; the numerical procedure used is described in Chapter 2. In Chapter 3 the development of a complete model for bulk melt polymerization of PLA in a Batch reactor is described. In Chapter 4 it's described the numerical procedure of detection of an optimal temperature trajectory for the polymerization reactor. This trajectory was calculated in order to reach the desired target ($M_w = 100,000$ [Da]) of the process in fewer time. Two temperature control systems were implemented. Firstly a PID control was implemented on the model and then an adaptive control system has been developed. Both controllers used the optimal temperature trajectory found as set-point curve. In Chapter 5 is described PLA synthesis carried out varying firstly the temperature, ranging from 140 °C to 200°C, and furthermore the ratios between monomer and catalyst and also cocatalyst and catalyst. These experiments were carried out in order to investigate the influence of reaction conditions on PLA final properties. Chapter 6 contains different kinds of analysis of the polymer produced in macro-scale such as: density, GPC, TGA, DSC, FT-IR, RDX, MEV and in vitro analysis. The aim is characterize the polymer under many aspects and not only the molecular weight in order to define if it can be used for its final application: scaffold in biomedical area. Chapter 7 contains conclusions and the outlook of the work.

CHAPTER 2

ROP of L-Lactide: kinetic study

2.1 Introduction

One of the goals of this thesis is to study ROP of L-Lactide in bulk melt polymerization process, in order to avoid the use of solvents and other external agents which would affect biocompatibility of the final product. In this case the catalysts used are heavy metals carboxylates, alkoxides or oxides and among them zinc and tin(II) based catalysts show the best catalytic activity [4]. 2-ethylhexanoic acid tin(II) salt ($\text{Sn}(\text{Oct})_2$) is the most widely used in both scientific research and industrial production and is the only catalyst that has been accepted by the U.S. Food and Drug Administration [29].

$\text{Sn}(\text{Oct})_2$ owes its widespread use to the following reasons [4]:

- Low toxicity (approved by U.S. FDA);
- Solubility in Lactide (this makes it suitable for bulk polymerization process);
- High catalytic activity;
- High monomer conversion presented (higher than 90%);
- Low racemization presented (less than 1%).

In presence of $\text{Sn}(\text{Oct})_2$ Lactide can undergo ROP through a coordination-insertion mechanism of the Lactide ring in the growing chain as can be seen in Fig. 2.1 [7].



Fig. 2.1 Generalized coordination–insertion mechanism of Lactide to PLA

R-OH in Fig. 2.1 represents a growing polymer chain with an hydroxyl end group. Almost all possible mechanisms on ROP of Lactide were proposed in the last 30 years, involving multiple different steps, such as initiation, propagation and chain transfer to low molecular species and between polymer chains. The key step of initiation was especially debated. It's worth to notice that all proposed mechanism involve the contribution of OH-bearing species, such as water, alcohols or carboxylic acids [29]. Two main initiation mechanisms can be found in literature for the ROP of Lactide in presence of Sn(Oct)₂. The first one has been developed mainly by Kricheldorf et al. [33,34] and it's based on a kind of "monomer activation" [29]. The activation of the monomer follows the reaction scheme reported in Fig. 2.1; monomer, catalyst and OH-bearing species, such as polymer chains with hydroxyl end groups, form a ternary complex which leads to the insertion of the monomer in the growing chain. Accordingly Sn atoms are not bonded to active chains (polymer chains containing Sn termination which can propagates chains growth), so the polymerization rate is simply first order with respect to the initial amounts of catalyst and OH-bearing species (which could be alcohols put in the reaction system as cocatalyst but also any environmental impurity which contain an hydroxyl group, like moisture). The second initiation mechanism was proposed by Penczek et al. [35] and is based on the "alkoxide initiation mechanism". Accordingly, Sn(Oct)₂ is not the true initiator of the polymerization. It first reacts with an OH-bearing specie to form an alkoxide which is the true initiator of the polymerization. Sn(Oct)₂ and OH-bearing species are respectively initiator and coinitorator of ROP and are often referred to as catalyst and cocatalyst. The direct observation of macromolecules containing Oct-Sn-O end groups by MALDI-TOF and the dependence of the polymerization rate upon monomer, catalyst and cocatalyst concentrations are solid evidences in favor of this mechanism which is now the accepted one in literature [29].

In order to take into account that the true initiation mechanism passes through the formation of an alkoxide specie the kinetic scheme developed by Yu et al. [30] was chosen. This kinetic scheme describes the bulk melt ROP of L-Lactide in presence of Sn(Oct)₂ as catalyst and 1-dodecanol as cocatalyst and it takes into account the "alkoxide initiation mechanism". The kinetic scheme is composed by the following class of reactions:

- Reversible activation (alkoxide initiation mechanism);
- Reversible propagation;
- Reversible chain transfer;

- Inter-molecular transesterifications;
- Non-radical random chain scission.

A more detailed description of each reaction step is given in the next sections. The same catalytic system used by Yu et al. [30] was used in this work and micro-scale experiments (in ampoules) were carried out in order to investigate the dynamic behavior of the ROP of L-Lactide. In particular experimental data about weight average molecular weight (M_w), number average molecular weight (M_n) and monomer's conversion (χ) were taken during polymerization time and at different temperatures. Monomer conversion was measured by gravimetric analysis while M_w and M_n were measured by GPC (Gel Permeation Chromatography) analysis.

The obtained experimental data were used to evaluate the kinetic constants of the kinetic model. To do this an isothermal model for ROP of L-Lactide in an ideal Batch reactor was developed. Population balances of polymer's chains were expressed using the method of the moments, a statistical method which allows to evaluate the average properties of a polymer (M_w and M_n). Experimental data were used to evaluate kinetic constants at each temperature and finally an Arrhenius expression of each kinetic constant presents in the model was evaluated.

2.2 Kinetic Scheme analysis

The range of temperature investigated goes from 140°C to 200°C (temperatures from 180°C to 230°C are typically in the range of work industrial production process of PLA [29]). Temperatures ranging from 140°C to 180°C are generally below the melting temperature of PLA which, depending upon polymer molecular weight, ranges from 135°C to 180°C [29]. For this reason polymer phase separation is expected under these conditions. Although also kinetic of this phase separation has to be considered: characteristic time of crystallization is quite large, ranging from 20 to 60[min] in absence of reactions and this time increases with polymer chain length [29]. In the work of Yu et al. [31] bulk melt ROP of L-Lactide has been carried out at 130°C. In order to check the actual presence of polymer solidification during this low temperature polymerization the physical state of the samples collected during a slow reaction producing high molecular weight was visually controlled; no signal of solidification was noticed during the first 3[h], thus indicating that the characteristic time of phase change is much longer than that of reaction. For this reason a maximum

polymerization time of 3[h] was taken as a constraint for the validity of the model which describes ROP of L-Lactide taking place in a single liquid phase.

2.2.1 Living behavior of ROP of L-Lactide

ROPs are often exhibiting living behavior; that is, the reaction proceeds at a constant number of growing chains [29]. For a living system with reversible propagation and reversible deactivation (chain transfer between active and dormant chains), the following relationships apply [29]:

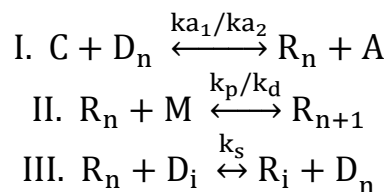
$$Y = \ln \left(\frac{[M]_0 - [M]_{eq}}{[M] - [M]_{eq}} \right) = k_p R^* t \quad [2.1]$$

$$M_n = \frac{[M]_0 \chi}{R^* + D} M_{mon} \quad [2.2]$$

where R^* is the concentration of living (active) chains, D is that of dormant (reversibly terminated) chains, χ is monomer conversion, defined as $([M]_0 - [M]) / [M]_0$, where $[M]$ is the monomer concentration and $[M]_0$ is the initial monomer concentration, M_{mon} is the molecular weight of monomer, and Y is the logarithm of the normalized conversion defined as in Eq. [2.1]. Note that such relationships apply when irreversible terminations are absent. Moreover, if propagation and reversible deactivations are only operative, then narrow molecular weight distributions are obtained, that is, with a polydispersity index (PDI), next to one. PDI is defined as:

$$PDI = \frac{M_w}{M_n} \quad [2.3]$$

PDI values next to one indicates that the product has a narrow molecular weight distribution (almost all the polymer chains present the same length). Finally, if the quantities Y and M_n exhibit linear behavior with time and conversion, respectively, then the concentrations of active and dormant chains are constant all along the reaction [29] (the polymerization system exhibits living behavior). This living behavior of the ROP of L-Lactide in presence of $Sn(Oct)_2$ can be described by the following simplified kinetic scheme [31]:



C represents the catalyst ($\text{Sn}(\text{Oct})_2$), A is octanoic acid formed during the activation of the catalyst to form tin alkoxide (and it can also represent any acid specie which negatively affects the activation step), M represents the monomer (L-Lactide), R_n a living chain (which presents Oct-Sn-O- as end group and so can propagate chain growth) of n repeating units and D_n a dormant chain (reversible terminated chain which presents a hydroxyl end group) of n repeating units. When n is set equal to 0, R_0 and D_0 represent respectively initiator (tin(II) alkoxide) and coinitiator (1-dodecanol) of ROP of Lactide.

Reaction I is reversible activation; in this step $\text{Sn}(\text{Oct})_2$ is converted to its active form (tin alkoxide). Direct kinetic constant of activation reaction is indicated with k_{a1} and reverse kinetic constant with k_{a2} . $\text{Sn}(\text{Oct})_2$ can be activated by any OH-bearing species, such as cocatalyst (1-dodecanol) or dormant chains which are converted into active chains.

Reaction II is reversible propagation; in this step an active chain of n repeating units adds a monomeric unit, forming an active chain of n+1 repeating units. Direct kinetic constant of propagation reaction is indicated with k_p and reverse kinetic constant with k_d . Reaction III is reversible chain transfer between a living chain and a dormant chain. Direct and reverse kinetic constants are set equal as this reaction is formally identical in both directions. Chain transfer kinetic constant is indicated with k_s . In these reactions direct and reverse kinetic constants are bonded by thermodynamic equilibrium constants (equilibrium constant of chain transfer reaction is set equal to one).

The living behavior of ROP of L-Lactide has been fully demonstrated by Yu in his PhD dissertation [29]. He showed that the quantity Y is linear with time, at least at conversion values lower than 95%, according with Eq. [2.1]. This means that the concentration of active chains is constant during most of the reaction and for sure up to conversion higher than 90%. At higher conversion the concentration of active chains decreases and the reaction is not living any longer. Furthermore Yu reported that Mn exhibits nice linearity with monomer conversion [29], according with Eq. [2.2]. This is another proof of the living behavior of the system. Living conditions are somehow lost during the reaction [29]. Discrepancy between Mn and Mw values becomes more important during time, indicating a broadening of the molecular weight distribution [29]. This has to be attributed to the presence of side reactions which do not affect the total number of chains or the polymerization rate (which is correctly predicted by the simplified kinetic scheme presented above), but only their length.

2.2.2 Transesterification reactions

In order to take into account the broadening of molecular weight distribution with time an additional set of reactions must be added to the previous kinetic scheme. These reactions don't affect the total number of chains (living and dormant) presents in the

system or the polymerization rate, but only the shape of polymer molecular weight distribution. Side reactions often mentioned as affecting the molecular weight distribution of polyesters are molecular interchange reactions called “transesterifications” [29]. Two types of transesterification can occur during the ROP of Lactide: intra-molecular transesterifications (as polymer chains contain both ester bonds and hydroxyl groups) and inter-molecular transesterifications (between two polymer chains). However inter-molecular transesterifications have been reported as the main mechanism responsible of the broadening of molecular weight distribution in catalyzed bulk ROP of L-Lactide [29,39,40]. The corresponding reaction scheme is shown in Fig. 2.2 [29]:

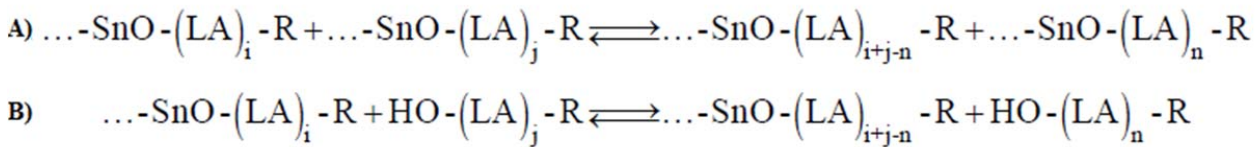


Fig. 2.2 Inter-molecular transesterifications

LA represents Lactide repeating unit in the polymer chain.

These reactions are reversible and the catalytic site is responsible of the chain reshuffling. Two types of inter-molecular transesterifications have to be distinguished: the one involving two active chains (which present an Sn-O group in the polymeric chain) which is reaction A showed in Fig. 2.2 and the one involving an active and a dormant chain (which presents an hydroxyl end group) which is reaction B showed in Fig. 2.2. In both cases an active chain attacks an ester bond internal to another chain which can be active or dormant [29]. As will be seen in the next paragraphs the nature of the attacking-attacked pair is relevant when writing chains’ population balances because it leads to different terms that must be accounted for active and dormant chains. For example, regarding reaction A, an active chain of n repeating units (R_n) can be formed by:

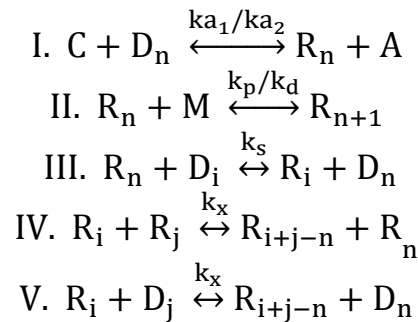
- The reaction between an active chain R_i of any length and an active chain R_j with a length greater than n;
- The reaction between an active chain R_i with a length smaller than n and an active chain R_j of any length.

Regarding reaction B:

- An active chain R_n can be formed by the reaction between an active chain R_i with a length smaller than n and a dormant chain D_j of any length;

- A dormant chain D_n of n repeating units can be formed by the reaction of an active chain R_i of any length and a dormant chain D_j of a length greater than n .

As can be seen three terms contribute to the production of R_n (Two from reaction A and one from reaction B), while only one term contributes to the production of D_n (the one in reaction B), leading to different terms that have to be accounted for transesterifications when writing population balances on active and dormant chains. Yu reported that propagation is dominant at low conversion (living behavior of ROP), while transesterification reactions broaden the molecular weight distribution at higher conversion only [29]. In order to take into account the growth of PDI with polymerization time the previous kinetic scheme must be modified, adding transesterification reactions. The modified kinetic scheme is showed below [30]:



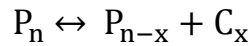
Reaction IV is transesterification reaction between two active chains and reaction V is transesterification reaction between an active and a dormant chain. Both reactions are reversible. As reported in Yu's PhD dissertation [29], although the two reactions involve different attacking-attacked pairs kinetic constants of both reactions are set equal. Furthermore as the two reactions are identical in both directions direct and reverse kinetic constants are set equal (which means that equilibrium constants of these reactions are set equal to one). Transesterification kinetic constant is indicated with k_x .

2.2.3 Non Radical Random Chain Scission

The previous kinetic scheme has been developed by Yu et al. [31] at a temperature of 130°C. This kinetic model describes in a very good way either the living behavior of ROP of L-Lactide, which lasts for almost the whole polymerization time (until conversion reaches a value of about 90%), or the broadening of molecular weight distribution due to transesterification reactions, which are typical side reactions that occur for polyesters. Although industrial production of PLA is usually run at higher temperature (at least 180°C) in order to achieve faster reaction rate and to avoid polymer crystallization (by working at temperature higher than the average melting temperature of PLA), and too high viscosity. Under such conditions the role of degradation reactions

become important and it can't be neglected [29]. Close to the range of temperature at which the industrial production of PLA is run (180°C-230°C) Wachsen et al. [41] proposed two possible degradation reactions: intramolecular transesterifications (back-biting reactions) and non-radical random chain scission, which respectively produce macro-cycles and acrylate-ended PLA chains. Since the reactions producing the acrylate-ended PLA chains require higher temperature values, one would expect that intramolecular transesterifications are the main mechanisms responsible for molecular weight decreasing with conversion in these conditions.

Although according to the theory of Jacobson and Stockmayer (J-S theory) [42], the concentration of the cycles is a strongly decreasing function of molecular size. Thermodynamics of the ring chain equilibrium quantitatively describes the conformational probability of two units along a polymer chain to meet and form a ring. In particular, the cycle formation reaction can be represented as:



And the corresponding equilibrium constant is [42]:

$$K = \frac{[C_x][P_{n-x}]}{[P_n]} \approx [C_x] = Ax^{-\frac{5}{2}} \quad [2.4]$$

Where P_n and P_{n-x} are linear chains of length n and $n-x$, respectively, while C_x is a cyclic polymer containing x repeating units with a concentration of $[C_x]$, and A is a constant which is characteristic for a given system. Assuming that P_n and P_{n-x} have almost the same concentration ($[P_n] \approx [P_{n-x}]$), the equilibrium constant of the back-biting reaction can be set equal to the concentration of the cyclic polymers. As this constant decreases with cycle dimensions (x) as described by Eq. [2.4], these reactions don't greatly affect the decreasing of PLA molecular weight at high temperature. The main mechanism of degradation at high temperature is the non-radical chain scission of PLA in presence of $Sn(Oct)_2$ [29]. This irreversible reaction leads to the formation of an acrylate-ended polymer chain from an original chain of greater length, as can be seen in Fig. 2.3 [29]. These acrylate-ended chains are irreversible terminated, therefore they can't propagate anymore. For this reason PLA molecular weight reaches a maximum and then, as non-radical chain scissions start to occur, decreases with time. Non-radical chain scission can involve active chains, dormant chains and also irreversible terminated chains which further decrease their length.

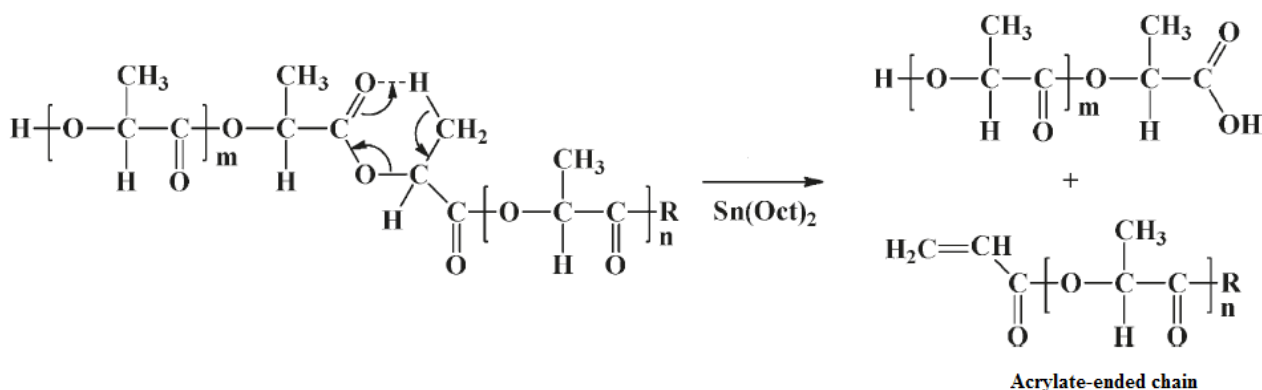
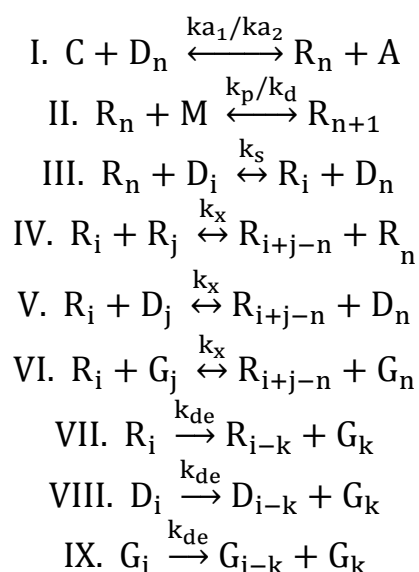


Fig. 2.3 Non-radical random chain scission

The kinetic scheme presented in the previous section must be modified in order to take into account polymer degradation by non-radical random chain scission.

The kinetic scheme chosen in this work was taken from Yu's PhD dissertation [29], as it considers: reversible activation (alkoxide initiation), reversible propagation, reversible chain transfer, inter-molecular transesterifications (between two active chains and between an active and a dormant chain) and non-radical random chain scission (on active, dormant and dead chains). The whole kinetic scheme is showed below:



Reactions VII, VIII and IX represent non-radical random chain scission of an active chain, a dormant chain and a dead chain (indicated with G), respectively. Reaction VI takes into account that also dead chains can be attacked by an active chain through a transesterification mechanism. Non-radical random chain scission leads to the formation of a shorter chain and an acrylate-ended chain (dead chain). Although each of these reactions involves a different type of chains, kinetic constants are set equal for all

reactions. These simplified assumption can be justify by the fact that the reactive act involved is independent by the type of, as it concerns the internal bonds of the chain. Obviously this assumption is true for infinite chain length, such as when the effect of the end groups of the chain (which differentiate the various types of chains) is negligible. The same assumption was made for reaction IV,V and VI (transesterifications). Non-radical random chain scission constant is indicated with k_{de} . Finally all kinetic constants present in the kinetic scheme showed above are assumed chain-length independent.

2.3 Experimental Section

2.3.1 Materials

(S,S)-3,6-Dimethyl-1,4-dioxane-2,5-dione(L,L-lactide;PURAC, PURASORB L; purity > 99.5%, water content <0.02%, Heavy metals <10 ppm, sulphated ash < 0.05%, residual solvent < 0.1%); 2-ethylhexanoic acid tin(II) salt (Sn(Oct)₂, Sigma Aldrich, 95% purity), and 1-dodecanol (Sigma Aldrich, 98% purity) were used as received. For the purification chloroform (J. T. Baker) and ethyl alcohol anhydrous (Labsynth 99,8% purity)were used. For GPC analyses, polystyrene standards from 1055 Da to 3 864 000 Da (Viscotek) were used for calibration, chloroform (J. T. Baker) was used as eluent and THF Tetrahydrofuran, Stabilized (J. T. Baker) HPLC Grade, 99.5% min. (by GC) was used as mobile phase.

2.3.2 Experimental Procedure

2.3.2.1 Ampoules sealing Procedure

Experiments were carried out in ampoules, following the same procedure used by Belincanta [46]. L,L-Lactide (LA), 2-ethylhexanoic acid tin(II) salt and 1-Dodecanol are mixed, the ampoules are connected to the vacuum system (Fig. 2.4 a), suddenly they are immersed in a container with liquid nitrogen (Fig. 2.4 b). When the samples are completely frozen (Fig. 2.4 c) (it takes about 2 minutes) they are removed from the container and the vacuum valves are opened. When all the ampoules are under vacuum and all the air, that acts as polymerization inhibitor, is removed vacuum is closed. This line is equipped with a system (*trap*) that prevents the flow of the reagents to the vacuum pump, for this reason is better to turn on the vacuum system and only a while later connect the trap.

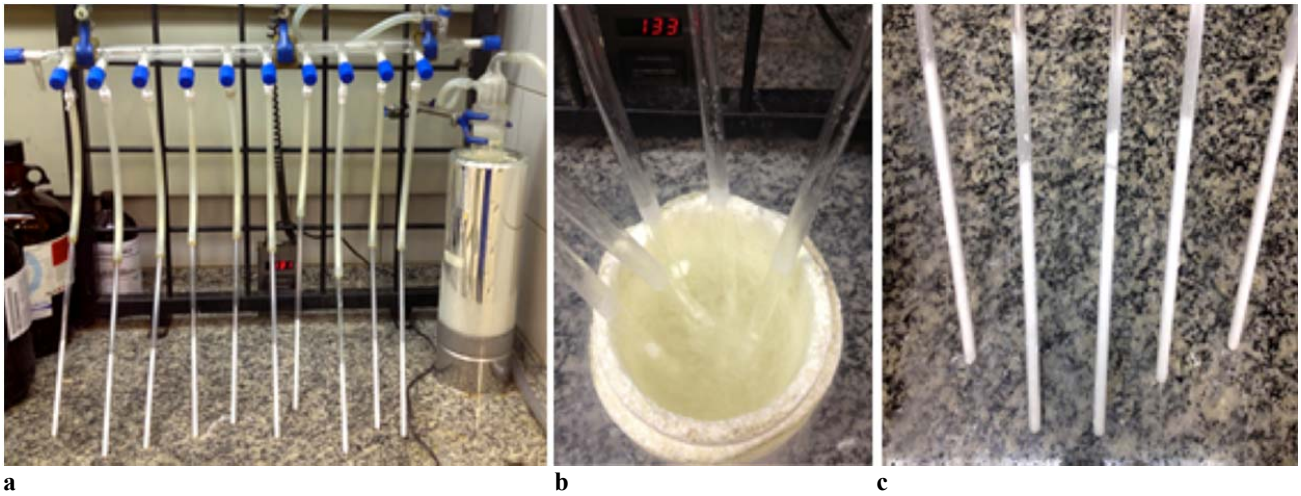


Fig. 2.4 Ampoules sealing experimental equipment (a: Ampoules under vacuum; b: Ampoules in nitrogen bath; c: Frozen ampoules)

When the vacuum valves are closed, the ampoules are thawed out using: ethanol, this must be done from the top to the bottom of the ampoules and during this process the air bubbles can be seen going out from the sample. When the ampoules are frozen, put them under vacuum and finally thawed out for minimum of three times and at the end they are maintained frozen for the next sealing process. At first the gas and the oxygen valves are opened. The nozzle is then ignited and the flame oxygen valve is regulated in order to have a blue flame (Fig. 2.5 a), then with rotational movements seal the ampoule without broke her (Fig 2.5 b). As final step, turn off the vacuum.

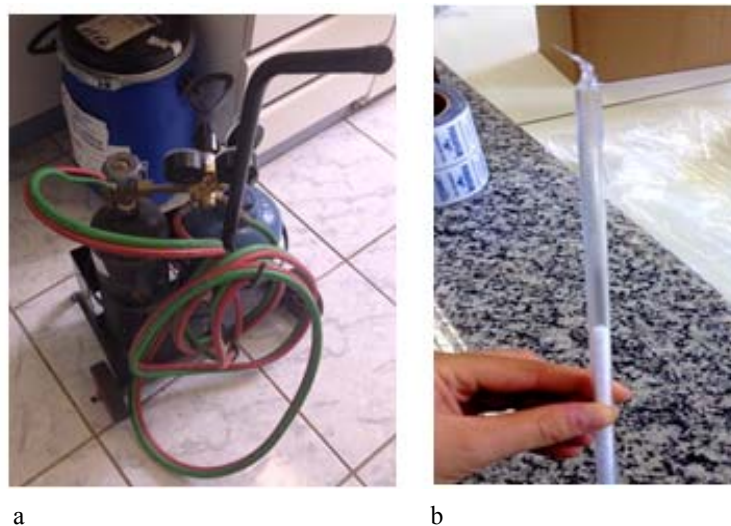


Fig. 2.5 Ampoules configuration (a: Oxyhydrogen torch; b: Sealed ampoule)

2.3.2.2 Reaction Procedure

First of all turn on the bath (Fig. 2.6 a) according to the arranged temperature (from 140° to 200° C) and define a plan for removing two ampoules after a predetermined time (two ampoules are used for each condition to compute a robust conversion). Insert all the ampoules at the same time in the bath and turn on the timer (Fig.2.6 b);

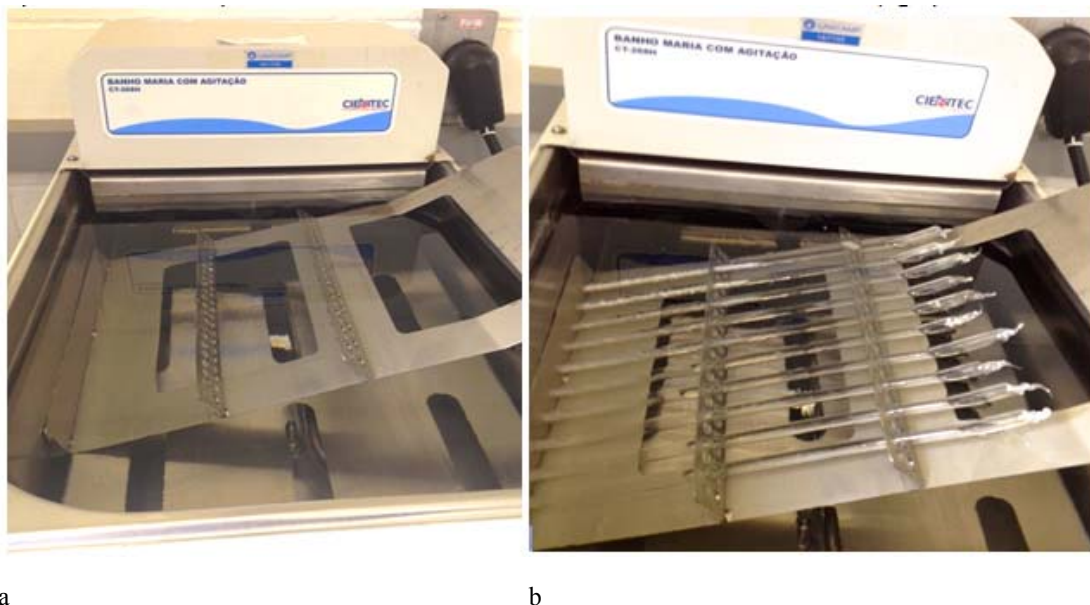


Fig. 2.6 Bath of diathermic oil (a: Empty batch, b: Bath with ampoules)

A becker must be taken for each ampoule and weighted: “mass 1”. When the predetermined time is reached remove the ampoules, they must be cleaned with a paper and quickly insert in a bath of water and ice (Fig. 2.7 a).

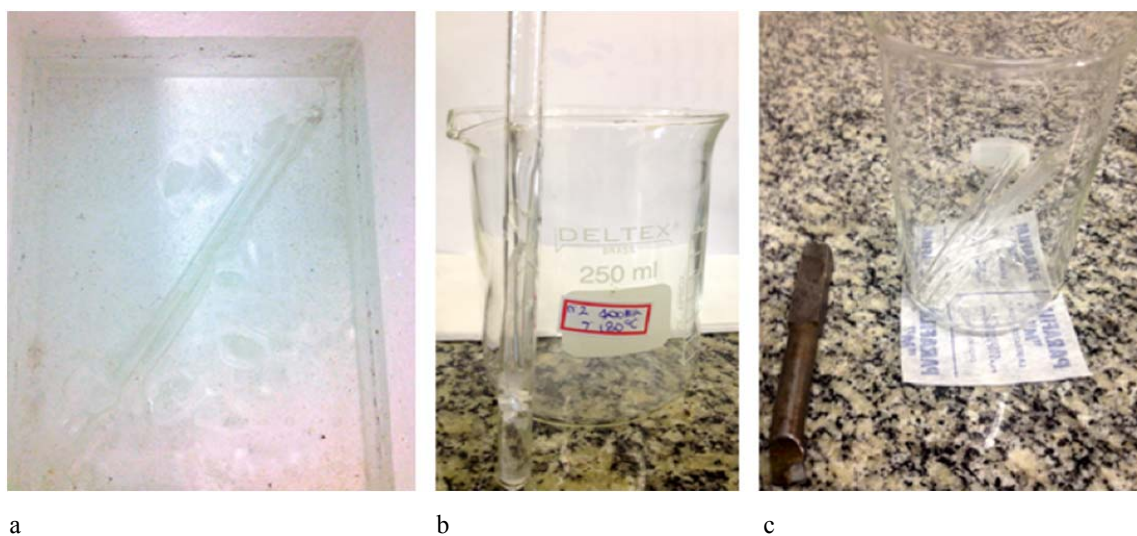


Fig. 2.7 Produced polymer after polymerization (a: Bath of ice, b: Ampoule after polymerization; c: Broken ampoule)

Retire the two ampoules from the bath and clean them with paper and alcohol or acetone and then weighted: “mass 2” (Fig. 2.7 b). The ampoules are taken, broken and the pieces of glass are insert in the relative becker (Fig. 2.7 c).

2.3.2.3 Polymer extraction

Chloroform and ethanol are added in the becker with the proportion of 4:1, subsequently the becker is closed with parafilm paper (Fig. 2.8 a), when the pieces of glass in the becker are complete cleaned, they are removed from the becker, weighted : “mass 3” and a further amount of ethanol is added. The function of the chloroform is to precipitate the polymer and the ethanol’s one is extract the monomer. The more polymer is present in the becker the more clear the solution is, if the solution doesn’t take a white color it means that the conversion is low (Fig. 2.8 b), The beckers are left in a fume cupboard, when the liquid level (solvents) is lower (Fig. 2.8 c), the beckers are put in the vacuum oven at 75 °C until the weight changes of a quantity less than 0.01 gr, (it could take more than 10 days). The polymer must be weighted “ mass 4” and collected in dark glass vials (Fig. 2.9 a,b)

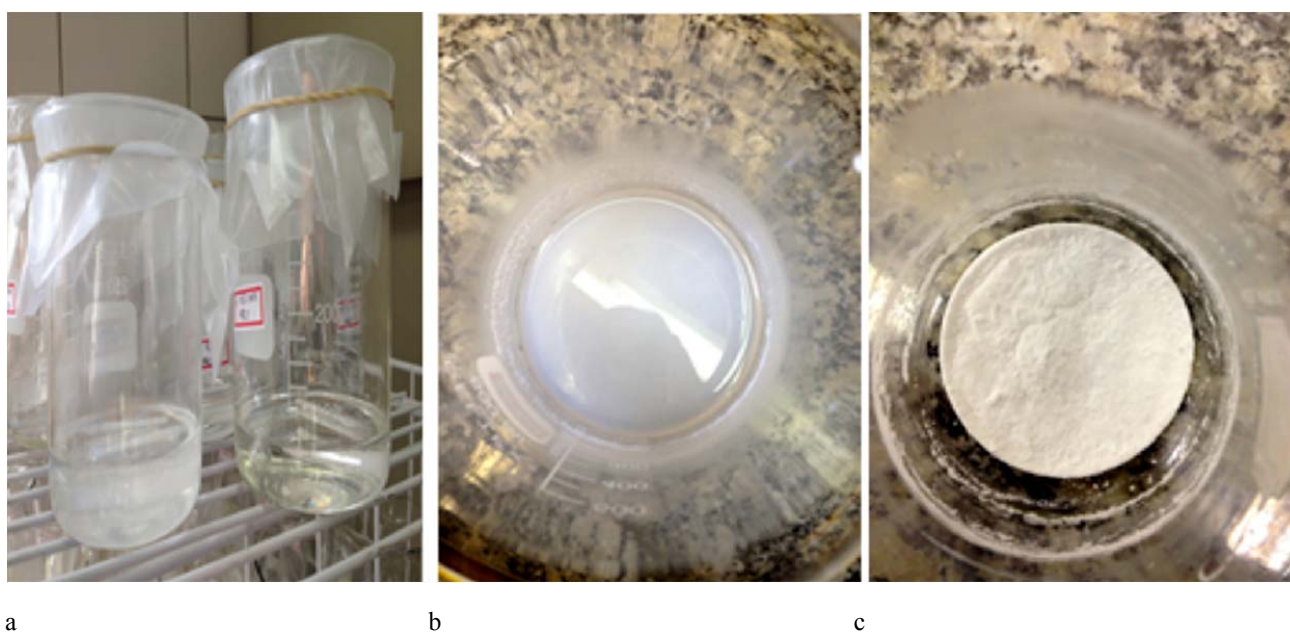


Fig. 2.8 Extraction polymer (a: first step of extraction; b: becker after addition of ethanol; c: Polymer retired from the cupboard)

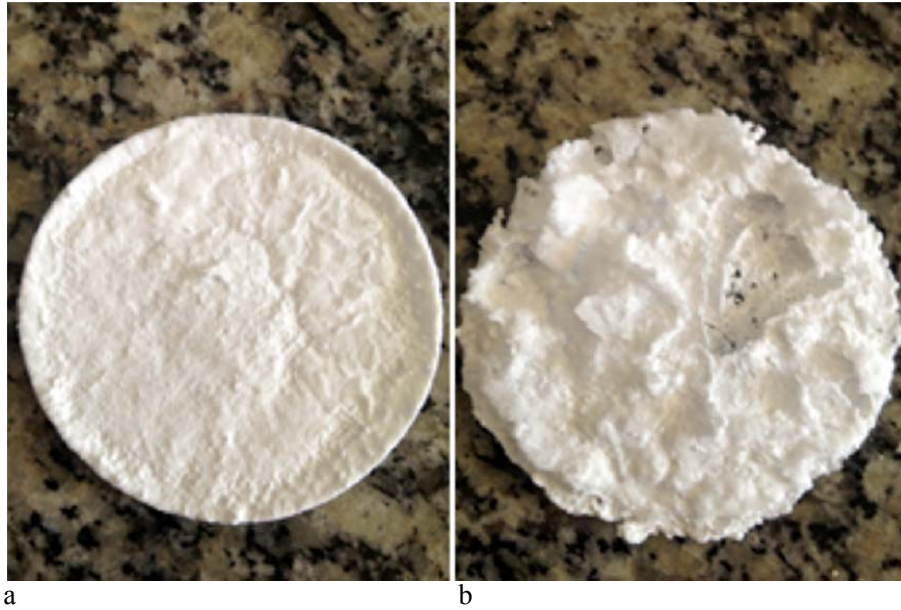


Fig. 2.9 Dry polymer (a: Example of dry polymer with high conversion; b: Example of dry polymer with low conversion)

2.3.3 Characterization Methods

2.3.3.1 Conversion

Starting from the polymers weighted previously (chapter 2.3.2.2 and 2.3.2.4) :

- Mass 1: becker weight;
- Mass 2: polymerized ampoule retired from the bath and cleaned with paper
- Mass 3: cleaned glass pieces of the ampoule retired from the becker
- Mass 4: weight of the dry polymer and the becker

$$\text{Conversion } (\chi) = \frac{\text{mass 4} - \text{mass 1}}{\text{mass 2} - \text{mass 3}} * 100 \quad [2.5]$$

That is equal to say:

$$\text{Conversion } (\chi) = \frac{([M]_0 - [M]_t)}{[M]_0} \quad [2.6]$$

2.3.3.2 Size Exclusion Chromatography Analysis (GPC)

Molecular weight distribution of all samples were characterized by size exclusion chromatography (GPC) (Viscotek) equipped with two detectors, Light Scattering (LS)

and differential refractive index (RI). Since the LS signal for Poly-L,Lactide is very low (confirmed by the dn/dc analysis), a LS detector was used. The GPC is equipped with two equals columns on series : ViscoGel I-MBHMW-3078 (7.8 mm x 30 cm). Tetrahydrofuran was used as eluent at flow rate of 1 mL min⁻¹ and temperature of 30 °C. Universal calibration was applied, based on polystyrene standards (Viscotek), three calibration curves are defined by relating respectively the retention volume RV [ml] with: weight average molecular weight, Mw [Da](Fig. 2.9), number average molecular weight, Mn [Da](Fig.2. 10) and the molecular weight of the highest peak, Mp [Da] (Fig. 2. 11).

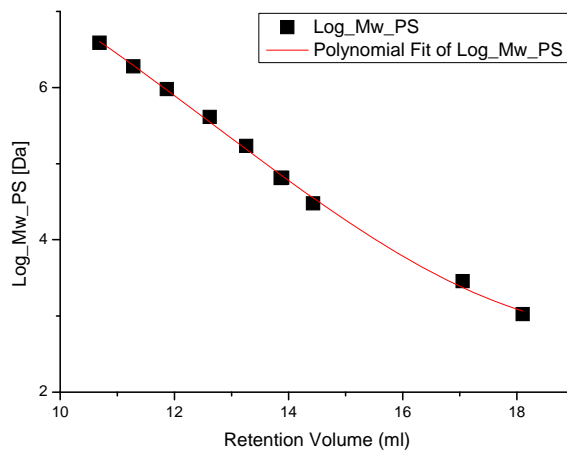


Fig. 2.9 Log_Mw of Polystyrene standards Vs. Retention Volume

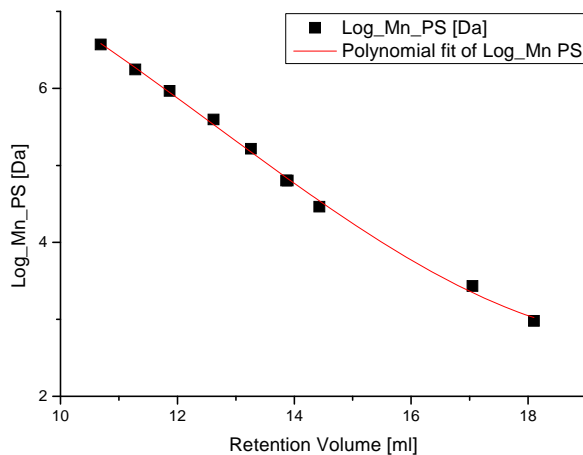


Fig. 1.10 Log_Mn of Polystyrene standards Vs. Retention Volume

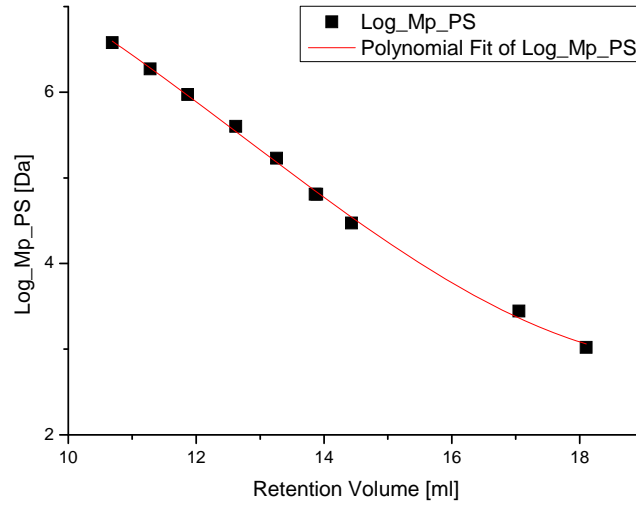
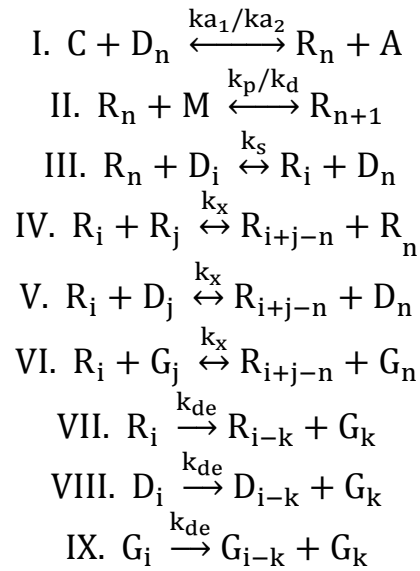


Fig. 2.11 Log_Mp of Polystyrene standards Vs. Retention Volume

2.4 Model Development

The kinetic scheme developed by Yu et al. [29,30] was chosen as the first building block of this work.



Kinetic constants was evaluated by Yu et al. [29,30,31] in a temperature range going from 130°C to 180°C. In order to adapt the previous kinetic model to the experimental conditions used in this work, kinetic constants of the model were evaluated using experimental data reported in section 2.4.

There are seven kinetic constants in the scheme reported above. Although, reverse kinetic constants are bond to direct ones by equilibrium constants.

$$\frac{k_{a1}}{k_{a2}} = K_{eq,a}(T) \quad [2.7]$$

$$\frac{k_p}{k_d} C_{TOT} = K_{eq,p}(T) \quad [2.8]$$

$K_{eq,a}$ and $K_{eq,p}$ are equilibrium constants of activation reaction and propagation reaction, respectively. For propagation reaction direct kinetic constant and reverse kinetic constant don't have the same measure units, as direct propagation is a bimolecular reaction and reverse is a unimolecular one. Propagation equilibrium constant must be divided for total concentration of the system in order to obtain homogeneity of measure units in Eq. [2.6]. As $K_{eq,p}$ is equal to:

$$K_{eq,p} = \frac{R_{n+1}}{R_n M} C_{TOT} \approx \frac{C_{TOT}}{M} \quad [2.9]$$

Ratio between direct and reverse propagation constants must be multiplied for the total concentration of the system. By assuming that C_{TOT} doesn't vary during time, it can be set equal to initial monomer concentration M_0 , which can be calculated as:

$$M_0 = \frac{\rho_{mon}(T)}{M_{mon}} \quad [2.10]$$

Where ρ_{mon} represents Lactide density which can be calculated as a function of temperature, by using the equation reported by Witke et al. [32]:

$$\rho_{mon}(T) = \frac{1145}{1 + 7.391 * 10^{-4}(T[^\circ C] - 150)} \left[\frac{g}{l} \right] \quad [2.11]$$

As already said, equilibrium constants of chain transfer and transesterification reactions are set equal to one. Equilibrium parameters are only function of temperature:

$$K_{eq} = \exp\left(-\frac{\Delta G_r^\circ(T)}{RT}\right) \quad [2.12]$$

$$\Delta G_r^\circ(T) = \Delta H_r^\circ - T\Delta S_r^\circ \quad [2.13]$$

From a theoretical point of view also ΔH_r° and ΔS_r° are temperature dependent; although assuming a linearization of ΔG_r° with temperature it's possible to set these two state functions as constant parameters.

In order to reduce the number of parameters that have to be estimated from the previous model, ΔH_r° and ΔS_r° of both activation and propagation reactions were taken from literature.

Reaction	ΔH_r° [kJ/mol]	ΔS_r° [J/(mol K)]	Reference
Activation	50.1	99.3	Yu et al. [29,30]
Propagation	-23.3	-22.0	Witke et al. [32]

Table 2.1 Thermodynamic parameters

It's necessary to underline that the thermodynamic parameters regarding activation were obtained by linear regression of the data point present in [29,30].

By doing so the number of parameters that have to be estimated from experimental data are 5: direct activation constant, direct propagation constant, chain transfer constant, transesterification constant and degradation constant. Reverse activation and propagation constant are function of the respective direct constant, according to Eq. [2.5] and [2.6].

The mathematical model used to describe the experimental data showed in section 2.4 refers to an ideal (well-stirred) isothermal Batch reactor. The model is formed by material balances on monomeric species (such as catalyst, octanoic acid and monomer) and chain population balances. Since three types of chains (active, dormant and dead) are present in the ROP of L-Lactide, three chain population balances must be written to describe the polymerization process.

Material balances on monomeric species:

$$\frac{dC}{dt} = k_{a2}A \sum_0^{\infty} R_n - k_{a1}C \sum_0^{\infty} D_n \quad [2.14]$$

$$\frac{dA}{dt} = -\frac{dC}{dt} \quad [2.15]$$

$$\frac{dM}{dt} = k_d \sum_0^{\infty} R_n - k_p M \sum_0^{\infty} R_n \quad [2.16]$$

It's worth to notice that the kinetic scheme chosen in this work expects that catalyst C reacts with an OH-bearing group, losing only an alkyl termination. Since it can lose its two alkyl termination forming a di-alkoxide as initiator, catalyst concentration in the model is twice the experimental one [43].

Material balance on initiator:

$$\frac{dR_0}{dt} = k_{a1} CD_0 - k_{a2} AR_0 + k_d R_1 - k_p MR_0 + k_s \left(D_0 \sum_0^{\infty} R_n - R_0 \sum_0^{\infty} D_n \right) \quad [2.17]$$

Material balance on activated monomer (open ring):

$$\begin{aligned} \frac{dR_1}{dt} = & k_{a1} CD_0 - k_{a2} AR_0 + k_d (R_2 - R_1) + k_p M (R_0 - R_1) \\ & + k_s \left(D_1 \sum_0^{\infty} R_n - R_1 \sum_0^{\infty} D_n \right) \\ & - k_x \left[R_1 \left(\sum_1^{\infty} nR_n - \sum_1^{\infty} R_n \right) - \sum_1^{\infty} R_n \sum_2^{\infty} R_i + R_1 \left(\sum_1^{\infty} nD_n - \sum_1^{\infty} D_n \right) \right. \\ & \left. - \sum_1^{\infty} R_n \sum_2^{\infty} D_i + R_1 \left(\sum_1^{\infty} nG_n - \sum_1^{\infty} G_n \right) - \sum_1^{\infty} R_n \sum_2^{\infty} G_i \right] \\ & + k_{de} \sum_2^{\infty} R_n \end{aligned} \quad [2.18]$$

Population balance on active chains:

$$\begin{aligned}
\frac{dR_n}{dt} = & k_{a1}CD_n - k_{a2}AR_n + k_d(R_{n+1} - R_n) + k_pM(R_{n-1} - R_n) \\
& + k_s \left(D_n \sum_0^\infty R_n - R_n \sum_0^\infty D_n \right) \\
& - k_x \left[R_n \left(\sum_1^\infty nR_n - \sum_1^\infty R_n \right) - \sum_1^\infty R_n \sum_{n+1}^\infty R_i + (n-1)R_n \sum_1^\infty R_n \right. \\
& - \sum_0^{n-1} R_i \sum_{n+1-i}^\infty R_k + R_n \left(\sum_1^\infty nD_n - \sum_1^\infty D_n \right) - \sum_1^\infty R_n \sum_{n+1}^\infty D_i \\
& \left. + R_n \left(\sum_1^\infty nG_n - \sum_1^\infty G_n \right) - \sum_1^\infty R_n \sum_{n+1}^\infty G_i \right] - k_{de}(n-1)R_n \\
& + k_{de} \sum_{n+1}^\infty R_n
\end{aligned} \tag{2.19}$$

Population balance on dormant chains:

$$\begin{aligned}
\frac{dD_n}{dt} = & k_{a2}AR_n - k_{a1}CD_n + k_s \left(R_n \sum_0^\infty D_n - D_n \sum_0^\infty R_n \right) \\
& + k_x(1 - \delta_{n,0}) \sum_0^{n-1} R_i \sum_{n+1-i}^\infty D_k - k_x(1 - \delta_{n,0})(1 - \delta_{n,1})(n-1)D_n \sum_1^\infty R_n \\
& - k_{de}(n-1)D_n + k_{de} \sum_{n+1}^\infty D_n
\end{aligned} \tag{2.20}$$

Population balance on dead chains:

$$\begin{aligned}
\frac{dG_n}{dt} = & k_x(1 - \delta_{n,0}) \sum_1^\infty R_n \sum_{n+1}^\infty G_i - k_x(1 - \delta_{n,0})(1 - \delta_{n,1})(n-1)G_n \sum_1^\infty R_n \\
& - 2k_{de}(1 - \delta_{n,0})(1 - \delta_{n,1})(n-1)G_n + 2k_{de}(1 - \delta_{n,0}) \sum_{n+1}^\infty G_i \\
& + k_{de}(1 - \delta_{n,0}) \sum_{n+1}^\infty R_i + k_{de}(1 - \delta_{n,0}) \sum_{n+1}^\infty D_i
\end{aligned} \tag{2.21}$$

Kronecker delta, $\delta_{i,j}$ is used in population balances when a chain of length $i = j$ is not interested by a specific term of the balance. Population balance on active chains (Eq. [2.19]) is valid for chains with at least two repeating units. Population balances' equations have been solved using the method of the moments. This method will be explained in the next section.

2.4.1 Method of the moments

The method of the moments is a statistical method which allows to estimate parameters related to a population distribution. The estimations evaluated by this method are punctual estimations of the population parameters, such as distribution's mean (μ) or distribution's amplitude (σ^2). This method is widely used in economics, but can be generalized for any case in which a parameters' estimation from a population distribution has to be done, starting from sample values.

Since polymerization processes involve chain length distributions (CLD), which can be connected to molecular weight distributions (MWD), the method of the moments can be applied in order to estimate the parameters related to this distributions. Parameters that characterize chain length distribution are average chain length and amplitude of the distribution.

Analyzing this method exclusively from a statistical point of view, let us suppose to have a random sample $X = \{x_1; x_2; \dots x_n\}$ with a probability density function (PDF), $p(x)$ and we want to know its parameters μ and σ^2 . In order to estimate PDF parameters, statistical functions must be defined. A statistical function is any function which binds together sample values: $f = f(x_1; x_2; \dots x_n)$. It's worth to notice that unknown parameters are contained in PDF $p(x)$ while f doesn't contain any unknown. Absolute sample moments (Eq. [2.22]) and relative sample moments (Eq. [2.23]) are examples of statistical functions:

$$M'_r = \frac{1}{n} \sum_1^n x_i^r \quad [2.22]$$

$$M_r = \frac{1}{n} \sum_1^n (x_i - x_{av})^r \quad [2.23]$$

M'_r represents the absolute sample moment of order r and M_r , the relative sample moment of order r ; x_{av} represents sample mean.

The problem related to the punctual estimation of parameters from a PDF, results in a research of a proper statistical function. A statistical function used to estimate

population parameters is called estimator. From a mathematical point of view an estimator can be represented as:

$$\theta' = t(x_1; x_2; \dots x_n) \quad [2.24]$$

Where θ' represents the estimation of the population parameter θ and is a random variable. The numerical value of θ' in correspondence of a specific sample value, X is called punctual estimation of θ .

In order to estimate the unknown population parameters with the method of the moments, the equivalence of the expected values of absolute sample moments (M'_r) with absolute distribution moments (μ'_r) is imposed.

$$\mu'_r = E\{X^r\} \quad [2.25]$$

Where μ'_r is function of population parameters $\theta_1, \theta_2, \dots \theta_k$.

Given a random sample X , the absolute sample moments are function of sample values through Eq. [2.22] while absolute distribution moments are function of the unknown parameters. When the condition showed in Eq. [2.25] is imposed the method of the moments leads to the following system:

$$\begin{aligned} \mu'_1(\theta_1, \dots \theta_k) &= M'_1(x_1, \dots x_n) \\ &\vdots \\ \mu'_r(\theta_1, \dots \theta_k) &= M'_r(x_1, \dots x_n) \end{aligned} \quad [2.26]$$

The solution of the system [2.23] is constituted by the estimations of population parameters: $\theta'_1(x_1; \dots x_n) \dots \theta'_k(x_1; \dots x_n)$.

This approach can be applied in polymerization process to obtain estimations of parameters from CLD. These parameters, such as average chain length (mean of the distribution) and amplitude of CLD (variance) are used to calculate the average molecular weight of the polymer: M_w and M_n . These two physical properties of the polymer are defined as:

$$M_n = \sum_1^\infty x_i M_i \quad [2.27]$$

$$M_w = \sum_1^\infty w_i M_i \quad [2.28]$$

Where x_i and w_i are respectively molar and weight fraction of polymer chains with a molecular weight of M_i . Since chains with higher molecular weight have an higher weight fraction than chains with lower molecular weight M_w is always higher than M_n . Ideally M_w could assume a minimum value equal to M_n if all polymer chains have the same length. As a result PDI is always higher than one.

If n_i is the number of chains with M_i as molecular weight, x_i and w_i can be written as:

$$x_i = \frac{n_i}{\sum_1^{\infty} n_i} \quad [2.29]$$

$$w_i = \frac{m_i}{\sum_1^{\infty} m_i} = \frac{n_i M_i}{\sum_1^{\infty} n_i M_i} \quad [2.30]$$

By combining Eq. [2.29] and [2.30] with Eq. [2.27] and [2.28] the following expressions are obtained:

$$M_n = \frac{\sum_1^{\infty} n_i M_i}{\sum_1^{\infty} n_i} \quad [2.31]$$

$$M_w = \frac{\sum_1^{\infty} n_i^2 M_i}{\sum_1^{\infty} n_i M_i} \quad [2.32]$$

If the polymerization occurs in liquid phase (as in the case of bulk melt ROP of L-Lactide) at constant reaction volume x_i and w_i can be written as:

$$x_i = \frac{P_i}{\sum_1^{\infty} P_i} \quad [2.33]$$

$$w_i = \frac{P_i M_i}{\sum_1^{\infty} P_i M_i} \quad [2.34]$$

Where P_i is the concentration of chains with a molecular weight of M_i . M_i can be written as the product of the number of repeating units (chain length n) multiply for M_{mon} .

$$M_i = n M_{\text{mon}} \quad [2.35]$$

Combining Eq. [2.31], [2.32], [2.33], [2.34] and [2.35] the following expressions of M_w and M_n are obtained:

$$M_n = \frac{\sum_1^{\infty} n P_n}{\sum_1^{\infty} P_n} M_{\text{mon}} \quad [2.36]$$

$$M_w = \frac{\sum_1^{\infty} n^2 P_n}{\sum_1^{\infty} n P_n} M_{\text{mon}} \quad [2.37]$$

Where the sum operator is no more extended to all molecular weights M_i , assumed by polymer chains, but to all chain lengths assumed.

As can be seen numerator and denominator of Eq. [2.36] and [2.37] are the moments of the CLD.

$$Q_i = \sum_1^{\infty} n^i P_n \quad [2.38]$$

Q_i represents the moment of order i of the CLD.

Eq. [2.36] and [2.37] can be reformulated as functions of the CLD moments.

$$M_n = \frac{Q_1}{Q_0} M_{\text{mon}} \quad [2.40]$$

$$M_w = \frac{Q_2}{Q_1} M_{\text{mon}} \quad [2.41]$$

It's worth to notice that only CLD moments of zero and first order have a physical meaning. Q_0 represents the total number of chains, while Q_1 represents the total number of repeating units in the system. Therefore the ratio between Q_1 and Q_0 represents the average chain length. Q_2 has only a statistical meaning (amplitude of CLD). When more than one chain population is involved during polymerization the sum of all chain populations' moments must be taken into account in the evaluation of M_w and M_n . Once chain population balances are known it's to evaluate the dynamic evolution of the moments of the CLD by applying the method of the moments.

For example to evaluate zero-order moment of CLD, the sum operator is applied to chain population balance.

$$\sum_1^{\infty} \frac{dP_n}{dt} = \frac{d(\sum_1^{\infty} P_n)}{dt} = \frac{dQ_0}{dt} = \sum_1^{\infty} r(P_n) \quad [2.42]$$

Where P_n represents concentration of chain with length n and $r(P_n)$ the global production rate of chain P_n .

Applying the method of the moments to chain population balances derived from the kinetic scheme used (Eq. [2.19], [2.20] and [2.21]) the following moments' balances have been found:

Moments' balances on active chains:

$$\frac{d\lambda_0}{dt} = \frac{dR_0}{dt} + \frac{dR_1}{dt} + \sum_2^{\infty} \frac{dR_n}{dt} = k_{a1}C\mu_0 - k_{a2}A\lambda_0 \quad [2.43]$$

$$\begin{aligned} \frac{d\lambda_1}{dt} &= \frac{dR_1}{dt} + \sum_2^{\infty} n \frac{dR_n}{dt} \\ &= k_{a1}C\mu_1 - k_{a2}A\lambda_1 + k_s(\lambda_0\mu_1 - \mu_0\lambda_1) + k_pM\lambda_0 - k_d\lambda_0 \\ &\quad - k_x \left[\lambda_1(\mu_1 - \mu_0) - \frac{1}{2}k_x\lambda_0(\mu_2 - \mu_1) + k_x\lambda_1(\gamma_1 - \gamma_0) - \frac{1}{2}k_x\lambda_0(\gamma_2 - \gamma_1) \right] \\ &\quad - \frac{1}{2}k_{de}(\lambda_2 - \lambda_1) \end{aligned} \quad [2.44]$$

$$\begin{aligned} \frac{d\lambda_2}{dt} &= \frac{dR_1}{dt} + \sum_2^{\infty} n^2 \frac{dR_n}{dt} \\ &= k_{a1}C\mu_2 - k_{a2}A\lambda_2 + k_s(\lambda_0\mu_2 - \mu_0\lambda_2) + k_pM(\lambda_0 + 2\lambda_1) + k_d(\lambda_0 - 2\lambda_1) \\ &\quad + k_x \left[\frac{1}{3}\lambda_0(\lambda_1 - \lambda_3) + \lambda_1(\lambda_2 - \lambda_1) - \lambda_2(\mu_1 - \mu_0) + \frac{1}{6}\lambda_0(2\mu_3 - 3\mu_2 + \mu_1) \right. \\ &\quad \left. - \lambda_2(\gamma_1 - \gamma_0) + \frac{1}{6}\lambda_0(2\gamma_3 - 3\gamma_2 + \gamma_1) \right] \\ &\quad - \frac{1}{6}k_{de}(4\lambda_3 - 3\lambda_2 - \lambda_1) \end{aligned} \quad [2.45]$$

Moments' balances on dormant chains:

$$\frac{d\mu_0}{dt} = \sum_0^{\infty} \frac{dD_n}{dt} = k_{a2}A\lambda_0 - k_{a1}C\mu_0 \quad [2.46]$$

$$\begin{aligned}
\frac{d\mu_1}{dt} &= \sum_1^{\infty} n \frac{dD_n}{dt} \\
&= k_{a2}A\lambda_1 - k_{a1}C\mu_1 + k_s(\mu_0\lambda_1 - \lambda_0\mu_1) \\
&\quad + k_x \left[\lambda_1(\mu_1 - \mu_0) - \frac{1}{2}\lambda_0(\mu_2 - \mu_1) \right] - \frac{1}{2}k_{de}(\mu_2 - \mu_1)
\end{aligned} \tag{2.47}$$

$$\begin{aligned}
\frac{d\mu_2}{dt} &= \sum_1^{\infty} n^2 \frac{dD_n}{dt} \\
&= k_{a2}A\lambda_2 - k_{a1}C\mu_2 + k_s(\mu_0\lambda_2 - \lambda_0\mu_2) \\
&\quad + k_x \left[\lambda_2(\mu_1 - \mu_0) + \lambda_1(\mu_2 - \mu_1) + \frac{1}{6}\lambda_0(-4\mu_3 + 3\mu_2 + \mu_1) \right] \\
&\quad - \frac{1}{6}k_{de}(4\mu_3 - 3\mu_2 - \mu_1)
\end{aligned} \tag{2.48}$$

Moments' balances on dead chains:

$$\frac{d\gamma_0}{dt} = \sum_0^{\infty} \frac{dG_n}{dt} = k_{de}(\lambda_1 - \lambda_0) + k_{de}(\mu_1 - \mu_0) \tag{2.49}$$

$$\begin{aligned}
\frac{d\gamma_1}{dt} &= \sum_1^{\infty} n \frac{dG_n}{dt} \\
&= k_x \left[\lambda_1(\gamma_1 - \gamma_0) - \frac{1}{2}\lambda_0(\gamma_2 - \gamma_1) \right] \\
&\quad + k_{de} \left[\frac{1}{2}(\lambda_2 - \lambda_1) + \frac{1}{2}(\mu_2 - \mu_1) - (\gamma_2 - \gamma_1) \right]
\end{aligned} \tag{2.50}$$

$$\begin{aligned}
\frac{d\gamma_2}{dt} &= \sum_1^{\infty} n^2 \frac{dG_n}{dt} \\
&= k_x \left[\lambda_2(\gamma_1 - \gamma_0) + \lambda_1(\gamma_2 - \gamma_1) + \frac{1}{6}\lambda_0(-4\gamma_3 + 3\gamma_2 + \gamma_1) \right] \\
&\quad + k_{de} \left[\frac{1}{6}(2\lambda_3 - 3\lambda_2 + \lambda_1) + \frac{1}{6}(2\mu_3 - 3\mu_2 + \mu_1) \right. \\
&\quad \left. - \frac{1}{3}(4\gamma_3 - 3\gamma_2 - \gamma_1) \right]
\end{aligned} \tag{2.51}$$

Mn and Mw are calculated as:

$$M_n = \frac{\lambda_1 + \mu_1 + \gamma_1}{\lambda_0 + \mu_0 + \gamma_0} M_{\text{mon}} \tag{2.52}$$

$$M_w = \frac{\lambda_2 + \mu_2 + \gamma_2}{\lambda_1 + \mu_1 + \gamma_1} M_{\text{mon}} \tag{2.53}$$

Where M_{mon} is the molecular weight of L-Lactide which is 144.13[g/mol].

As PDI is calculated as reported in Eq. [2.3], its expression with population moments is:

$$PDI = \frac{(\lambda_2 + \mu_2 + \gamma_2)(\lambda_0 + \mu_0 + \gamma_0)}{(\lambda_1 + \mu_1 + \gamma_1)^2} \tag{2.54}$$

It's worth to notice that the method of the moments doesn't allow to estimate polymer MWD with time but only its average value. Knowing the dynamic evolution of the moments of chain population, the dynamic evolution of Mw and Mn can be evaluated by Eq. [2.52] and [2.53].

Since transesterification and non-radical chain scission reactions involve the internal bonds of the chain, the corresponding reaction rates in population balances are function of chain length, n. When applying the method of the moments to population balances, the dependence of these reactions rate from chain length leads to the presence of (i+1)-order moments in i-order moments balances. So, as can be seen in Eq. [2.45], [2.48] and [2.52], second-order moments' balances present third-order moments in their expressions. Closing formula for third-order moments were taken from [29].

$$\lambda_3 = \frac{\lambda_2(2\lambda_2\lambda_0 - \lambda_1^2)}{\lambda_1\lambda_0} \tag{2.55}$$

$$\mu_3 = \frac{\mu_2(2\mu_2\mu_0 - \mu_1^2)}{\mu_1\mu_0} \quad [2.56]$$

$$\gamma_3 = \frac{\gamma_2(2\gamma_2\gamma_0 - \gamma_1^2)}{\gamma_1\gamma_0} \quad [2.57]$$

Material balances on catalyst, acid and monomer (from Eq. [2.11] to [2.13]) together with moments' balances on active dormant and dead chains (from Eq. [2.43] to [2.51]) form an ODE system of 12 differential equations. This ODE system represents the mathematical model of an isothermal Batch reactor for the ROP of L-Lactide.

Initial conditions of the system are fixed, once reaction temperature and molar ratios between monomer to catalyst (M/C) and cocatalyst to catalyst (ROH/C) are fixed. Initial concentration of monomer can be calculated through Eq. [2.10], which is a function of reaction temperature through Eq. [2.11]. So once reaction temperature is fixed also M_0 is. Eq. [2.10] assumes that reaction volume is equal to monomer volume. Since ROP of L-Lactide is carried out through bulk melt polymerization process this assumption is very reasonable, as catalyst and cocatalyst contributions to reaction volume are negligible. Once M/C and ROH/C are fixed, it's possible to evaluate either catalyst concentration or cocatalyst concentration.

This model allows to evaluate the dynamic evolution of Mw, Mn (with Eq. [2.53] and [2.52]) and monomer conversion χ .

2.5 Parameters Estimation

In order to validate the kinetic model with the experimental data obtained through the procedure described in section 2.3, the following problem was formulated. It was imposed that kinetic constants have to minimize the following objective function:

$$\text{SSE} = \sum_1^{\text{NE}} \left[w_i^{\text{Mn}} (\text{Mn}(t_i) - \text{Mn}^{\text{exp}}(t_i))^2 + w_i^{\text{Mw}} (\text{Mw}(t_i) - \text{Mw}^{\text{exp}}(t_i))^2 + w_i^{\chi} (\chi(t_i) - \chi^{\text{exp}}(t_i))^2 \right] \quad [2.58]$$

Where $\text{Mn}(t_i)$, $\text{Mw}(t_i)$ and $\chi(t_i)$ are number average molecular weight, weight average molecular weight and monomer conversion calculated at each sampling time, t_i from the model. $\text{Mn}^{\text{exp}}(t_i)$, $\text{Mw}^{\text{exp}}(t_i)$ and $\chi^{\text{exp}}(t_i)$ are the corresponding values obtained experimentally at each sampling time. NE it's number of samples. Since molecular weight and conversion differ one from the other of several orders of magnitude, each term of the objective function (sum of square errors, SSE) was multiplied for a proper

weight. The problem that was solved to find kinetic constants through experimental data was a constrained multivariable (as 5 kinetic constants must be evaluated) optimization problem. The constrain of the problem is represented by the mathematical model of the isothermal Batch reactor.

Optimization problem:

$$\begin{aligned} \min_{\mathbf{k}} \text{SSE}(\mathbf{k}) \\ \text{s. t.} \\ \frac{d\mathbf{y}}{dt} = \mathbf{f}(\mathbf{y}, t) \end{aligned}$$

In the previous expression vectors are marked as bold.

In the numerical procedure adopted a function containing the objective function was written in C++. This function contains the ODE system discretized in time; thus Euler method was applied to solve the mathematical model.

$$\mathbf{y}_{i+1} = \mathbf{y}_i + h\mathbf{f}(\mathbf{y}_i, t_i) \quad [2.59]$$

Where h is the integration step of the method. In order to guarantee convergence of the method and a good accuracy a very small integration step has been chosen. It was seen that good previsions were obtained when h was set equal to 10^{-5} [hr]. The test was made by solving the isothermal model using kinetic constants evaluated by Yu et al. at 130°C [31], using $M/C = 3771$ and $\text{ROH}/C = 10$. It was seen that with this integration step the results obtained from Euler method and from *BzzOdeNonStiff* class (class from *BzzMath*© numerical library which implements Adams-Moulton algorithms to solve ODE system) were practically identical.

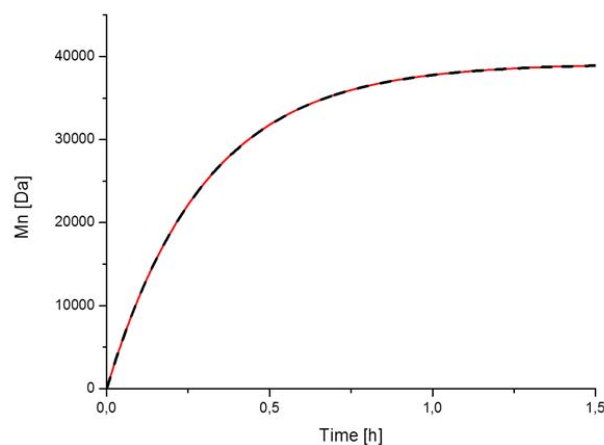


Fig. 2.12 Mn vs time. Continuous line: Euler algorithm, Dash line: *BzzOdeNonStiff* solver

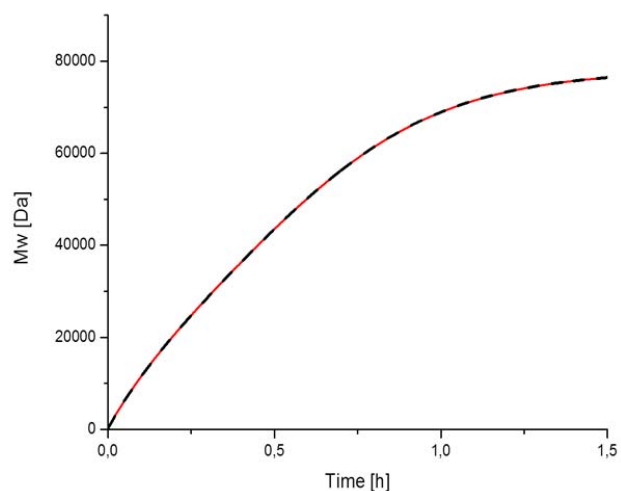


Fig. 2.13 Mw vs time. Continuous line: Euler algorithm, Dash line: *BzzOdeNonStiff* solver

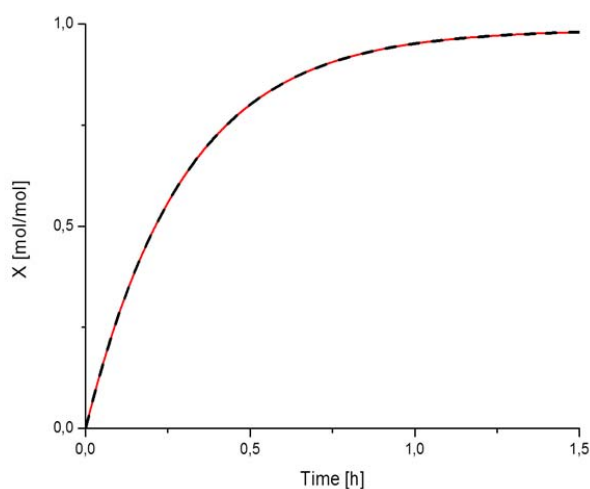


Fig. 2.14 χ vs time. Continuous line: Euler algorithm, Dash line: *BzzOdeNonStiff* solver

At each sampling time the values of moments of chain population and monomer concentration are taken in the function to evaluate $M_n(t_i)$, $M_w(t_i)$ and $\chi(t_i)$. These values are used to evaluate SSE which is the return value of the function. In the main program *BzzMinimizationRobust* class is used. This class implements robust optimization algorithms (e.g. Simplex method) to solve multivariable optimization problems. The object generated by this class calls the function described above and finds the vector of kinetic constants \mathbf{k} which optimize its return value. This procedure was used for each set of experimental data taken at different temperature.

2.6 Results and discussions

Initial amounts of monomer, catalyst and cocatalyst were chosen in order to obtain high molecular weight PLA ($M_w = 50,000$ [Da] at least) in polymerization process. Thus a value of M/C equal to 1000 and ROH/C equal to 4, were chosen. In order to prevent solidification of PLA during the process at lower temperature than polymer melting temperature polymerization time was set lower than 3 hours. A 2 hours polymerization time was chosen for experiments carried out at 140°C . As higher polymerization rates are achieved at higher temperatures, lower times were used. 1.5 hours polymerization time was used for 160°C and 170°C and 1 hour polymerization time was used for 180°C and 200°C . Kinetic constants found with the optimization procedure described above are reported in Table 2.2.

$T[^\circ\text{C}]$	$k_{a1}[\text{l}/(\text{mol h})]$	$k_p [\text{l}/(\text{mol h})]$	$k_s[\text{l}/(\text{mol h})]$	$k_x[\text{l}/(\text{mol h})]$	$k_{de}[\text{h}^{-1}]$
140	$1.57 \cdot 10^6$	112.	$3.88 \cdot 10^6$	1.00	$9.35 \cdot 10^{-7}$
160	$2.24 \cdot 10^6$	462	$4.15 \cdot 10^6$	1.01	10^{-6}
170	$2.81 \cdot 10^6$	537	$4.44 \cdot 10^6$	1.16	$5.74 \cdot 10^{-6}$
180	$3.03 \cdot 10^6$	951	$4.97 \cdot 10^6$	1.46	$5.74 \cdot 10^{-6}$
200	$4.53 \cdot 10^6$	1950	$5.47 \cdot 10^6$	1.64	$2.52 \cdot 10^{-5}$

Table 2.2 Kinetic constants calculated by *BzzMinimizationRobust* solver

Comparison between model and experimental data at 140°C:

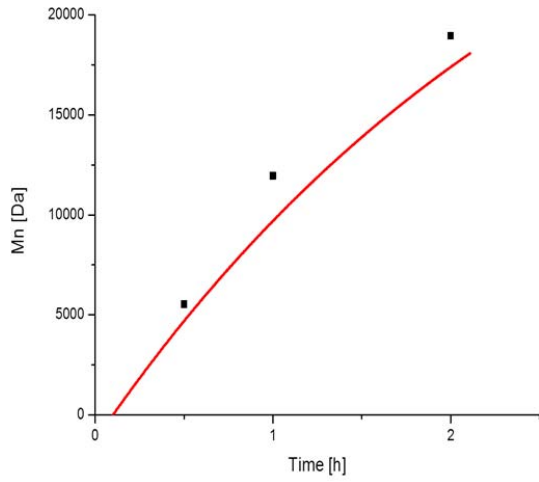


Fig. 2.15 Mn vs time at 140°C.
(•): Experimental data, Continuous line: model

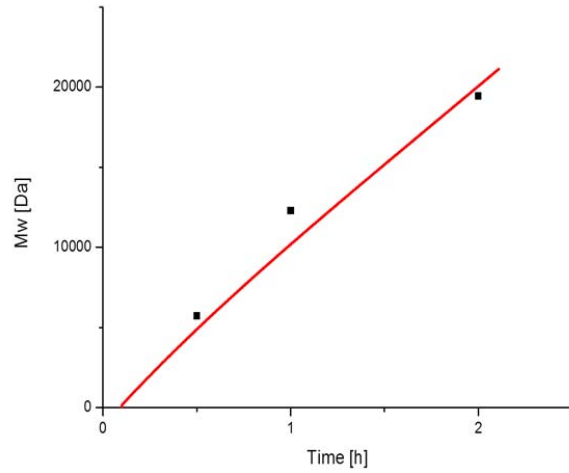


Fig. 2.16 Mw vs time at 140°C.
(•): Experimental data, Continuous line: model

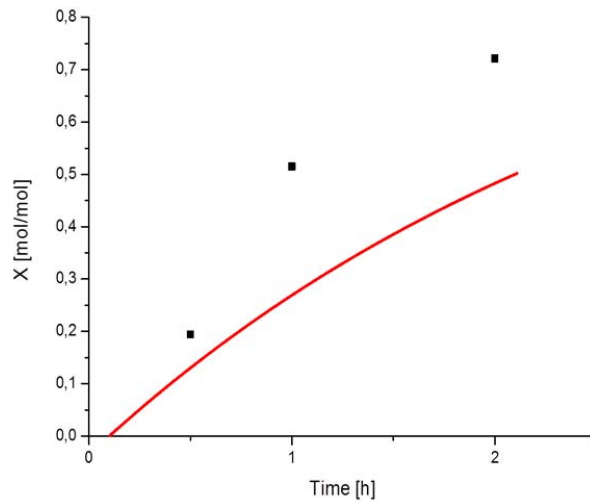


Fig. 2.17 X vs time at 140°C
(•): Experimental data, Continuous line: model

Comparison between model and experimental data at 160°C:

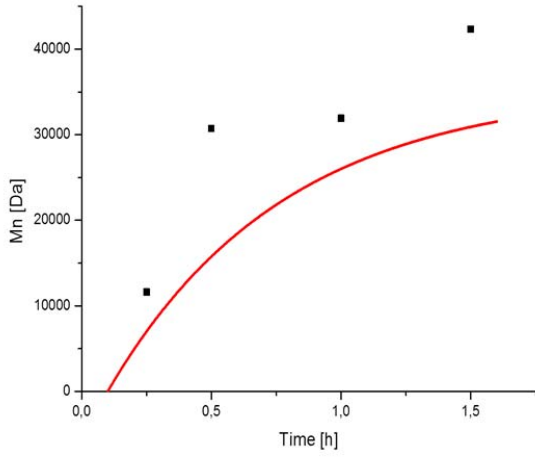


Fig. 2.18 Mn vs time at 160°C.
(▪): Experimental data, Continuous line: model

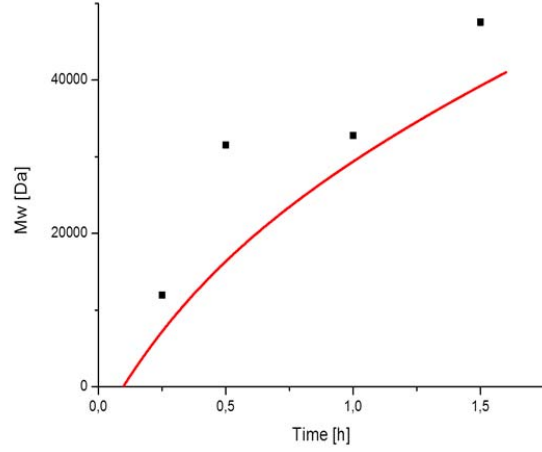


Fig. 2.19 Mw vs time at 160°C
(▪): Experimental data, Continuous line: model

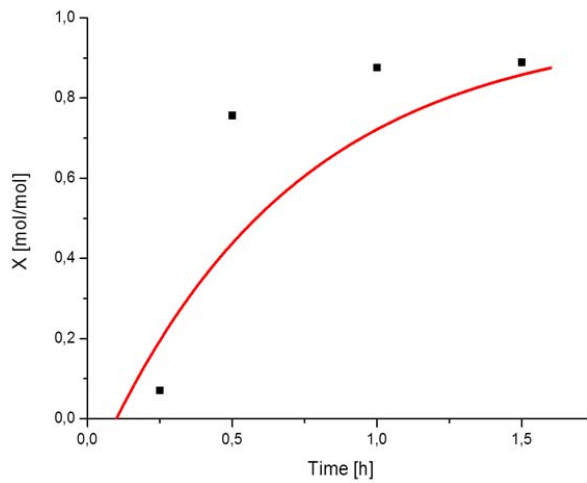


Fig. 2.20 χ vs time at 160°C.
(▪): Experimental data, Continuous line: model

Comparison between model and experimental data at 170°C:

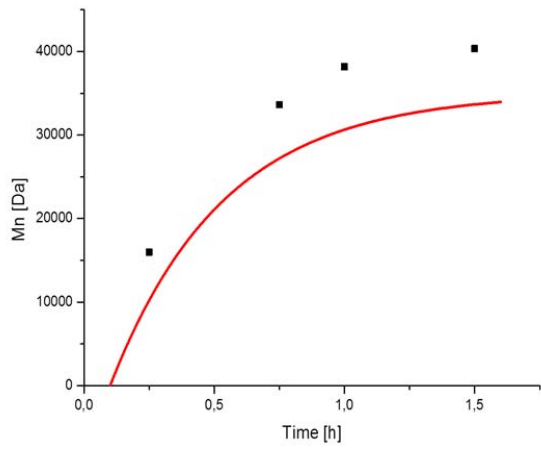


Fig. 2.21 Mn vs time at 170°C.
(•): Experimental data, Continuous line: model

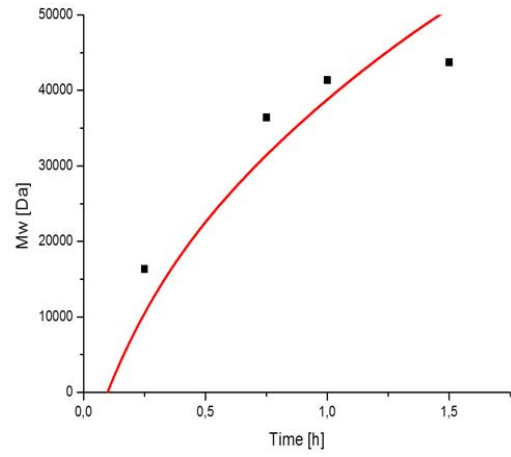


Fig. 2.22 Mw vs time at 170°C.
(•): Experimental data, Continuous line: model

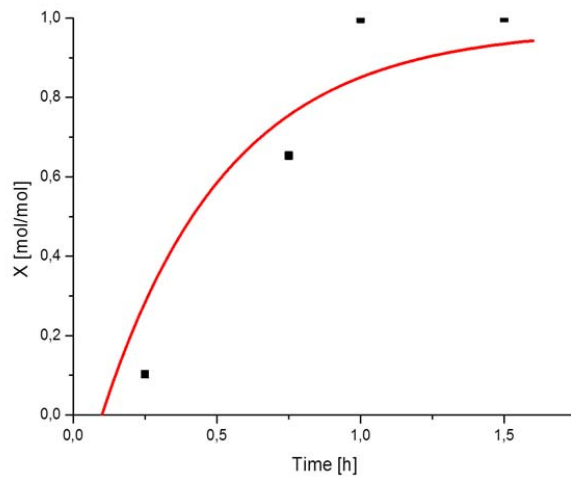


Fig. 2.23 χ vs time at 170°C.
(•): Experimental data, Continuous line: model

Comparison between model and experimental data at 180°C:

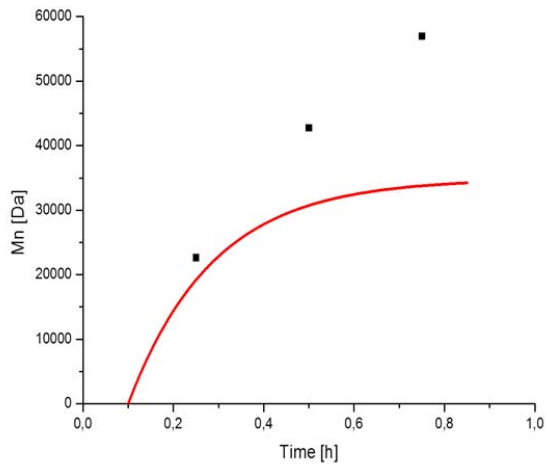


Fig. 2.24 Mn vs time at 180°C.
(•): Experimental data, Continuous line: model

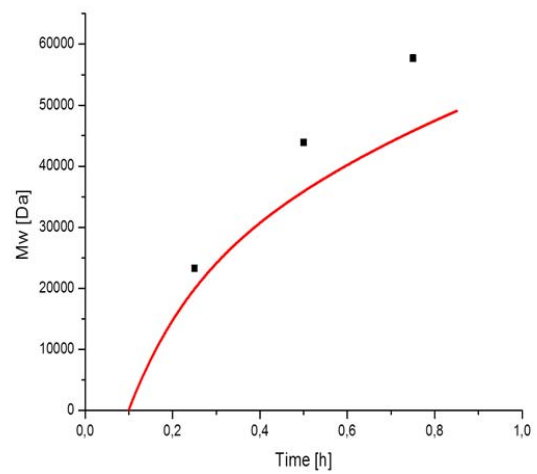


Fig. 2.25 Mw vs time at 180°C.
(•): Experimental data, Continuous line: model

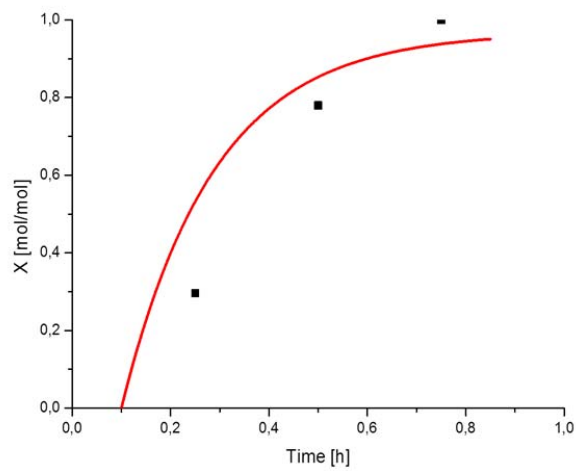


Fig. 2.26 χ vs time at 180°C.
(•): Experimental data, Continuous line: model

Comparison between model and experimental data at 200°C:

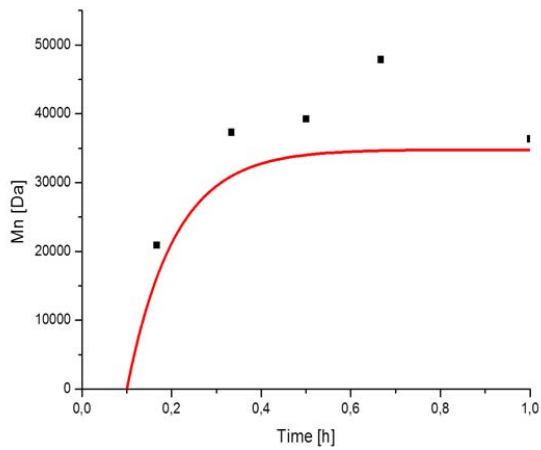


Fig. 2.27 Mn vs time at 200°C.
(•): Experimental data, Continuous line: model

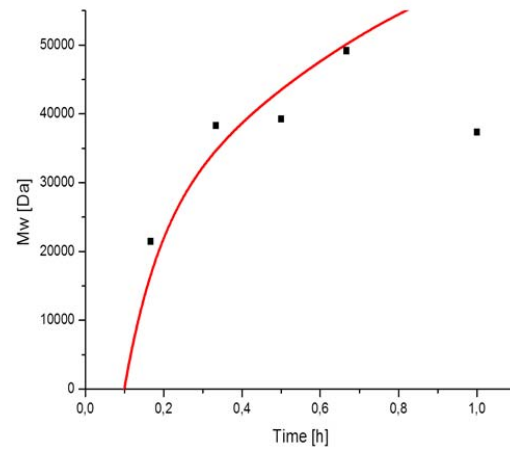


Fig. 2.28 Mw vs time at 200°C.
(•): Experimental data, Continuous line: model

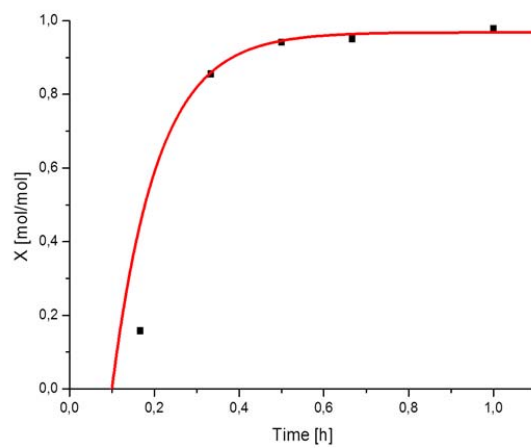
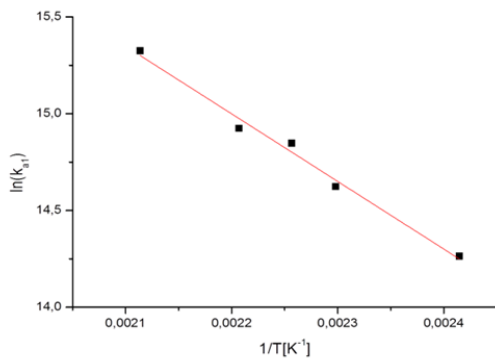


Fig. 2.29 χ vs time at 200°C.
(•): Experimental data, Continuous line: model

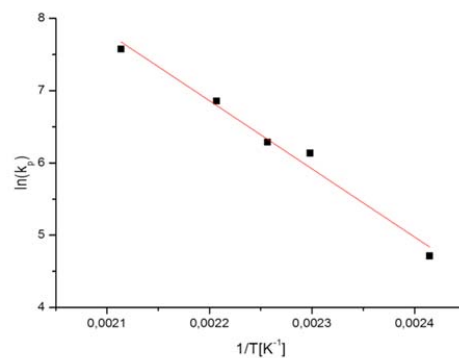
In order to have a better fitting of experimental data, a characteristic delay time of reaction of 1 hour was set for each set of data. This delay time can be seen as the time necessary to start up the polymerization. Quite good agreement can be seen between model previsions and experimental data, although there are some discrepancies between them. As can be seen in Fig. 2.17 monomer conversion is largely underestimated at 140°C. Under vacuum conditions, at this temperature vaporization of Lactide and low molecular species (e.g. oligomers) may occur. Probably at low temperature characteristic time of phase change is smaller than the polymerization one and this leads to M/C values lower than the nominal one (the initial one). As monomer conversion increases with the decreasing of M/C this, eventually leads to higher conversion achieved during polymerization. As temperature of reaction increases underestimation of Lactide conversion is reduced. A remarkably good agreement can be seen in Fig. 2.29 between conversion experimental data and model previsions at 200°C. At higher temperatures characteristic time of polymerization is smaller than the one of phase change and this leads to effective M/C values close to the nominal one.

GPC analyses showed that every samples had a PDI next to one, so that PLA synthesized had a very narrow CLD. This fact is in contrast to what is reported in literature [29,30,31] and leads to discrepancies between model previsions and experimental data on Mn. Since experiments were carried out in ampoules well-stirred conditions weren't reached in the experimental configuration. For this reason diffusion limitations played an important role on bimolecular reactions. Since transesterification involves two polymer chains which must diffuse one towards the other to react. Due to the absence of a proper stirring system during polymerization transesterification reactions were slowed down, leading to an underestimation of k_x . As diffusion rate decreases with increasing chain length (i.e. Mn), greater discrepancies are seen for higher temperature (Fig. 2.18, 2.21, 2.24, 2.27) where higher molecular weight are achieved in lower times, while a better agreement is observed for lower temperatures (Fig. 2.15).

Finally an underestimation of k_{de} is observed at 200°C.



a



b

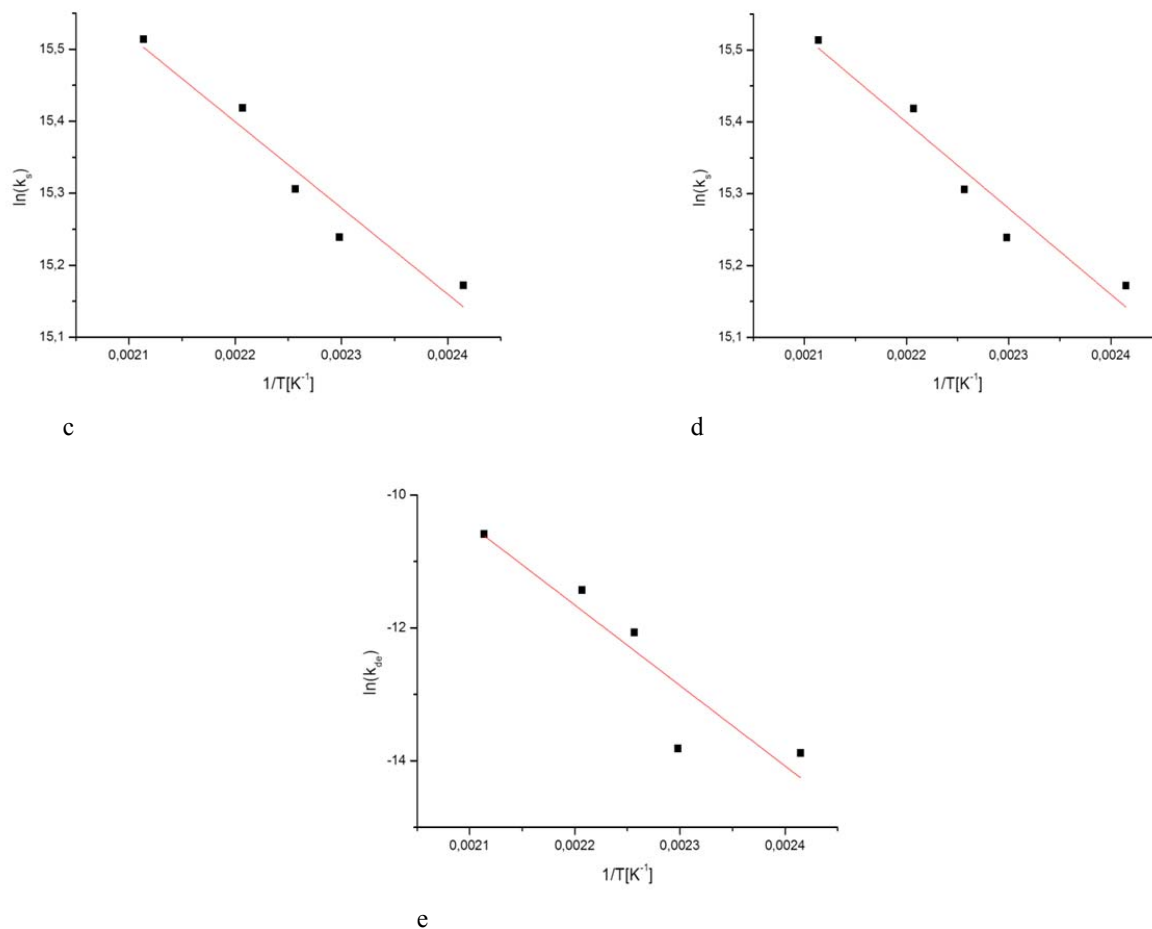


Fig. 2.30 Arrhenius plots. a) activation, b) propagation, c) chain transfer, d) transesterification, e) non-radical random chain scission

Reaction	k°	E_A [kJ/mol]
Activation	$8.11 \cdot 10^9$ [l/(mol h)]	29.5
Propagation	$8.04 \cdot 10^{11}$ [l/(mol h)]	77.7
Chain transfer	$6.33 \cdot 10^7$ [l/(mol h)]	9.70
Transesterification	62.1 [l/(mol h)]	14.5
Non-radical random chain scission	$7.29 \cdot 10^5$ [h ⁻¹]	96.0

Table 2.3 Kinetic parameters estimations: pre-exponential factor k° and activation energy E_A

Pre-exponential factor of propagation constant is in good agreement with the value reported by Yu [29], while its activation energy is almost equal to the values reported by Witzke et al. [32] and by Safrit et al. [45].

Although at 200°C experimental data show that degradation of the polymer occurs in less than 2 hours (Fig. 2.27 and 2.28), model previsions show that more time is needed before degradation starts. Thus the optimization procedure used in this work, led to underestimation of k_{de} . This underestimation regards the value of pre-exponential factor while activation energy is in good agreement with literature values [29], [44], [45].

CHAPTER 3

Batch Reactor modeling

3.1 Introduction

In this Chapter the developing of a complete Batch reactor is described. The developed model is based on *Biofabris* pilot plant used by Linan et al. [47] for PMMA (Poly-methyl-methacrylate) synthesis. This reactor configuration was taken as the reference one for the model.

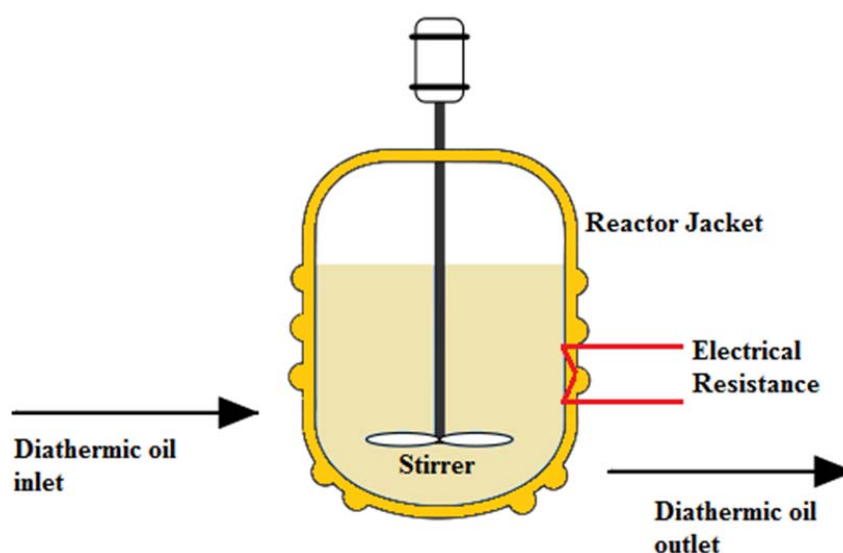


Fig. 3.1 Reactor configuration

The reactor is a stirred reactor, which works at atmospheric pressure. As polymerization is an exothermic process, a cooling system is needed in order to take off reaction heat. Since reference reactor used in this work is used for solution polymerization of PMMA, its operating temperature is around 70°C [50]. This temperature is well below the minimum temperature at which it was observed a significant polymerization (140°C). For this reason some original parameters of the

reactor were changed in order to meet operating conditions of bulk melt ROP of L-Lactide. Two main parameters were changed:

- Water was substituted with diathermic oil as cooling media (since reaction temperature ranges from 140°C to 200°C),
- Electrical resistance maximum power was changed from 500[W] to 20[kW] in order to reach higher temperature of the oil in the jacket.

The reactor has a cooling jacket in which diathermic oil is fluxed. Since this oil is pumped to the jacket at room temperature (which is well above its pour point that is - 24°C [56]), an electrical resistance is installed in the jacket, in order to maintain oil temperature at the desired value. Jacket temperature is modulated by varying a normalized signal (from 0 to 1) of electrical power. When a signal of 0 is applied, no electrical power is supplied to the jacket, while when a signal of 1 is applied, the maximum one is supplied. Geometric features and operating parameters of the reference reactor are reported in Table 3.1.

Parameter	Symbol	Value	U.O.M
Stirrer diameter	d_s	184	[mm]
Stirrer speed	N_R	500	[rpm]
Internal reactor diameter	D_i	266.1	[mm]
Reactor thickness	t_r	5	[mm]
Reactor height	h_r	260	[mm]
Jacket volume	V_j	5.44	[l]
Jacket diameter	D_j	315.9	[mm]

Table 3.1 Reactor parameters

Using this reference reactor a complete mathematical model of a Batch reactor for PLA production was developed. This model results in a ODE system of 15 differential equations and it has been implemented in C++ environment. *BzzOdeNonStiff* class, from *BzzMath*© [27], was used to solve the model. This model is able to predict dynamic evolution of χ , Mn, Mw, reactor temperature (T), liquid level (h) and jacket temperature (T_j).

3.2 Isothermal model

The isothermal model described in Chapter 2 (Eq. [2.14] to [2.16] and Eq. [2.43] to [2.51]) was solved using *BzzOdeNonStiff* class. Effect of reaction conditions, such as M/C ratio, ROH/C ratio, acid to catalyst ratio (A/C) and polymerization temperature (T) on reactor performances (χ reached) and PLA properties (Mw and Mn) were investigated.

3.2.1 ROH/C effect

As reported by Yu et al. [30,31] and by Zhang et al. [48] activation step of ROP of L-Lactide proceeds via tin(II) alkoxide formation. Any OH-bearing specie, present in the reactor can react with Sn(Oct)₂ leading to the formation of the true initiator of ROP. In fact alkoxide opens the monomeric ring which can be added by a growing chain. For this reason increasing the amount of cocatalyst (ROH) in the reactor leads to higher conversions as Sn(Oct)₂ is converted to its active form (alkoxide).

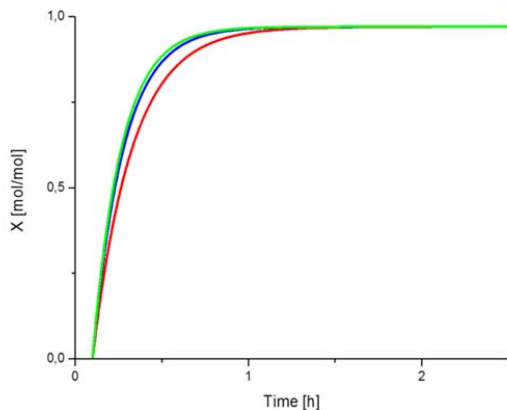


Fig. 3.2 χ vs time. T=180°C, M/C=6000
ROH/C=4 (-), ROH/C=10 (-), ROH/C=15 (-)

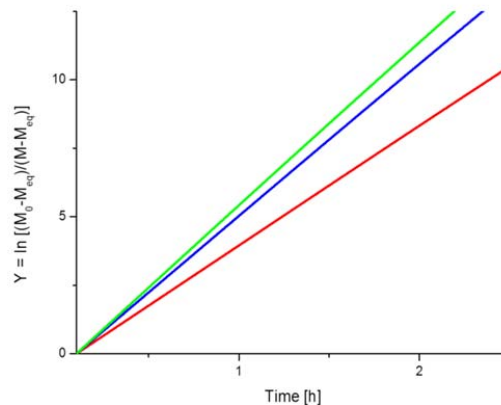


Fig. 3.3 Y vs time. T=180°C, M/C=6000
ROH/C=4 (-), ROH/C=10 (-), ROH/C=15 (-)

In Fig. 3.3 is reported the logarithm of normalized conversion, Y defined in Chapter 2 by Eq. [2.1]. As can be seen this variable shows a linear trend with time, indicating that the model is able to predict the living behavior typical of ROP of L-Lactide for most of polymerization time [29]. Either Fig. 3.2 or Fig. 3.3 show that the effect of an increasing of initial amount of 1-dodecanol in the reactor, leads to higher conversions, as Sn(Oct)₂ is converted to alkoxide more rapidly.

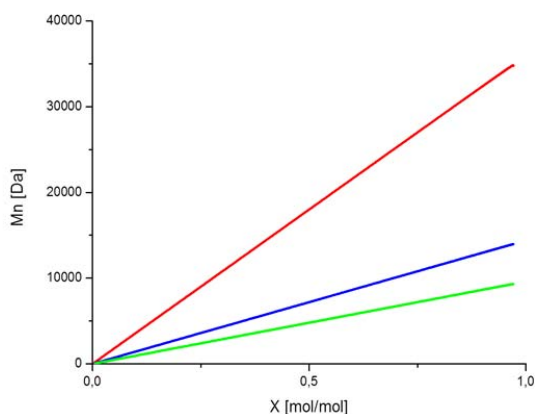


Fig. 3.4 Mn vs χ . T=180°C, M/C=6000
ROH/C=4 (—), ROH/C=10 (—), ROH/C=15 (—)

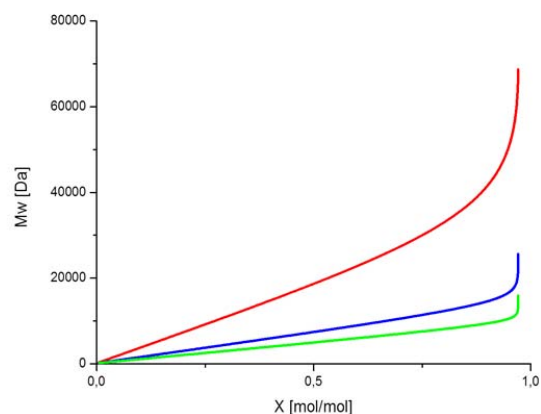


Fig. 3.5 Mw vs χ . T=180°C, M/C=6000
ROH/C=4 (—), ROH/C=10 (—), ROH/C=15 (—)

As can be seen in Fig. 3.4 Mn shows a linear trend with conversion χ , in agreement with Eq. [2.2] reported in Chapter 2. This is another evidence that the model is able to simulate the living behavior of ROP of L-Lactide. Mw shows a linear trend with χ , until high values of conversion are reached. Then the presence of transesterification reactions leads to a non-linear increasing of Mw with χ (Fig. 3.5). Fig. 3.4 and 3.5 a decreasing of Mn and Mw with increasing amount of cocatalyst can be observed. At large amount of cocatalyst chain transfer reactions lead to the presence of a huge amount of dormant chains (containing hydroxyl groups) which reduce the value of Mw and Mn reached at equilibrium. As reported in Yu's PhD dissertation [29] there's a limit value of ROH/C ratio at which further amounts of cocatalyst don't affect any more dynamic of conversion. This limit condition is reached at ROH/C values of 20.

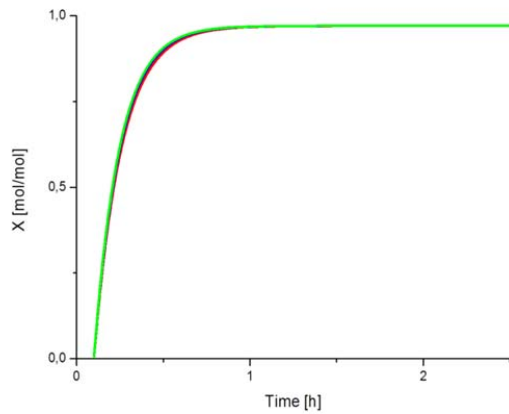


Fig. 3.6 χ vs time. $T=180^{\circ}\text{C}$, $M/C=6000$
 $\text{ROH}/C=20$ (—), $\text{ROH}/C=30$ (—), $\text{ROH}/C=40$ (—)

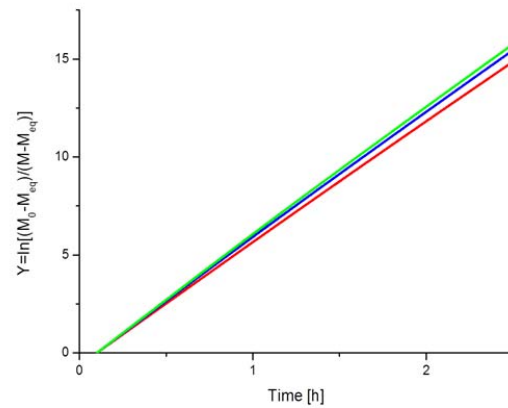


Fig. 3.7 χ vs time. $T=180^{\circ}\text{C}$, $M/C=6000$
 $\text{ROH}/C=20$ (—), $\text{ROH}/C=30$ (—), $\text{ROH}/C=40$ (—)

As can be seen in Fig. 3.6 and 3.7 the three curves of χ and Y overlap each other, indicating that ROH/C ratio higher than 20 doesn't affect significantly monomer conversion evolution in the reactor. Actually in Fig. 3.2 and 3.3 it can be seen that also ROH/C values higher than 10 don't significantly change the dynamic of χ and Y , indicating that the model used in this work reached the limit condition at ROH/C values of 10.

3.2.2 M/C effect

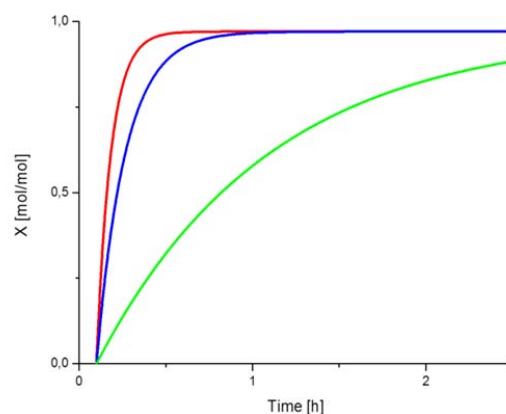


Fig. 3.8 χ vs time. $T=180^{\circ}\text{C}$, $\text{ROH}/C=15$
 $M/C=500$ (—), $M/C=1000$ (—), $M/C=6000$ (—)

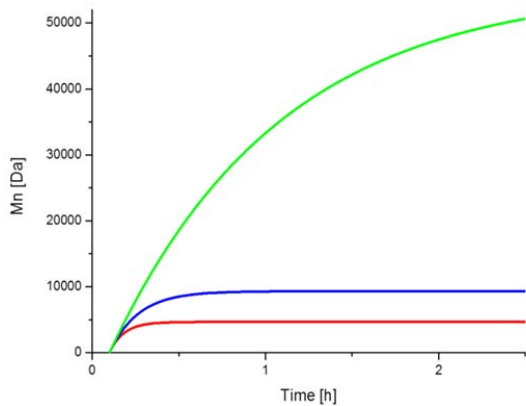


Fig. 3.9 Mn vs time. T=180°C, ROH/C=15
M/C=500 (—), M/C=1000 (—), M/C=6000 (—)

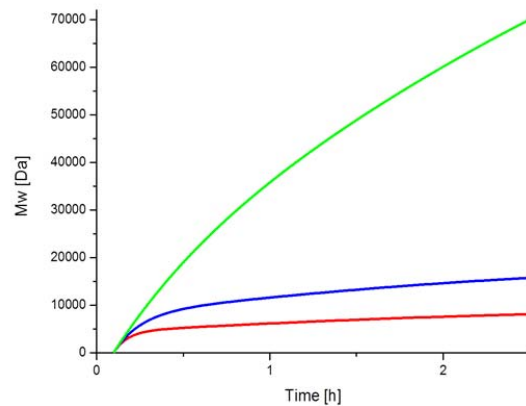


Fig. 3.10 Mw vs time. T=180°C, ROH/C=15
M/C=500 (—), M/C=1000 (—), M/C=6000 (—)

Obviously increasing M/C ratio leads to higher Mn and Mw, as higher amounts of L-Lactide is present in the reactor. Although fewer catalyst is available for ROP and a small number of active chains grows, limiting the conversion reached in the reactor.

3.2.3 A/C Effect

As reported by Zhang et al. [48] either hydroxyl or carboxyl impurities influence PLA molecular weight and conversion. Both types of impurities reduce Mn and Mw of PLA. Although, while hydroxyl impurities speed up activation step leading to higher χ , carboxyl impurities inhibit it leading to lower χ . The effect of carboxyl impurities can be taken into account by setting the initial amount of octanoic acid A, equal to the amount of carboxyl impurities in the reactor.

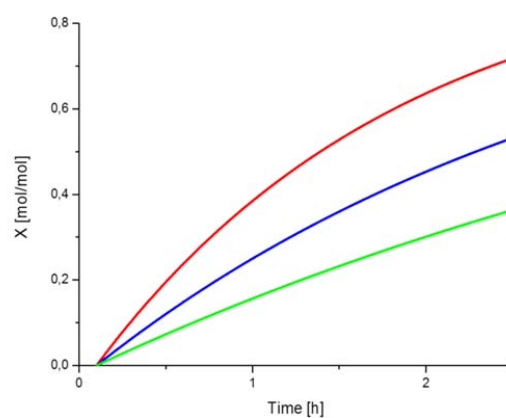


Fig. 3.11 χ vs time. T=180°C, M/C=6000, ROH/C=15. A/C=4 (—), A/C=10 (—), A/C=20 (—)

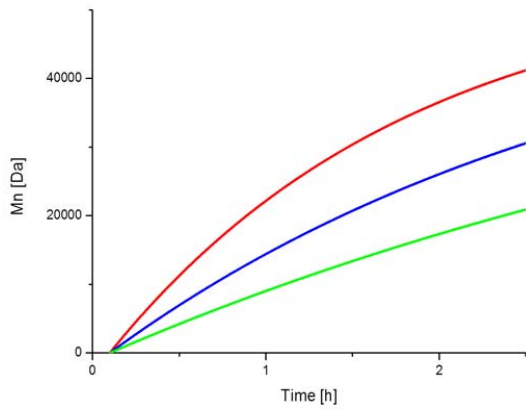


Fig. 3.12 Mn vs time. T=180°C, M/C=6000
ROH/C=15 A/C=4 (—), A/C=10 (—), A/C=20 (—)

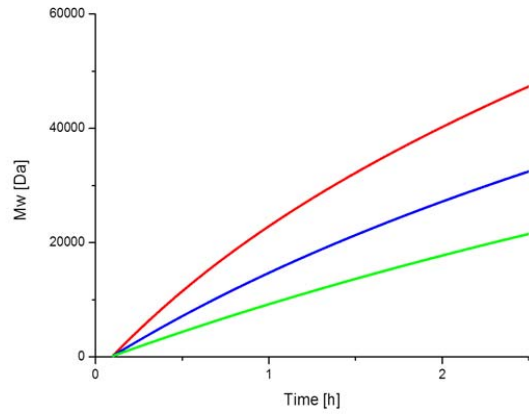


Fig. 3.13 Mw vs time. T=180°C, M/C=6000,
ROH/C=15, A/C=4 (—), A/C=10 (—), A/C=20 (—)

3.2.4 Temperature Effect

The range of temperatures in which the isothermal model described in Chapter 2 was validated, goes from 140°C to 200°C. 140°C is the minimum temperature at which a significant production of PLA was observed with experiments.

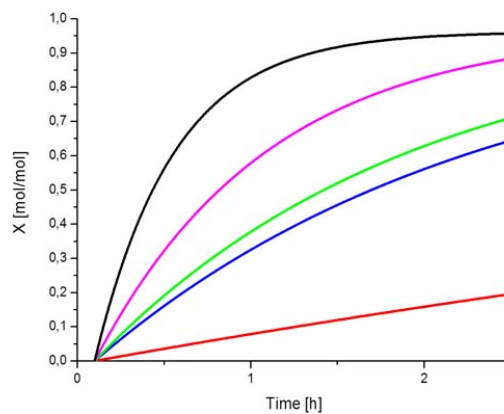


Fig. 3.14 χ vs time. M/C=6000, ROH/C=15
T=140°C (—), T=160°C (—), T=170°C (—), T=180°C (—), T=200°C (—)

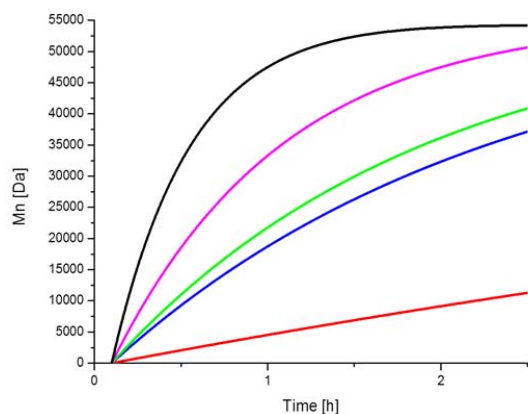


Fig. 3.15 Mn vs time. M/C=6000, ROH/C=15
T=140°C (-), T=160°C (-), T=170°C (-),
T=180°C (-), T=200°C (-)

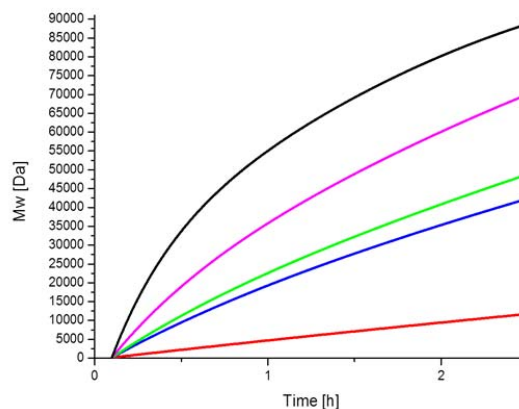


Fig. 3.16 Mw vs time. M/C=6000, ROH/C=15
T=140°C (-), T=160°C (-), T=170°C (-),
T=180°C (-), T=200°C (-)

Low polymerization temperatures lead to low reaction rates. In particular, low propagation rates lead to lower χ , Mn and Mw in 2.5[h] polymerization time. Furthermore the increasing of transesterification rates with temperature leads to broader MWD at higher temperatures (i.e. 180°C and 200°C), while narrower MWD is obtained at lower temperatures (i.e. 140°C). At low polymerization temperature Mn, Mw and χ show linear trends with time. As polymerization temperature increases these variables start to show the dynamic trend typical of first-order systems. These variables eventually reach an asymptotic (equilibrium) value. Actually this is true for conversion only. If higher polymerization times are used, degradation reactions can occur leading to a decreasing of Mn and Mw after having reached a maximum value. Although maximum polymerization time was always set equal to 2.5[h] (lower than the characteristic time of solidification observed by Yu et al. [30]) for the simulations carried out in this work, in order to avoid PLA solidification during reaction and consequent loss of validity of the model.

3.3 Adiabatic model

In order to represent in more detail the physics of ROP of L-Lactide a complete Batch reactor model was developed. Modeling procedure followed several steps; at each step more details were added to reactor model. The first step of this procedure involved the implementation of reactor energy balance, in order to describe temperature evolution during PLA polymerization. Therefore an adiabatic model of PLA Batch reactor was developed. As a Batch reactor is a closed system, the energy balance is equal to an internal energy balance.

$$\frac{dE}{dt} = \frac{dU}{dt} \quad [3.1]$$

Where E is the total energy of the reactor and U its internal energy. Since PLA polymerization occurs in a single liquid phase, pumping work in internal energy can be neglected as liquids are incompressible fluids.

$$\frac{dU}{dt} \approx \frac{dH}{dt} \quad [3.2]$$

Where H represents reactor enthalpy. Therefore energy balance can be expressed as an enthalpy balance on reactor. For an adiabatic Batch reactor enthalpy balance is expressed as:

$$m_{TOT}C_p \frac{dT}{dt} = \sum_1^{N_r} (-\Delta H_{r,j})r_j(T, C_j) V_r \quad [3.3]$$

Where m_{TOT} is the whole reaction mass, C_p is specific heat of reaction mixture (which is assumed constant with temperature), $\Delta H_{r,j}$ is the reaction enthalpy of the j th reaction, r_j is

the reaction rate of the j th reaction (which is a function of T and concentration C_j of reactants involved by the reaction) and V_r is reaction volume. In almost all polymerization reactors' models, only propagation reaction heat is considered in the energy balance [50,57]. In this work two reaction contributions have been considered in the energy balance: propagation and activation.

$$m_{\text{TOT}}C_p \frac{dT}{dt} = [(-\Delta H_{r,a})r_a + (-\Delta H_{r,p})r_p]V_r \quad [3.4]$$

Where r_a is activation rate and r_p , propagation rate.

$$r_a = k_{a1}(T)C\mu_0 - k_{a2}(T)A\lambda_0 \quad [3.5]$$

$$r_p = k_p(T)M\lambda_0 - k_d(T)\lambda_0 \quad [3.6]$$

Activation reaction is an endothermic reaction, while propagation is obviously an exothermic one. As ROP of L-Lactide shows a living behavior for most of the polymerization time, the total number of active and dormant chains remains constant during polymerization. Thus, activation rate reaches equilibrium conditions in short times and its contribution to reactor energy balance is zero for almost the whole polymerization time. Since reactor model doesn't refer any more to an isothermal model, reaction volume will vary during time. In order to evaluate this variation during time, a global material balance, expressed in terms of volumes, has been added to the model. Total reaction volume is equal to:

$$V_r(t) = V_{\text{mon}}(t, T) + V_{\text{cat}}(t) + V_{\text{CoCat}}(t) + V_{\text{Acid}}(t) + V_{\text{PLA}}(t, T) \quad [3.7]$$

Where V_{mon} is monomer volume, V_{cat} is catalyst volume, V_{CoCat} is cocatalyst volume, V_{Acid} is octanoic acid volume and V_{PLA} is PLA volume. Since catalyst and cocatalyst are

added in catalytic quantities to the reactor, their contributions to volume changing is lower than the one of L-Lactide and PLA. For this reason catalyst, cocatalyst and octanoic acid densities were assumed constant with temperature. Rewriting species volumes as the ratio between mass and density and, when applying differential operator, substituting mass balances of species, Eq. [3.8] is derived.

$$\frac{dV_r}{dt} = \left(\frac{r_{\text{mon}}}{\rho_{\text{mon}}(T)} - \frac{M V_r M_{\text{mon}}}{\rho_{\text{mon}}^2(T)} \frac{d\rho_{\text{mon}}}{dT} \frac{dT}{dt} + \frac{r_{\text{cat}}}{\rho_{\text{cat}}} + \frac{r_{\text{CoCat}}}{\rho_{\text{CoCat}}} + \frac{r_{\text{Acid}}}{\rho_{\text{Acid}}} \right) \left(1 - \frac{1}{\rho_{\text{PLA}}(T)} \right) - \frac{m_{\text{TOT}} - (M M_{\text{mon}} + C M_{\text{cat}} + \text{ROH} M_{\text{CoCat}} + A M_{\text{Acid}}) V_r}{\rho_{\text{PLA}}^2(T)} \frac{d\rho_{\text{PLA}}}{dT} \frac{dT}{dt} \quad [3.8]$$

Where r_{mon} , r_{cat} , r_{CoCat} and r_{Acid} are global rate of formation of monomer, catalyst, cocatalyst and acid, respectively.

$$r_{\text{mon}} = -r_p \quad [3.9]$$

$$r_{\text{cat}} = -r_a \quad [3.10]$$

$$r_{\text{CoCat}} = k_{a2} A \lambda_0 - k_{a1} C \mu_0 \quad [3.11]$$

$$r_{\text{Acid}} = r_a \quad [3.12]$$

Physical parameters used in Eq. [3.8] are reported in Table 3.2.

Parameter	Symbol	Value	U.O.M
Lactide molecular weight	M_{mon}	144.13	[g/mol]
Sn(Oct) ₂ molecular weight	M_{cat}	405.1	[g/mol]
1-dodecanol molecular weight	M_{CoCat}	186.34	[g/mol]
Octanoic acid molecular weight	M_{Acid}	144.22	[g/mol]
Lactide density	ρ_{mon}	Eq. [2.11]	[g/l]
Sn(Oct) ₂ density	ρ_{cat}	1200	[g/l]
1-dodecanol density	ρ_{CoCat}	820	[g/l]
Octanoic acid density	ρ_{Acid}	908.8	[g/l]
PLA density	ρ_{PLA}	Eq. [2.11]	[g/l]
Reaction mixture specific heat	C_p	2.06	[kJ/(kg °C)]

Table 3.2 Physical parameters of reaction mixture

Densities of Sn(Oct)₂, 1-dodecanol and octanoic acid were taken from material safety data sheet provided by Sigma Aldrich. As can be seen from Table 3.2 PLA density was set equal to L-Lactide density, thus neglecting any shrinking effect, due to polymer production. Although this is not true, since PLA density is obviously higher than the monomer one, ROP of L-Lactide is not affected by the so called *gel effect*. This effect, which is typical of radical polymerization like PMMA polymerization [50], leads to a slowing down of termination reactions when high molecular weights (so high chain lengths) are reached and a consequent increasing of radical chains. This radical chains increasing in the reactor, leads to an increasing of irreversible propagation rate with consequent uncontrolled release of reaction heat. Thus, the reactor can go in runaway conditions. Since this event could result in a reactor explosion, all models regarding radical polymerization take into account the shrinking effect due to polymer production. Since ROP of L-Lactide isn't characterized by the presence of irreversible termination and propagation, *gel effect* doesn't occur in the polymerization system studied. For this reason shrinking effect, due to polymer formation has a lesser effect on PLA polymerization. Obviously, if diffusional limitations have to be described by the model the simplifying assumption used in this work must be removed and a more precise correlation for PLA density has to be used. Specific heat of reaction mixture C_p has been assumed constant with temperature and equal to specific heat of monomer. This value was calculated using experimental data obtained by Kulagina et al. [49]. In this work specific heat of liquid DL-Lactide was measured by calorimetric analysis in a temperature range from 397[K] to 430[K]. The value of C_p reported in Table 3.2 was calculated as average value of data obtained in [52]. Since reaction volume is no more constant during polymerization, material balances presented in Chapter 2 must be modified. A dilution term has been added to material and moments balances (from Eq. [2.14] to [2.16] and from Eq. [2.43] to [2.51]).

$$\frac{dC_i}{dt} = r_i - \frac{C_i}{V_r} \frac{dV_r}{dt} \quad [3.13]$$

Where C_i represents the concentration of the generic specie i and r_i its global rate of formation. Modified material and moments balances, along with reactor energy balance and total volume balance form an ODE system of 14 differential equations. This ODE system represents the mathematical model of a Batch adiabatic reactor, used for PLA production through bulk melt ROP of L-Lactide. For the simulation of the adiabatic

reactor model, initial reaction temperature has been set equal to 140°C, which is the lower boundary for the validity of the kinetic model described in Chapter 2. M/C and ROH/C ratios have been set equal to 6000 and 15 respectively. Initial amount of L-Lactide has been calculated, taking into account that the minimum load needed by the reactor described in section 3.1 to make the stirrer working, is equal to 70% of reactor total capacity. Approximating reactor geometry to a cylindrical one (as the heights of dished bottoms can be neglected) initial volume of monomer is calculated as:

$$V^{\circ}_{\text{mon}} = 0.7 \frac{\pi D_i^2}{4} h_r \quad [3.14]$$

Through monomer density and monomer molecular weight, it's possible to find the initial amount of monomer in moles. By knowing this value, initial amounts of catalyst and cocatalyst are derived from M/C and ROH/C ratios.

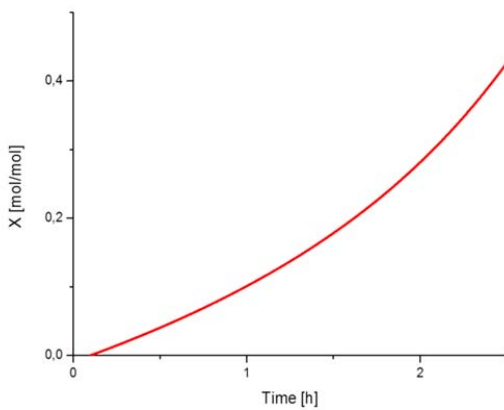


Fig. 3.17 χ vs time. Adiabatic model

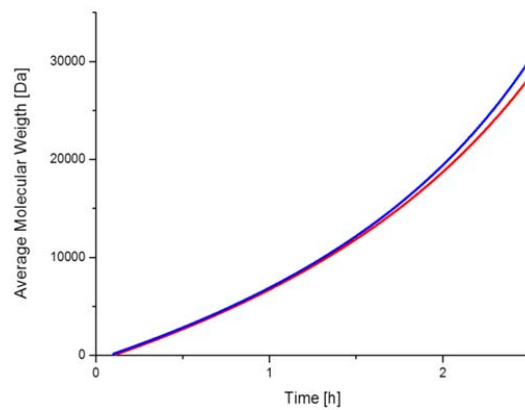


Fig. 3.18 (-)Mn, (-) Mw vs time. Adiabatic model

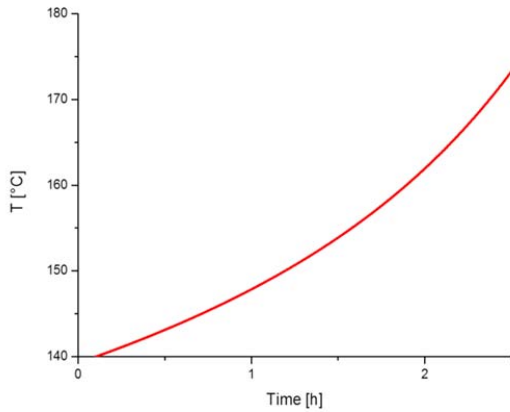


Fig. 3.19 T vs time. Adiabatic model

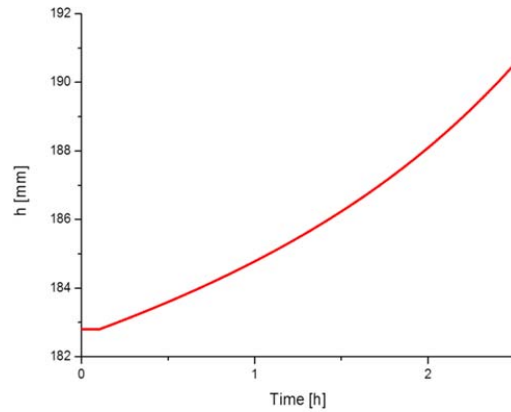


Fig. 3.20 h vs time. Adiabatic model

As can be seen from the diagrams reported above the reactor can't operate in adiabatic conditions. Since heat release from polymerization reaction is rather low, reaction rates reached in the system are low and don't even lead to equilibrium conditions. In fact all the curves monotonically increase with time in 2.5[h]. Slow system dynamics result in low χ (around 43%), M_n and M_w (both around 30,000 [Da]). Furthermore low transesterification rates lead to narrow MWD as can be seen in Fig. 3.18, in which the curves regarding M_w and M_n overlap each other. In Fig. 3.20 is reported the dynamic trend of liquid level (h) with time. Liquid level is function of time through reaction volume.

$$h(t) = \frac{4V_r(t)}{\pi D_i^2} \quad [3.15]$$

As no shrinking effect is considered ($\rho_{PLA} = \rho_{mon}$), reaction volume and liquid level have the same trend of reactor temperature. One difference between the trends assumed by process variables in the adiabatic model with the trends assumed in the isothermal model is the initial concavity. In isothermal model process variables show a downward concavity in their trends, which is typical of first-order systems. In adiabatic model, process variables show an upward concavity in their trends. If all variables reached equilibrium conditions in 2.5[h], they would show sigmoid trends, which are typical of

second-order systems. As reactor can't operate in adiabatic conditions an external heat exchange system must be provided to the reactor, in order to lead the system from starting reaction temperature (140°C) to desired reaction temperature and remove reaction heat at this temperature.

3.4 Open loop model

A complete model of a Batch reactor for bulk melt ROP of L-Lactide was derived from the model described in the previous section, by adding an heat transfer term to reactor energy balance and an energy balance on reactor jacket.

Eq. [3.4] becomes:

$$m_{TOT} C_p \frac{dT}{dt} = [(-\Delta H_{r,a}) r_a + (-\Delta H_{r,p}) r_p] V_r + U A (T_j - T) \quad [3.16]$$

Where U is the overall heat transfer coefficient, A is reactor exchange surface and T_j is jacket temperature.

Reactor exchange surface has been assumed equal to the wet surface of the reactor.

$$A(t) = \pi D_i h(t) \quad [3.17]$$

Reactor energy balance is function of another process variable: jacket temperature. For this reason an energy balance on reactor jacket must be added to the model. The jacket is modeled as a CSTR with no reaction. A simplifying assumption of completely full jacket was made; thus mathematical model of the jacket results in a single equation of energy balance.

$$\rho_{oil} V_j C_{p,oil} \frac{dT_j}{dt} = Q_{oil} \rho_{oil} C_{p,oil} (T_j^o - T_j) + U A (T - T_j) + pS P_e \quad [3.18]$$

Where ρ_{oil} , $C_{p,oil}$ and Q_{oil} are oil density, specific heat and volumetric flow, respectively. P_e represents the heat provided by the electrical resistance installed in the jacket, which has a maximum value of 20[kW]. Normalized power signal is indicated with pS. As can be observed, both balances (Eq. [3.17] and [3.18]) depend on overall heat transfer coefficient U . This parameter depends on fluid dynamics of reactor and jacket. Therefore a proper theory has to be used in order to evaluate U in the model.

3.4.1 Overall heat transfer coefficient evaluation

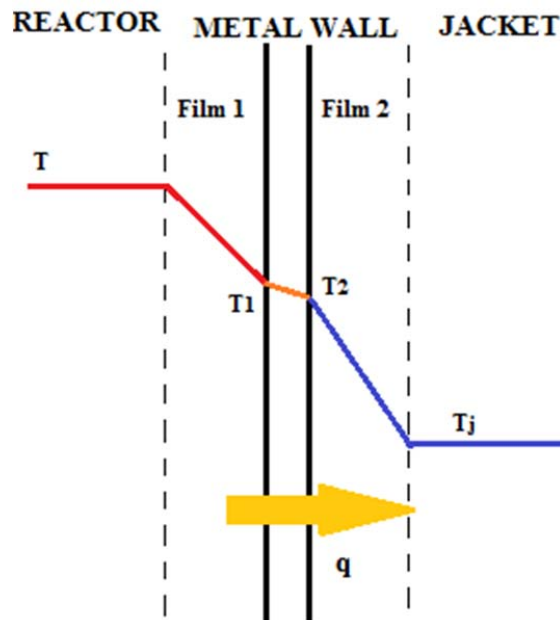


Fig. 3.21 Thermal resistances encountered by heat flux q

The highest temperature gradients in the reactor and in the jacket are concentrated in two thin liquid films (respectively Film 1 and Film 2, showed in Fig. 3.21) next to reactor wall. Exchanged heat is transferred from reactor to jacket by convection through Film 1 and Film 2 and conduction through reactor wall.

Heat flux passing through Film 1 is:

$$q_1 = h_i(T - T_1) \quad [3.19]$$

Where h_i is the laminar heat transfer coefficient of the reaction mixture and T_1 the internal wall temperature. Heat flux passing through reactor wall is:

$$q_2 = \frac{k_s}{t_r} (T_1 - T_2) \quad [3.20]$$

Where k_s is thermal conductivity of reactor wall and T_2 the external wall temperature. Heat flux passing through Film 2 is:

$$q_3 = h_e (T_2 - T_j) \quad [3.21]$$

Where h_e is the laminar heat transfer coefficient of diathermic oil. Assuming stationary conditions for heat fluxes leads to: $q_1 = q_2 = q_3 = q$. Therefore the heat flux going from reaction mixture to diathermic oil in the jacket can be expressed as the product of the whole temperature difference between reactor and jacket, with an overall heat transfer coefficient U .

$$q = U (T - T_j) \quad [3.22]$$

U takes into account all thermal resistances encountered by flux q in its way. As these thermal resistances are in series, U can be calculated as:

$$\frac{1}{U} = \frac{1}{h_i} + \frac{t_r}{k_s} + \frac{1}{h_e} \quad [3.23]$$

Since reference reactor is made of carbon steel, k_s has been set equal to 54 [W/(m² K)], which is the thermal conductivity of this material. Laminar heat transfer coefficients depend on flow conditions in the reactor and in the jacket. In fact h_i and h_e can be expressed as:

$$h_i = \frac{Nu_i k_{mix}}{D_i} \quad [3.24]$$

$$h_e = \frac{Nu_e k_{oil}}{L_j} \quad [3.25]$$

Where Nu_i and Nu_e are Nusselt numbers referred to reaction mixture and diathermic oil respectively. Since Nusselt number depends on Reynolds number, both h_i and h_e depend on flow conditions of the respective systems. Thermal conductivity of reaction mixture and oil are indicated with k_{mix} and k_{oil} . L_j represents the jacket width. Nusselt number is function of flow conditions, through Reynolds number, and thermal properties of the fluid, through Prandtl number. Semi-empiric relationship of Nusselt as function of the other two dimensionless number, is generally given in the form:

$$Nu = a Re^b c Pr^d \quad [3.26]$$

Semi-empiric relationships in the form of Eq. [3.26] were taken from literature. Evaluation of Nu_i was carried out using the correlation reported in [50]:

$$Nu_i = 0.555 Re_i^{0.5875} Pr_i^{0.33} \quad [3.27]$$

For the evaluation of Nu_e the correlation reported in [58] was used:

$$Nu_e = 0.36 Re_e^{0.67} Pr_e^{0.33} \quad [3.28]$$

Expressions of Re and Pr referred to reactor and jacket are reported below.

$$Re_i = \frac{\rho_{mix} N_R d_s^2}{\eta_{mix}} \quad [3.29]$$

$$Pr_i = \frac{\eta_{mix} C_p}{k_{mix}} \quad [3.30]$$

$$Re_e = \frac{\rho_{oil} \left(\frac{Q_{oil}}{A_j} \right) L_j}{\eta_{oil}} \quad [3.31]$$

$$Pr_e = \frac{\eta_{oil} C_{p_{oil}}}{k_{oil}} \quad [3.32]$$

Physical properties of diathermic oil were taken from technical data sheet of *DelcoTerm S Db* a synthetic oil produced by *D.E.L.CO. srl* [56]. This oil has a maximum operating temperature of 350°C, before cracking of the oil starts. Oil viscosity (η_{oil}) and thermal conductivity (k_{oil}) have been evaluated as function of jacket temperature from data reported in [56] at different temperatures.

$$k_{oil} = 0.1488 - 7 * 10^{-5} T_j [K] \left[\frac{W}{m K} \right] \quad [3.33]$$

$$\eta_{oil} = \exp \left(-16.039 + \frac{4434.3}{T_j [K]} \right) [Pa * s] \quad [3.34]$$

Density of reaction mixture have been evaluated with time as:

$$\rho_{\text{mix}} = \frac{m_{\text{TOT}}}{V_r(t)} \quad [3.35]$$

Other parameters used to evaluate Re and Pr number referred to reactor and jacket are reported in Table 3.3.

Parameter	Symbol	Value	U.O.M.	Reference
Oil density	ρ_{oil}	944	[kg/m ³]	[59]
Oil specific heat	C_{poil}	2.025	[kJ/(kg K)]	[59]
Mixture thermal conductivity	k_{mix}	0.289	[W/(m K)]	[60]

Table 3.3 Thermal properties of diathermic oil and reaction mixture

Volumetric flow of diathermic oil (Q_{oil}), pumped to the jacket has been set equal to 130 [l/h]. Interspace between reactor wall and jacket wall (L_j) is 19.9 [mm]; assuming that the oil passes through a circular cross-section with a radius L_j (simplification of reactor geometrical configuration), cross-section of the oil in the jacket can be calculated as:

$$A_j = \pi L_j^2 \quad [3.36]$$

For the evaluation of viscosity of reaction mixture a rheological characterization was done on PLA produced in a laboratory-scale reactor (see Chapter 5).

3.4.1.1 PLA Rheological characterization

Since PLA is a thermoplastic material it shows pseudo-plastic behavior. Thus, apparent viscosity of PLA decreases with an increasing of applied shear rate.

Generally for non-Newtonian fluids, power-law equation [53] is used for the evaluation of apparent viscosity (η).

$$\eta = \eta_0 \gamma^{n-1} \quad [3.37]$$

Where γ is shear rate applied to the polymer melt, n the power index (lower than 1 for pseudo-plastic fluids) and η_0 is defined as zero shear rate. η_0 is generally evaluated as a function of Mw. Dorgan et al. [54] studied melt rheology of variable L-content PLA. They made several rheological measurements on a well-characterized set of PLA homopolymers and copolymers, spanning a wide range of molecular weights (10^5 - 10^6 [Da]) and stereoisomer proportions. A universal equation describing PLA zero shear rate, was evaluated at a reference temperature of 180°C [54]. In the work of Dorgan et al. [54] also critical PLA molecular weight of entanglement was evaluated. This is a limit value of Mw above which, η_0 have an higher increasing with Mw, due to entanglements between polymer chains. Piyamanocha et al. [55] studied the effect of pressure and temperature on rheological behavior of PLA melt, by using capillary rheometer equipped with backpressure device. All the works found in literature refer to PLA melt viscosity. Since viscosity needed in the mathematical model is referred to reaction mixture, rheological characterization of PLA samples produce with lab-scale reactor (see Chapter 5) was carried out. Four samples were analyzed with variable Mw and monomer content, in order to evaluate the evolution of reaction mixture viscosity with time.

Sample	Mw [Da]	L-content [%]
1	37000	70.4
2	50000	14.4
3	68000	22.0
4	70000	4.18

Table 3.4 Samples used for rheological characterization of PLA reaction mixture

PLA samples were analyzed with rotary viscometer (*PSL Systemtechnik HPHT Viscosimeter*). After having melted the sample measurements of PLA viscosity, varying

Shear rate applied by the equipment. Experimental data obtained were fitted using Carreau-Yasuda model.

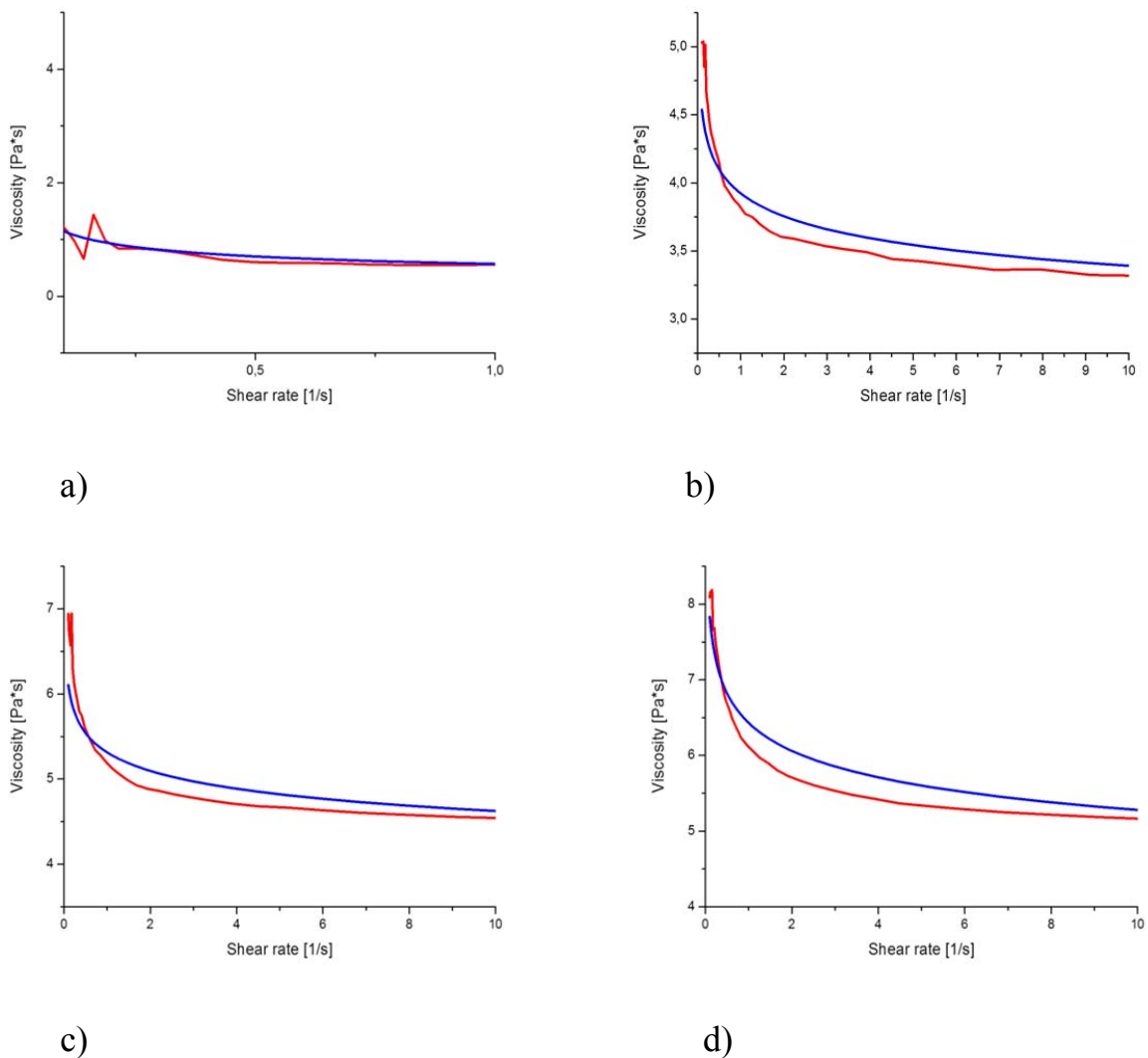


Fig. 3.21 a) Sample 1, b) Sample 2, c) Sample 3, d) Sample 4 (–) Experimental data, (–) Carreau-Yasuda model

As can be seen from Fig. 3.21, except for sample 1, viscosity of reaction mixture follows a pseudo-plastic behavior, since its viscosity decreases with shear rate. Sample 1 (the one containing the higher monomer content and the lower molecular weight PLA) shows Newtonian behavior, as can be seen in Fig. 3.21a. Carreau-Yasuda model is used for evaluating reaction mixture apparent viscosity.

$$\eta = \eta_{\infty} + (\eta_0 - \eta_{\infty})(1 + (\lambda\dot{\gamma})^2)^{\frac{n-1}{2}} \quad [3.38]$$

Where η_{∞} is viscosity at infinite shear rate, λ the polymer relaxation time and n the power index. Eq. [3.38] predict that if the applied shear rate is lower than relaxation rate (inverse of relaxation time), the fluid behaves as a Newtonian fluid ($\eta = \eta_0$). On the other hand, if the applied shear rate is higher than relaxation rate, the fluid behaves as a power-law (non-Newtonian) fluid. Parameters of Carreau-Yasuda equation evaluated by *Haake® Viscotester VT550* software, are reported in Table 3.5.

Sample	η_0 [Pa*s]	η_{∞} [Pa*s]	λ [s]	n [-]
1	6.372	0	2900	0.6970
2	6.615	0	3887	0.9368
3	8.401	0	1965	0.9396
4	11.33	0	740.9	0.9143

Table 3.5 Carreau-Yasuda parameters

As reaction mixture shows pseudo-plastic viscosity, Carreau-Yasuda model (Eq. [3.38]) was chosen for the evaluation of reaction viscosity in the model. Relaxation time and power index of polymeric mixture in the reactor were set constant and equal to average values of samples data ($\lambda = 2373$ [s], $n = 0.8719$). Strain rate applied to reaction mixture in Batch reactor is equal to stirrer speed (N_R). For zero shear viscosity a relationship of this variable with Mw was developed, by fitting data obtained from Carreau-Yasuda with an exponential function.

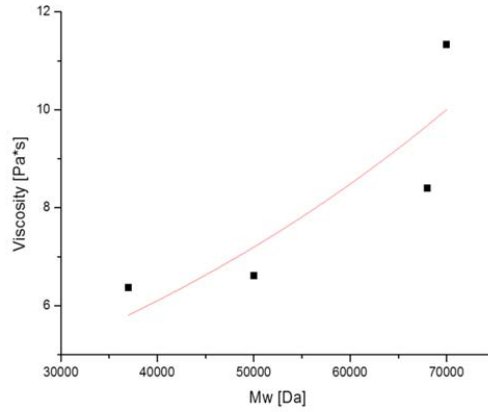


Fig. 3.22 Zero shear viscosity vs Mw. Experimental data fitting

The following equation was found:

$$\eta_0 = 3.585 \exp(1.949 * 10^{-5} Mw[Da]) \text{ [Pa * s]} \quad [3.39]$$

Since Eq. [3.39] was obtained for high molecular weight PLA (Mw higher than 20,000[Da]), another relationship has to be used to evaluate reaction mixture viscosity during the first part of polymerization. As reported by Codari[50] at low Mw, PLA shows Newtonian behavior. Consequently apparent viscosity is equal to zero shear viscosity for low molecular weight PLA. A relationship for low molecular weight PLA viscosity was taken from [50]. This correlation takes into account the variation of η with Mw and reaction temperature (T).

$$\eta = \eta_0 = c_1 Mw[Da]^{c_2} \text{ [Pa * s]} \quad [3.40]$$

$$c_1 = \exp\left(-\frac{8262.7}{T[K]} + 6.4361\right) \quad [3.41]$$

$$c_2 = -1.4 * 10^{-2}T[K] + 7.41 \quad [3.42]$$

If PLA weight molecular weight is lower than 10,000 [Da] (polymerization has produced oligomers), Eq. [3.40] is implemented in the model, while at higher Mw values Eq. [3.38] is used.

3.4.2 Simulation results

Adding Eq. [3.8],[3.16] and [3.18] to isothermal model presented in Chapter 2, a complete model of a Batch reactor of ROP of L-Lactide is derived. This model results in a ODE system of 15 differential equations. This system has been implemented in C++ environment and *BzzOdeNonStiff* class, from *BzzMath*©, has been used to solve it. Initial conditions for the model are:

- Starting polymerization temperature: $T^\circ = 140^\circ\text{C}$;
- $V_r^\circ = 0.7 * V_{\text{REACTOR}}$;
- $M/C = 6000$;
- $\text{ROH}/C = 15$;

These are the same initial conditions used for the adiabatic model described in section 3.3. An additional condition has to be set for jacket temperature. This was set, imposing a minimum temperature difference between oil and reaction mixture of 10°C ($T_j^\circ = 150^\circ\text{C}$) to have heat exchange as polymerization starts. Furthermore as diathermic oil is pumped to the jacket at 25°C , a normalized power signal (pS) of 60% was set for power resistance. This value leads to a stationary jacket temperature of about 191°C .

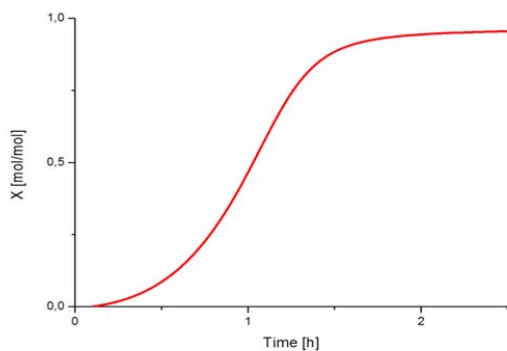


Fig. 3.23 χ vs time. Open loop model

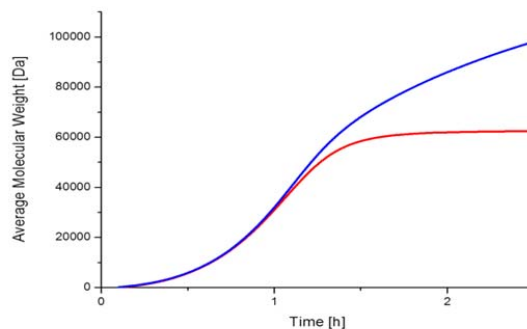


Fig. 3.24 (-)Mn, (-)Mw vs time. Open loop model

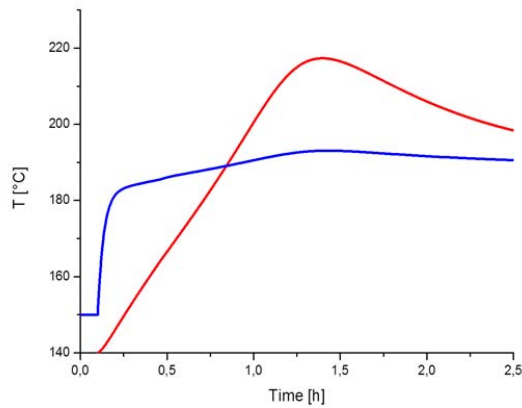


Fig. 3.25 (-)T, (-)T_j vs time. Open loop model

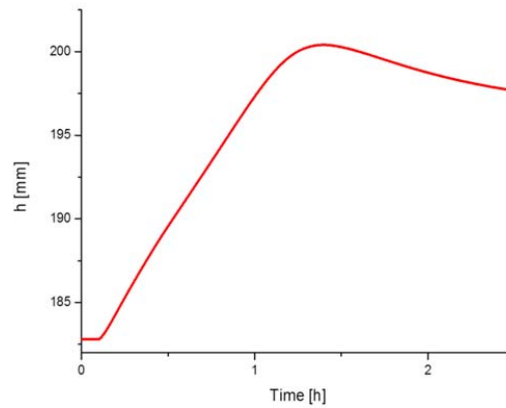


Fig. 3.26 h vs time. Open loop model

As can be seen in Fig. 3.23 and 3.24 χ , Mn and Mw presents a sigmoid trend which is typical of over-damped second order system. Reactor temperature (Red line of Fig. 3.25) shows an initial linear increasing of temperature, in which diathermic oil heats reaction mixture. Once passed jacket temperature, reactor temperature increases in a non-linear way, due to the releasing of reaction heat. Reactor temperature reaches a maximum value of almost 216°C and then starts to decrease, due to the cooling done by diathermic oil. Jacket temperature (Blue line of Fig. 3.25) has an initial first-order dynamic behavior, which is due to the power supplied by the electrical resistance installed in the jacket. The heat of reaction released by polymerization leads jacket temperature to reach a maximum value (around 193°C), more or less in correspondence of maximum reactor temperature (more or less 1.25[h]). Although, jacket temperature maximum is well less marked than reactor temperature one. Liquid level in the reactor follow the same dynamic behavior of temperature, as reaction volume is function only of reaction temperature through Eq. [2.11]. As can be seen from Fig. 3.23 and 3.24, the addition of a heat exchange system leads to higher conversion and Mw reached in 2.5[h] polymerization. Simulation results of the model presented in this Chapter show that final PLA has:

- Mn = 62,407[Da];
- Mw = 98,058[Da];
- L-lactide content (calculated as: $1-\chi$): 4.47%.

CHAPTER 4

Temperature Control

4.1 Introduction

The model presented in Chapter 3 describes PLA production through ROP of L-Lactide in a Batch reactor. PLA produced in this reactor must have appropriate mechanical characteristics, in order to be used as polymeric material for the building of biomedical devices, such as scaffolds for bone-tissue engineering. For this reason a minimum value of PLA molecular weight must be reached in the polymerization process, in order to have desired mechanical characteristics of the final product. Razak et al. [28] reviewed applications of biodegradable materials like PGA, PCL and PLA as polymeric matrix for composite scaffolds made of PLA and hydroxyl-apatite (Calcium-based ceramic material). This composite material mimics the structure of bones; in fact polymeric matrix performs the role of collagen in bones, while hydroxyl-apatite is the chemical state assumed by Calcium in bones. In this work [28] several PLAs, with different Mw, mechanical characteristic and processing methods (hot pressing, extrusion etc.) were reported for composite scaffolds. Minimum Mw value reported in [28] was 100,000 [Da].

For this reason a weight average molecular weight of 100,000[Da], was chosen as process target. Another process target assumed in PLA production process was monomer conversion. The value of this variable was set at 95[%], in order to minimize or even remove PLA purification processes after polymerization. In order to reach process targets a proper control system must be included in the model. Since the model regards a close system (Batch reactor), the only controllable variable for PLA production process is the reactor temperature. This variable is controlled manipulating the power supplied to the jacket, thus the normalized power signal p_S . Set-point conditions must be found for the developing of the control system. Therefore, optimal polymerization temperature has to be evaluated, in order to achieve process targets reported above ($M_w = 100,000$ [Da] and χ higher than 95%).

4.2 Optimal temperature trajectory detection

The final goal of the process is to obtain PLA with a weight average molecular weight of 100,000 [Da] and monomer conversion higher than 95[%]. Since the only controllable variable of the polymerization process is Reactor temperature, an optimal temperature trajectory must be evaluated in order to achieve process targets.

Optimal temperature trajectory detection was carried out using the following numerical procedure.

1) Selection of the optimization time-step

Since a temperature trajectory with time must be evaluated, the problem presented is a dynamic optimization problem. For this reason the polymerization time (set equal to 2[h]) is divided in several time step. In each of this time-step a proper objective function, chosen in order to reach as fast, as possible the desired process targets, is optimized. Since the optimal trajectory estimated with this procedure will be implemented as the set-point trajectory in the closed-loop model, the optimization time-step must be higher than the response time of the system. It was observed that a minimum optimization time-step of 0.5[h] has to be used for set-point changing in the closed-loop model, in order to leave to the system sufficient time to reach set-point temperature.

2) Selection of the objective function

The objective function chosen in this procedure was:

$$f_{\text{obj}} = (\text{Mw}[\text{Da}] - 100,000[\text{Da}])^2 \quad [4.1]$$

This function is called by the Optimization class (*BzzMinimizationMono*) at each time-step in order to evaluate the optimal temperature, in that time-step that leads to the desired Mw as fast, as possible. Monomer conversion was not included in the objective function, since it was seen that high molecular weights were reached at high conversions.

3) Discretization of the isothermal model

Since reactor temperature was the degree of freedom that has to be optimized, the isothermal mathematical model has to be chosen for the evaluation of Mw, used in the objective function. For this reason the same procedure used for the evaluation of kinetic constants from experimental data (see Chapter 2), was implemented for the optimal temperature trajectory detection. The isothermal model was discretized in time and solved, using Euler method. In order to assure either a good accuracy, or convergence of the integration method an integration step of 10^{-5} [h] was chosen. Discretized model was implemented in a function in which objective function showed in Eq. [4.1] was evaluated.

4) Dynamic optimization

The function containing discretized isothermal model and the objective function is called by *BzzMinimizationMono* class in the main program at each optimization time-step, in order to evaluate the optimal condition for that time-interval. Since the optimization procedure is carried out dynamically, the mathematical model is integrated more than one time at each time-step. Once found the optimal temperature in a time-step, results of model integration in that time-step will be initial conditions of the next one. M/C and ROH/C ratios at the beginning of the polymerization ($t=0$ [h]) are set equal to 6000 and 15, respectively.

Thus the mathematical formulation of the optimization problem is:

$$\text{for } t = 0: dt = 0.5[\text{h}]: t = 2[\text{h}]$$

$$\min_{\mathbf{T}} ((Mw - 100,000)^2)$$

$$\text{s. t. } \frac{d\mathbf{y}}{dt} = \mathbf{f}(\mathbf{y}, t)$$

$$\mathbf{y}^{\circ} = \mathbf{y}(t_{i-1})$$

Where \mathbf{y}° represents the initial conditions vector of ODE system which is equal to the output vector found in the former optimization time-step ($\mathbf{y}(t_{i-1})$). Fig. 4.1 shows the optimal temperature trajectory found using kinetic parameters

estimated in this work (see Chapter2) and kinetic parameters reported by Yu [29]. It's important to underline that in both cases optimum research field was limited by upper and lower bound of temperature in which was validated the kinetic model (140°C-200°C, in this work and 130°C-180°C in the work of Yu[29]).

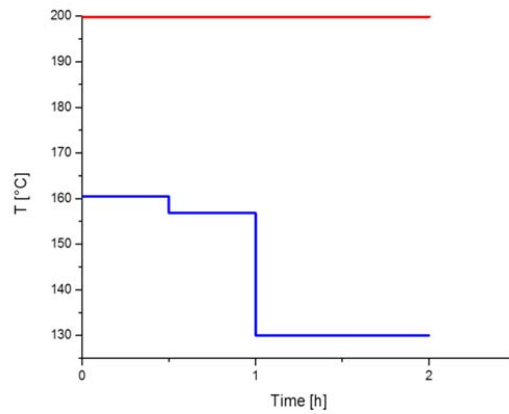


Fig. 4.1

- (-) Optimal trajectory with Yu[29] kinetic constants
- (-) Optimal trajectory with kinetic constants derived in this work

As can be seen in Fig. 4.1 the optimization procedure led to a single temperature value (the maximum one) for the isothermal model based on kinetic constants estimated in this work. Since this procedure led to an optimal temperature trajectory for the isothermal model based on Yu[29] kinetic constants which decreases with time, this isn't due to defects of C++ code used. The main reason for which the numerical procedure used, led to a single temperature of 200°C as optimum trajectory is that degradation constant (k_{de}) estimated in this work is significantly lower than the one reported by Yu[29]. As PLA degradation doesn't occur in 2[h], polymerization temperature is kept to its maximum value in order to achieve higher propagation rate and so higher Mw in less time. Although, as can be seen in Chapter 2, degradation of the polymer occurs in less than 1[h]. Thus, degradation constant is underestimated in this work and optimal temperature trajectory is more likely similar to the one derived with kinetic constants reported in the work of Yu[29].

4.3 PI Temperature Control

Once found the optimal temperature trajectory, this is implemented as set-point trajectory in a Closed-loop model. As already said the only controllable variable in the Batch reactor is reactor temperature. Thus, variables pairing leads to have:

- Reactor temperature T as controlled variable,
- Power signal pS as manipulated variable.

A conventional control, such as a PI (Proportional-integral) control has been implemented in the model. Derivative term was omitted, as it led to incorrect previsions which resulted in instability of system response.

Temperature control law is:

$$pS = pS_{bias} + k_C \left[(T_{sp} - T) + \frac{1}{\tau_I} \int_t^{t+dt} (T_{sp} - T) dt \right] \quad [4.2]$$

Where set-point temperature T_{sp} is equal to 200°C (optimal temperature found with the procedure described in section 4.2), pS_{bias} the bias power signal at which the power of electrical resistance is set, k_C is the proportional gain and τ_I the integral time. This control law is implemented every dt, which represents the control time-step. This time-step was set equal to 10^{-3} [h], thus normalized power signal is manipulated almost every second.

Control parameters used in PI controller are reported in Table 4.1.

Control parameter	Value	U.O.M
pS_{bias}	0.6	[-]
k_C	0.05	[°C ⁻¹]
τ_I	1	[h]

Table 4.1 PI controller parameters

Simulation results of closed-loop model are reported below.

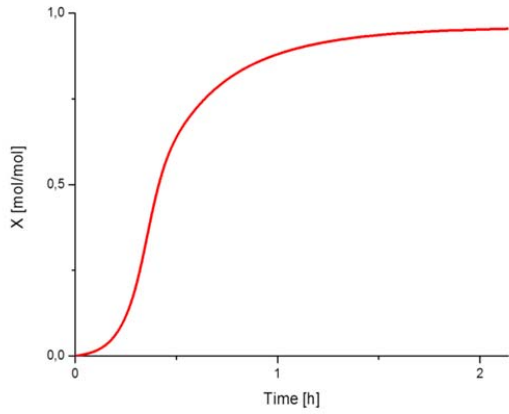


Fig. 4.2 χ vs time. Closed-loop model

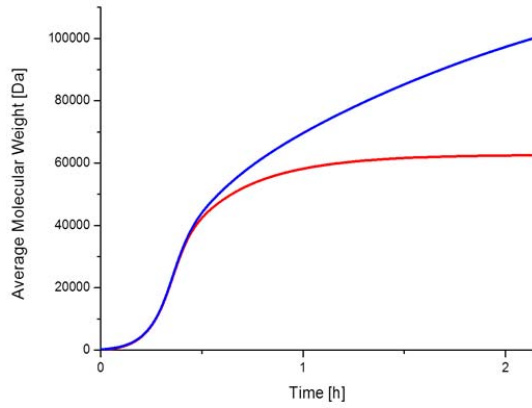


Fig. 4.3 $(-)$ M_n , $(-)$ M_w vs time. Closed-loop model

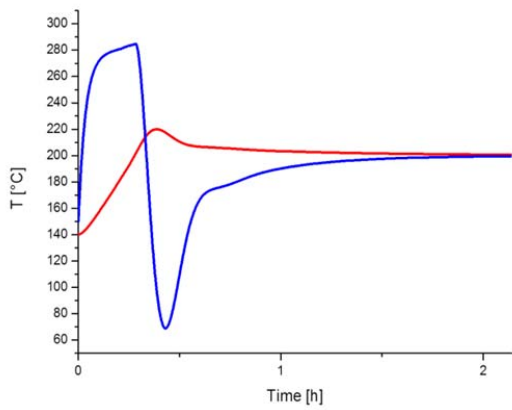


Fig. 4.4 $(-)$ T , $(-)$ T_j vs time. Closed-loop model

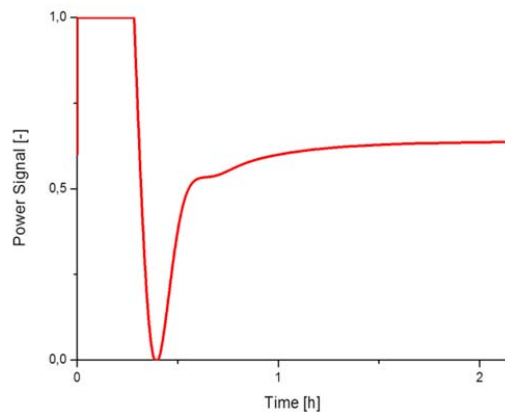


Fig. 4.5 p_S vs time. Closed-loop model

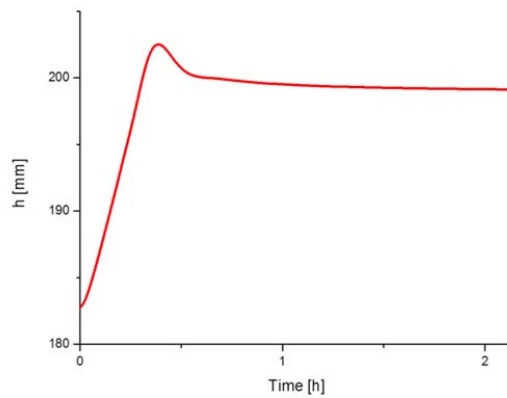


Fig. 4.6 h vs time. Closed-loop model

Control parameters k_C and τ_I were chosen in order to have an over-damped response of reactor temperature, avoiding so oscillations of reactor temperature and normalized power signal. Jacket temperature has a series of first-order responses, due to variation of power signal p_S . In the first part of polymerization, maximum available power is supplied to the jacket leading to an increasing of oil temperature of about 285°C (lower than oil cracking temperature). Then normalized power signal suddenly decreases to 0 and jacket temperature decreases rapidly to about 70°C. This is due to the fact that reaction heat released by polymerization further increases reaction temperature. In order to remove it, jacket temperature decreases until a minimum value which is more or less in correspondence of the maximum value reached by reactor temperature (around 220°C). Then both reactor and jacket temperature reach equilibrium conditions. The asymptotic value reached by the power supplied by electrical resistance to the jacket is 63.65% of the maximum power. Rise time of reactor temperature is equal to 18[min] and total polymerization time needed to satisfy process targets is 2.14[h]. PLA produced in the closed-loop Batch reactor presents the following properties:

- $M_n = 62,496[\text{Da}]$,
- $M_w = 100,014[\text{Da}]$,
- L-Lactide content: 4.54%

4.3 Adaptive Temperature Control

In order to optimize polymerization time (so achieve process targets in less time) an adaptive control system was developed and implemented in the closed-loop model. Control law was maintained in the form of a PID (Proportional-integral-derivative) law. Derivative term was added to control law because PI control law led manipulated variable p_S to assume only its boundary values (0 and 1). The addition of derivative term led to a more reliable dynamic behavior of the normalized power signal p_S . Control logic of the controller system developed is show in Fig. 4.7.

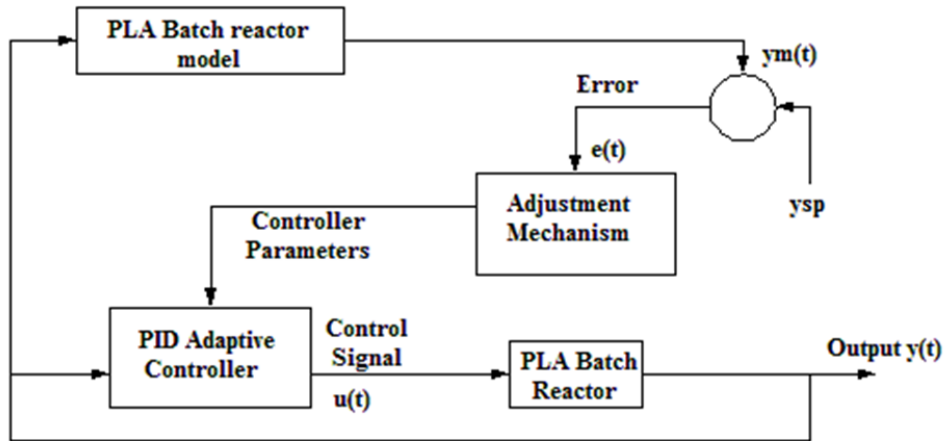


Fig. 4.7 Control loop of Adaptive controller

Output reactor temperature ($y(t)$) is implemented both in controller and in PLA Batch reactor model. With this, model prevision of reactor temperature ($y_m(t)$) is carried out in a certain time-step, which is the time-interval in which control-law is implemented. Difference between set-point temperature and model prevision generates an error signal. This signal is used in a proper objective function which is optimized to find controller parameters (Adjustment mechanism). Thus, the two blocks regarding *PLA Batch reactor model* and *Adjustment mechanism* are linked together in a single block in which an optimization subject to reactor model is carried out. By doing this Controller parameters of PID Adaptive controller are modified with time. The problem related to the research of controller parameters is a dynamic optimization problem and its mathematical formulation can be schematized as:

for $t = 0: dt_{\text{Control}}: t_{\text{poly}}$

$$\min_{k_C, \tau_I, \tau_D} f_{\text{obj}}$$

$$\text{s. t. } \frac{dy}{dt} = \mathbf{f}(\mathbf{y}, t)$$

$$\mathbf{y}^\circ = \mathbf{y}(t_{i-1})$$

Mathematical formulation of this problem is similar to the one of Optimal Temperature Trajectory detection. Objective function used in dynamic optimization is obviously a function of error. This error is calculated not as the difference between output reactor

temperature and set-point temperature, but as the difference between the prevision made by the model and the set-point temperature. Thus, controller parameters estimated are the ones that should lead to a reactor temperature close to the optimal model prevision $y_m(t)$. Two objective functions were implemented in the adaptive controller:

$$f_{\text{obj},1} = \varepsilon^2(t) = \left(T_{\text{sp}} - T(t)\right)^2 \quad [4.3]$$

$$f_{\text{obj},2} = |\varepsilon(t)| = \left|T_{\text{sp}} - T(t)\right| \quad [4.4]$$

Two function were written in C++ code. One function contains the Batch reactor model (open-loop). The other function has the value of the objective function as return value and controller parameters as input values. In this function *BzzOdeNonStiff* class is used to solve the Batch reactor model among with the control law. Once solved the ODE system which constitutes Batch reactor model, objective function is evaluated. These two functions represents the single block formed by *PLA Batch reactor model* and *Adjustment mechanism* blocks in Fig. 4.7. The function containing the objective function is called in the main program by the optimization object generated by *BzzMinimizationRobust* class which optimize the values of controller parameters. Thus, integration of the ODE system is done several times at each control time-step (dt_{control}). Once found optimal controller parameters, these are used to solve the closed-loop model by using *BzzOdeNonStiff* class in the main program. This step of the numerical procedure is represented by the implementation of the control signal generated on manipulated variable ($u(t)$) in the pilot plant. As this procedure involves either integration or optimization problems, the adaptive control system developed has an higher response time than PI controller. For this reason an higher control time-step is used for adaptive control. A control-time step of 10^{-2} [h] (6 [min]) was selected for the implementation of the control law. Control-time steps higher than 10^{-2} [h] lead to a worsening of reactor performances, while control-time steps lower than 10^{-2} [h] lead to higher calculation times for the code. A total polymerization time of 2[h] has been set in the program and optimization of controller parameters, thus implementation of the control law, was done every 10^{-2} [h]. Simulation results of the closed-loop model with adaptive control are reported below.

Objective function used in the optimization: $\epsilon^2(t)$.

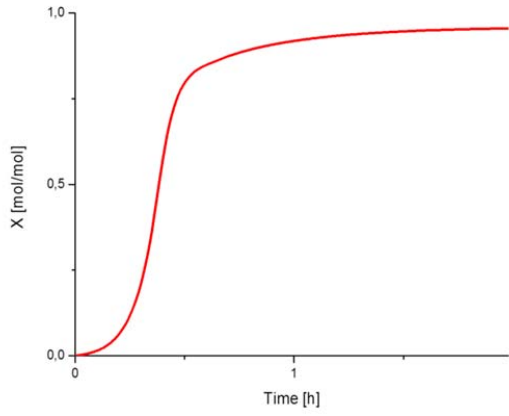


Fig. 4.8 χ vs time. Adaptive Control

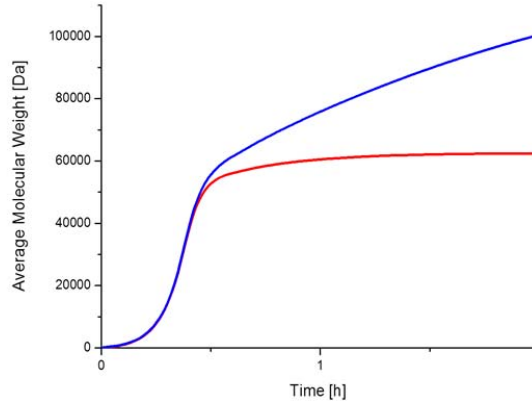


Fig. 4.9 $(-)$ Mn, $(-)$ Mw vs time. Adaptive Control

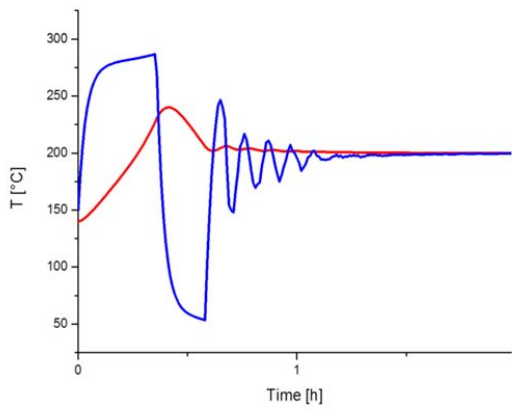


Fig. 4.10 $(-)$ T, $(-)$ T_j vs time. Adaptive Control

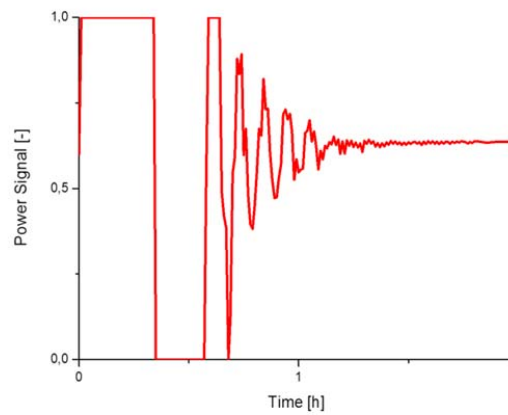


Fig. 4.11 pS vs time. Adaptive Control

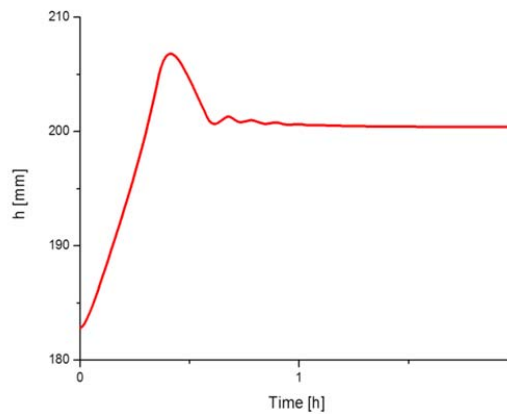


Fig. 4.12 h vs time. Adaptive Control

Objective function used in the optimization: $|\varepsilon(t)|$.

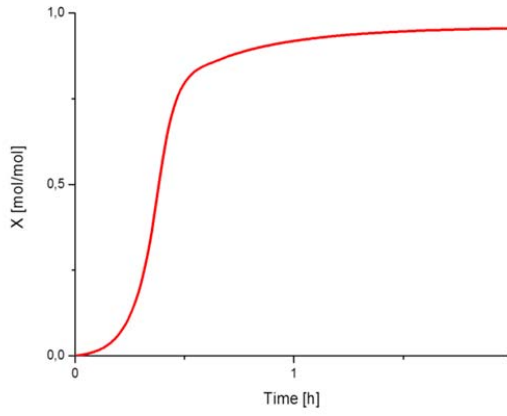


Fig. 4.13 χ vs time. Adaptive Control

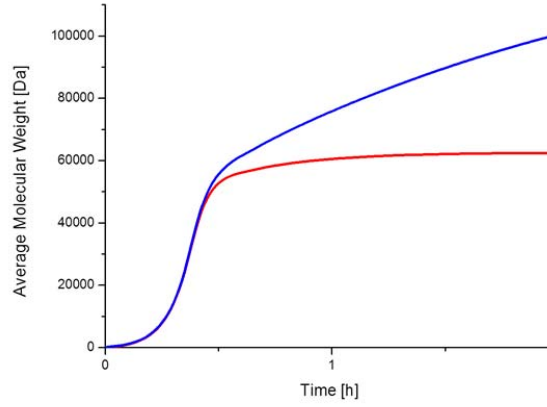


Fig. 4.14 $(-)$ Mn, $(-)$ Mw vs time. Adaptive Control

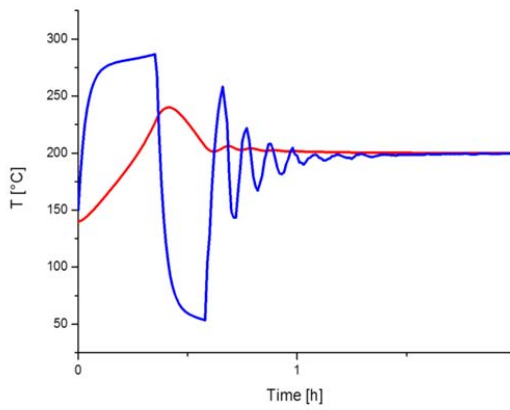


Fig. 4.15 $(-)$ T, $(-)$ T_j vs time. Adaptive Control

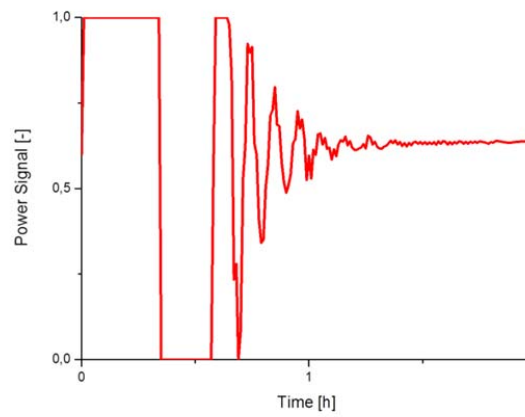


Fig. 4.16 pS vs time. Adaptive Control

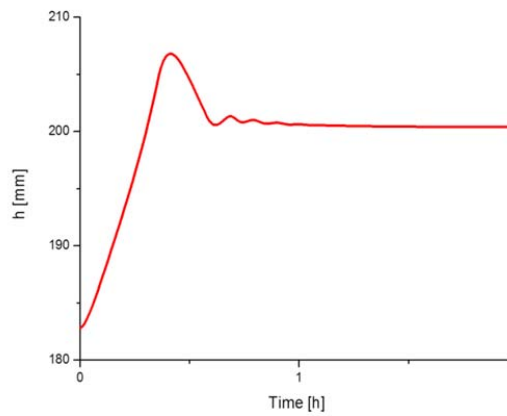


Fig. 4.17 h vs time. Adaptive Control

Implementation of Adaptive temperature control leads reactor temperature response to be under-damped. Since the power supplied by electrical resistance influences directly jacket temperature, the amplitude of jacket temperature oscillations is higher than the one of reactor temperature oscillations. Both objective functions used in the adaptive controller lead to a similar dynamic behavior of the Batch reactor. In both cases maximum temperature reached by reactor (overshoot) is 240°C, while maximum temperature reached by the jacket is 287°C. Minimum temperature reached by the jacket is equal to 54°C, in correspondence of the overshoot related to reactor temperature. Rise time of reactor temperature is equal to 18[min], the same value observed with PI Controller, and polymerization time needed to reach process targets is equal to 1.98[h]. PLA final properties produced in the closed-loop Batch reactor, using an Adaptive Temperature controller are reported below.

Objective function	Mn[Da]	Mw[Da]	L-Lactide content [%]
$\varepsilon^2(t)$	62,443	100,142	4.45
$ \varepsilon(t) $	62,443	100,139	4.45

Table 4.2 PLA final properties obtained, implementing Adaptive temperature control

As can be observed in Table 4.2 both objective functions lead to same PLA properties. A problem of this control system is that the continuous updating of controller parameters leads to excessive oscillations in the manipulated variable pS. For this reason the objective function was modified, adding an anti-ringing term. Since both objective functions chosen lead to the same dynamic behavior, only square of the error was left as objective function in the Adaptive temperature control. The modified objective function implemented in the Adaptive temperature control is:

$$f_{obj} = \varepsilon^2(t) + c |pS_i - pS_{i-1}| \quad [4.5]$$

The second term of Eq. [4.5] is the anti-ringing term, which keeps under control the variation of the manipulated variable between a control action (pS_i) and the previous one (pS_{i-1}). Absolute difference between two control signals in the anti-ringing term, is multiplied for a constant c. This constant was set equal to 10^5 . For c values lower than

10^5 the dynamic behavior of the manipulated variable still shows excessive oscillations, while for values higher than 10^5 no further improvements are observed in the dynamic behavior of the manipulated variable. Simulation results of the closed-loop model, using the new Adaptive control are reported below.

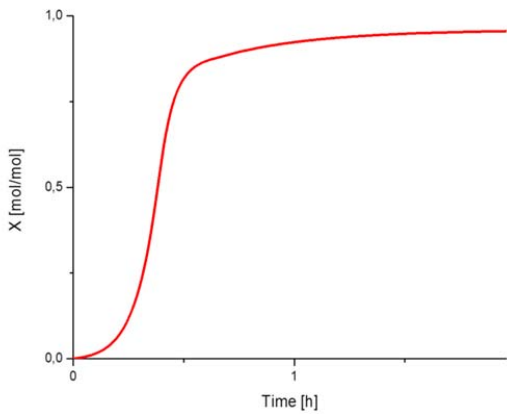


Fig. 4.18 χ vs time. Adaptive Control with anti-ringing term

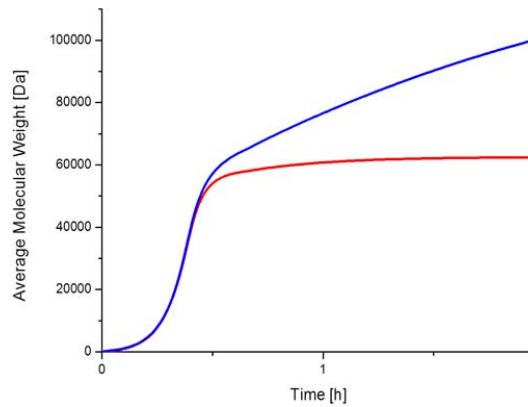


Fig. 4.19 (-)Mn, (-)Mw vs time. Adaptive Control with anti-ringing term

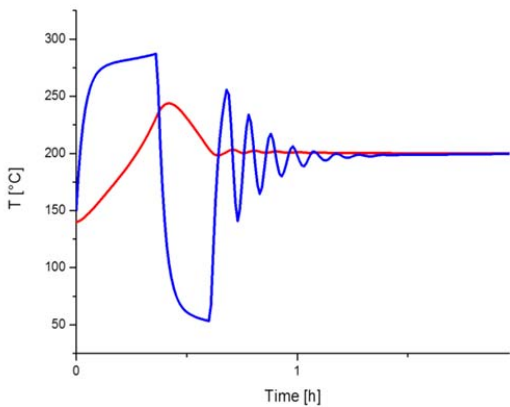


Fig. 4.20 (-)T, (-)T_j vs time. Adaptive Control with anti-ringing term

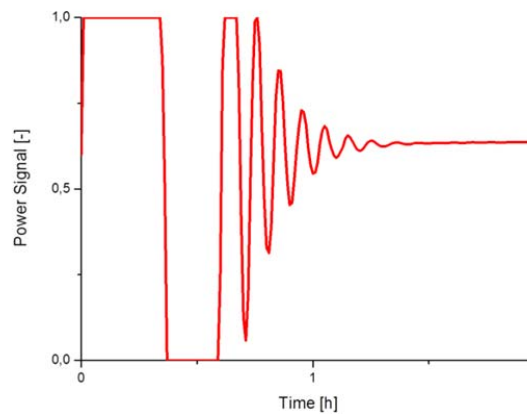


Fig. 4.21 pS vs time. Adaptive Control with anti-ringing term

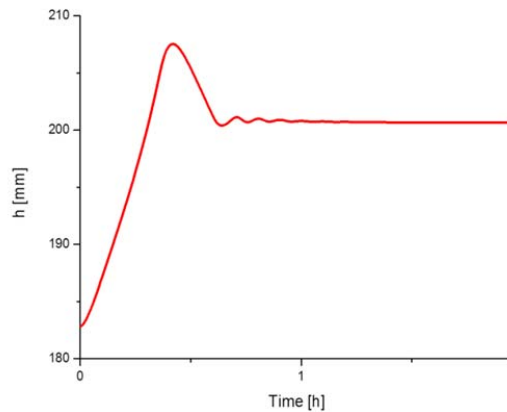


Fig. 4.22 h vs time. Adaptive Control with anti-ringing term

As can be observed in Fig. 4.21 the addition of the anti-ringing term leads to a smoothing of power signal dynamic behavior. Jacket temperature shows two first-order responses which are in correspondence of the time interval in which, power signal assumes its boundary values. After these responses the variable starts to oscillate until thermal equilibrium is reached with reactor temperature (200°C). Reactor temperature overshoot reaches 244°C and rise time for reactor temperature is, again, around 18[min]. Maximum temperature reached by diathermic oil is 287°C , while the minimum one is 53°C . Power supplied by electrical resistance to the jacket, when reactor temperature is kept to 200°C (equilibrium conditions between jacket and reactor) is equal to 63.69% of the maximum one. A polymerization time of 1.96[h] is needed in order to satisfy process targets.

PLA final properties are:

- $M_n = 62,415[\text{Da}]$,
- $M_w = 100,161[\text{Da}]$,
- L-Lactide content: 4.42%.

CHAPTER 5

Influence of reaction conditions on PLA polymerization

5.1 Introduction

Up to this point of the work, all kinds of polymers produced were analyzed only under average molecular weight and conversion aspects. Since one of the aim of the work is to produce Poly L-Lactide for biomedical application, it's important to find out the main characteristics, in addition to a high molecular weight and a high conversion, that the polymer must have. Taking as starting point literature works on PLA analysis, it was observed that fundamental analyses to define both polymer produced and its applications are: DSC analysis (from which crystallization temperature, glass transition temperature, fusion temperature, enthalpy of crystallization and enthalpy of fusion are obtained), TGA analysis (to define polymer thermal stability) and FT-IR analysis (to verify the presence of PLA chemical groups). All these analytical techniques are deeply studied in the work of Signori [61]. Following the same procedure reported by Fernández [59], RDX analysis was done on synthesized PLA samples, in order to obtain their crystallinity degrees. Finally all tests regarding polymer applications in human body, such as MEV analysis and in vitro experiments [60], were carried out.

5.2 Experimental Section

5.2.1 Materials

(S,S)-3,6-Dimethyl-1,4-dioxane-2,5-dione(L,L-lactide;PURAC, PURASORB L; purity > 99.5%, water content <0.02%, Heavy metals <10 ppm, sulphated ash < 0.05%, residual solvent < 0.1%); 2-ethylhexanoic acid tin(II) salt (Sn(Oct)₂, Sigma Aldrich, 95% purity), and 1-dodecanol (Sigma Aldrich, 98% purity) were used as received. For the purification chloroform (J. T. Baker) and ethyl alcohol anhydrous (Labsynth 99,8% purity)were used. For GPC analyses, polystyrene standards from 1055 Da to 3 864 000 Da (Viscotek) were used for calibration, chloroform (J. T. Baker) was used as eluent and THF Tetrahydrofuran, Stabilized (J. T. Baker) HPLC Grade, 99.5% min. (by GC) was used as mobile phase. In the reactor synthetic oil (Labsynth) was used with a becker of 250 ml (Labcenter, Brazil).

5.2.2 Experimental Procedure

The L,L-Lactide (LA) with 2-ethylhexanoic acid tin(II) salt and 1-Dodecanol are weighted directly in the beaker. Then the beaker is inserted in the reactor, which is closed and the stirrer is switched on. Nitrogen flux is connected to one of the three exits of the top of the reactor, the bigger one is occupied by the stirrer and the small one is left open. A low flux of nitrogen is maintained for about 15 minutes, then it is disconnected and the exit closed (Fig. 5.1).



Fig. 5.1 Reactor for macro-experiments equipment

Time of reaction, temperature and M/C and ROH/C ratios depend on the particular case under study. When reaction time is reached, the beaker is removed from the synthetic oil bath and inserted in a bigger beaker filled of water and ice. PLA is left in the beaker until polymer solidification occurs (Fig. 5.2). Then the beaker is broken with a hammer, the glass is removed and the polymer is cleaned from small pieces of glass still on it (Fig. 5.3).

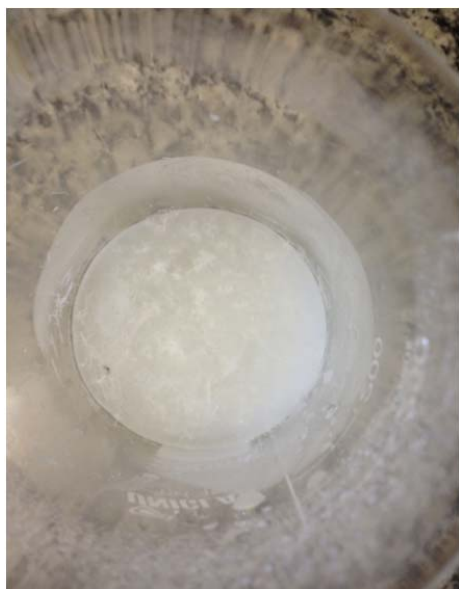


Fig 5.2 Polymer in the becker

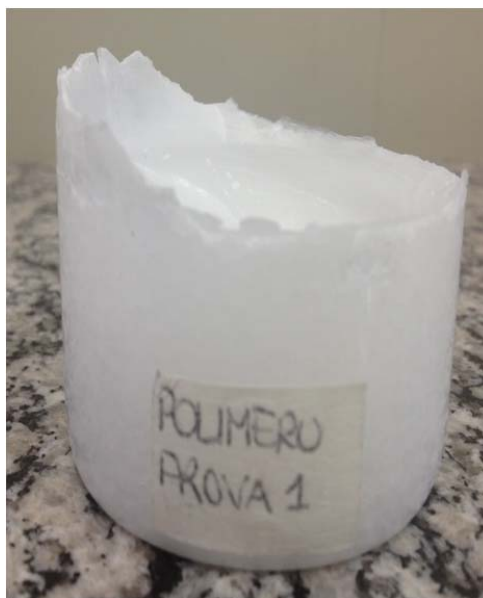


Fig. 5.3 Final polymer out from the becker

5.3 Experiments at different temperatures

Since temperature plays an effective role during polymerization, it's interesting to define how much this parameter influences final polymer properties. To do this a set of temperatures was used: 140°C - 160°C - 175°C - 185°C – 200°C. For all the experiments constant M/C and ROH/C ratios were used: M/C was set equal to 500 and ROH/C to 2. The choice of these two values depends on the fact that ROH /C (experimental value) it's stoichiometric ratio, in order to have complete activation of stannous octoate $\text{Sn}(\text{Oct})_2$ into tin(II) alkoxide. An M/C ratio equal to 500 was used as reported by Gonçalves in her work [62], in order to achieve almost complete conversion at the end of polymerization.

5.3.1 Characterization Methods

5.3.1.1 GPC analysis

Procedure and equipments are the same used for the ampules system and they are described in section 2.3.3.2. The obtained results are showed below (Fig. 5.4, Fig. 5.5, Fig. 5.6).

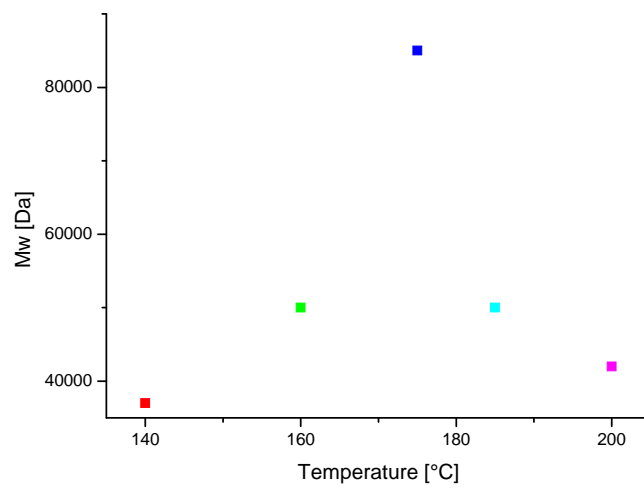


Fig. 5.4 Final values of Mw at different temperatures

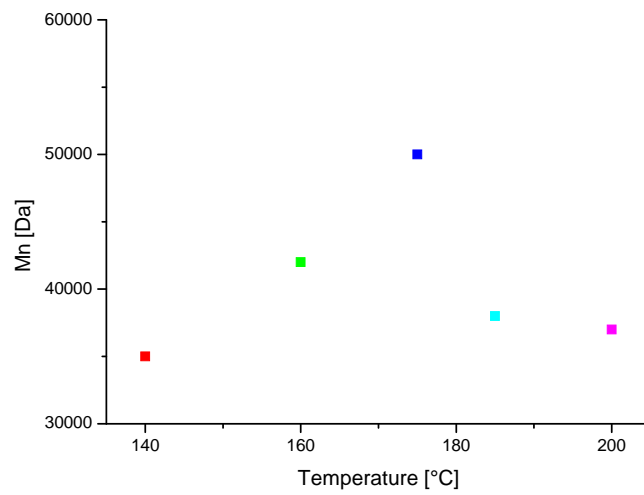


Fig. 5.5 Final values of Mn at different temperatures

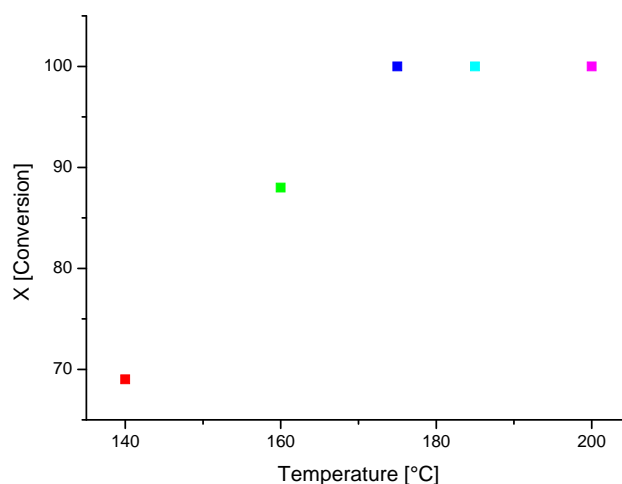


Fig. 5.6 Final values of conversion at different temperatures

The values of weight average molecular weight increases to 85000 [Da] at 175°C, and then decreases for higher temperatures. This behavior can be easily explained with the beginning of degradation phenomena that take place at 180 °C. The same behavior can be detected for the number average molecular weight and the two values are almost similar, except for the temperature equal to 175°C. Small differences between M_n and M_w are probably due to diffusive limitations, which influence transesterification reactions (see Chapter 2). In the third diagram (Fig. 5.6) conversion values for each temperature are showed. It's observed that from 175°C the system already reaches complete conversion, but this doesn't mean that high molecular weight are achieved. At the same time for temperatures higher than 185°C, even if molecular weight decreases because of the degradation of polymer chains, monomer conversion doesn't drop down.

5.3.1.2 Density

To measure polymer density a quite easy method was used: Archimedes' method. Archimedes' principle indicates that the upward buoyant force exerted on a body immersed in a fluid, whether fully or partially submerged, is equal to the weight of the fluid that the body displaces. In his treatise on hydrostatics, *On Floating Bodies*, Archimedes states:

“Any object, wholly or partially immersed in a fluid, is buoyed up by a force equal to the weight of the fluid displaced by the object.”

Archimedes of Syracuse

We may observe for any immersed object that the volume of the submerged portion equals the volume of displaced fluid. Also, we may observe for any immersed object that buoyancy equals the weight of displaced fluid. Objects weight more in air than they do in water. If a 30-kilogram object displaces 20 kilograms of fluid when immersed, then its apparent weight equals the weight of 10 kilograms (98 Newtons). This is because 30 kilograms of weight pushing down are counteracted by 20 kilograms of weight pushing up. The "missing weight" is equal to the weight of the water displaced, which is the buoyant force. The apparent weight of a submerged object is its weight under standard conditions minus the buoyant force.

Because the density of water is 1 g/cm³ (or 1 kg/L), an object that has displaced 20 kg of water, must have a volume of 20 liters. Archimedes' Principle can therefore be used to measure the volume of any solid, regardless of its shape. The experiment was carried out using a graduated cylinder, pieces of polymers (better if in rock) and a balance. The polymers were previously weighted (mass_n), the cylinder filled up with water up to a certain volume (volume_n). Once the volume was known, the polymer rock was inserted in the cylinder and final volume was taken.

$$\rho_n = \frac{\text{mass}_n}{\text{volume}_n} \quad [5.1]$$

The measure was repeated five times for each sample and the average value was taken as density measure. Results showed that the density increases in a range of 1.0 to 1.3 with the molecular weight (Table 5.1).

Mw [Da]	Density [g/cm³]
37000	1,0826
42000	1,1317
50000	1,1386
75000	1,2734
85000	1,3007

Table. 5.1

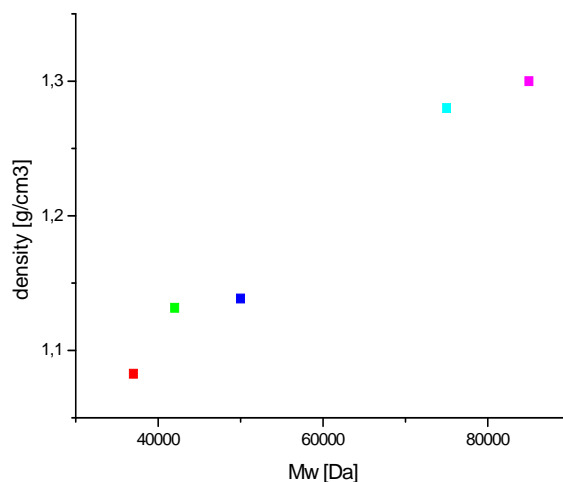


Fig. 5.7 Density profile as function of molecular weight (Mw)

5.4 Experiments at different M/C and ROH/C ratios

Procedure, materials and instrumentation are the same of section 5.2 Chapter 5. What change is the fact that this time the temperature is considered constant at 140°C and M/C and ROH/C ratios are variable. The reason why 140°C was chosen as reaction temperature depends on the fact that we want to analyze concentration influence in mild polymerization conditions and the minimum temperature at which a significant polymerization was observed experimentally is 140°C. The ratios used are showed in Table 5.2.

M/C	ROH/C
500	2
1500	10
1500	20
20000	45
20000	125

Table 5.2

These conditions were chosen starting from the values used in the ampoules (M/C=1000- ROH/C=4) and in the experiments at constant temperature (M/C=500-

ROH/C=2) in order to cover a wide range of conditions to define how the polymerization occurs and how much these parameters influence the final polymer characteristics.

5.4.1 Characterization Methods

5.4.1.1 GPC analysis

Procedure and equipments are the same used for the ampules system and are described in section 2.3.3.2. The obtained results are represented below (Fig. 5.8, Fig. 5.9, Fig. 5.10).

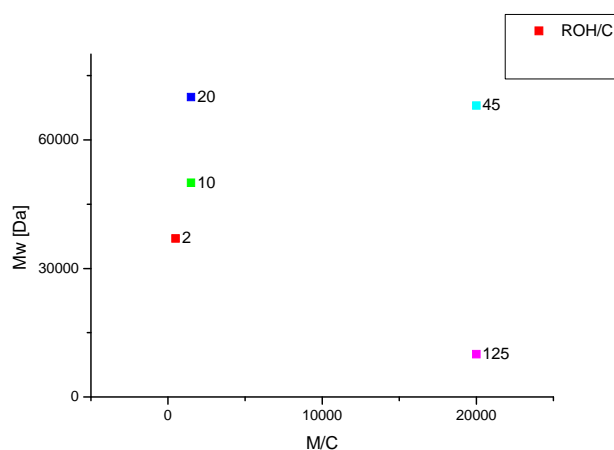


Fig. 5.8 Final values of Mw at different M/C and ROH/C

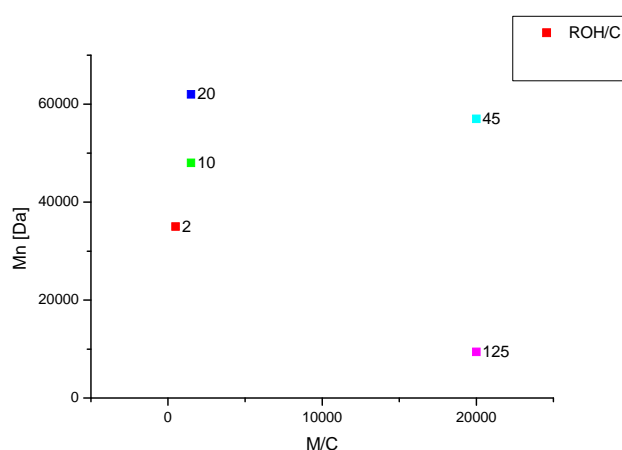


Fig. 5.9 Final values of Mn at different M/C and ROH/C

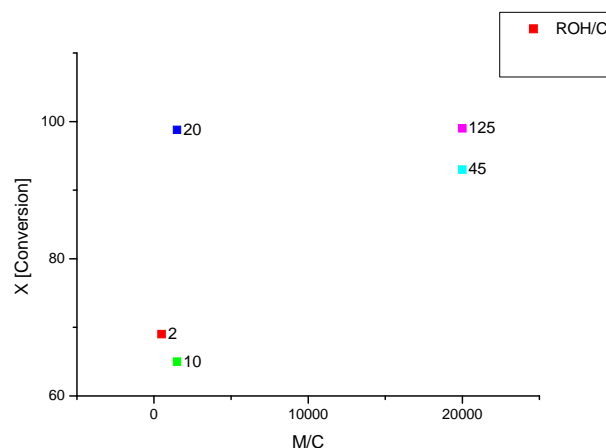


Fig. 5.10 Final values of conversion at different M/C and ROH/C

From the obtained results and considering all the kinetics evaluations done in Chapter 2 it's possible to conclude that final molecular weight is deeply influenced by the combination of M/C and ROH/C ratio. The combination 20000-125 reach the lowest molecular weight because the high quantity of cocatalyst allows to reach high conversion in a very small time, as catalyst is rapidly converted into its active form (tin(II) alkoxide), but the high amounts of 1-dodecanol favor chain transfer reactions between active chains and cocatalyst, reducing PLA molecular weight. Combination M/C = 500 and ROH/C=2 gives a molecular weight equal to 37 000 Da. This value is a little bit smaller than the molecular weight obtained with M/C = 1000 and ROH/C = 4 because increasing both M/C and the ROH/C ratios leads to higher Mw (50 000 Da). At the same time comparing ROH/C = 10 with ROH/C = 20 is possible to see that Mw reached in this case (70 000 Da) is the highest. We can compare this final value with the molecular weight obtained using M/C = 20000 and ROH/C = 125 where a large increasing of M/C ratio is sufficiently balanced with a value of ROH / C properly increased. For Mn all the considerations explained in section 5.3.1.1 can be done considering that the system is exactly the same.

5.4.1.2 Density

To evaluate polymer density a quite easy method is used: Archimedes' method as described in section 5.3.1.2. Obtained experimental data are shown below.

Mw [Da]	Density [g/cm ³]
10000	1,0626
37000	1,0826
50000	1,1386
68000	1,1764
70000	1,1827

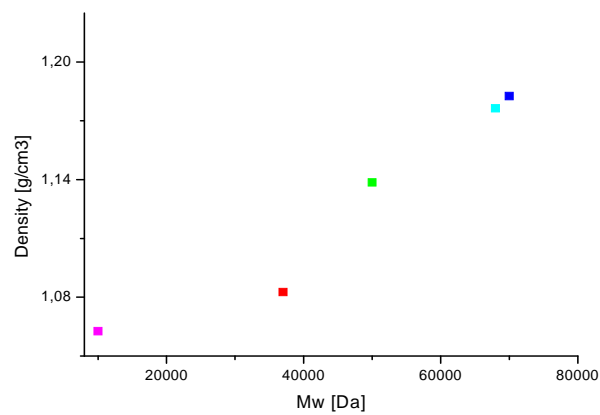


Fig. 5.11 Density profile as function of molecular weight (Mw)

Considering only the molecular weight, it's also possible to compare all the polymers produced (Fig. 5.12). It can be observed that in all the cases the density increases with Mw.

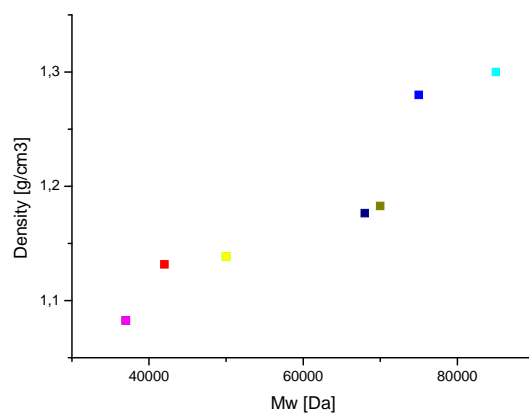


Fig. 5.12 Density profile as function of molecular weight (Mw)

CHAPTER 6

PLA characterization analyses

6.1 Introduction

In order to have a whole vision of the polymers produced different kinds of analysis were done such as: thermal analysis, spectroscopic analysis, microscopic analysis and, finally, in vitro experiments. This investigation was done in order to understand the effects of process variables (concentration, temperature and time of polymerization) on PLA properties and thus, its application in biomedical area.

6.2 Thermal analysis

Thermal analysis is defined by the International Confederation of Thermal Analysis and Calorimetry (ICTAC) [63,64] as “a group of techniques in which a property of a sample is monitored against time or temperature while the temperature of the sample, in a specified atmosphere, is programmed.” Actually, temperature of the oven which contains the sample is programmed, while temperature of the sample in some cases may differ from programmed temperature. Exothermic or endothermic reactions or phase transitions in the sample subjected to the programmed temperature variation may cause temperature difference between the sample and the oven up to several degrees. The most popular technique for polymer applications is DSC followed by TGA (along with its derivative, DTGA).

6.2.1 DSC - Differential scanning calorimetry

6.2.1.1 Introduction

The development and introduction of DSC in 1964 [67] was a major innovation in thermal analysis. Several competitive commercial instruments were developed shortly afterward. Basically, there are two types of DSC instruments: the first is the Perkin-Elmer version (called the “power compensation” DSC) and the second is the DSC unit that operates in a “heat flux” mode. DSC used in this work, belongs to the second group and it’s a Mettler-Toledo DSC. Its operation is similar to the one of DTA (i.e., it generates a ΔT signal). However, the associated hardware and software, carefully integrated into the system, quantitatively converts ΔT to ΔH and compensates for other deficiencies, such as the temperature dependence of thermal transport and sensor sensitivity. Figure 6.1 shows two types of heat-flux calorimeters along with a schematic

diagram taken from Boerio-Goates and Callanan [68] (Fig. 6.1c). In Fig. 6.1c symbols T_B , T_{SC} , T_R and T_{RC} refer to block, sample container, reference and reference container respectively. Capital R refers to heat transfer resistance in the instrument. Fig. 6.1a represents the Boersma-type instrument used by TA Instruments. In this unit, single thermocouples are in good thermal contact with the sample and the reference holders. In the Tian-Calvet-type calorimeter, shown in Figure 6.1b, a thermopile is used. The latter tends to give greater temperature sensitivity and better temperature averaging over the whole sample and reference containers. The analysis is described by Wunderlich [66]. Each type of DSC gives satisfactory enthalpy data [69] with an accuracy around 1–2%. Some heat-flux DSC instruments can operate at temperatures up to 1500° C, while the power-compensation instrument operation is limited to 725° C.

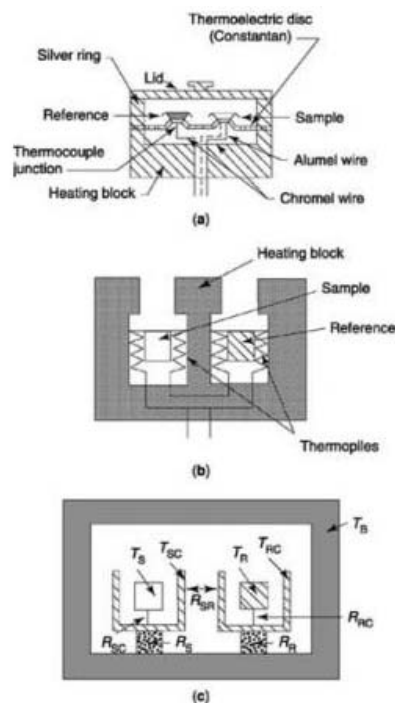


Fig. 6.1 Boersma-type instrument used by TA Instruments

6.2.1.2 Instrumentation

For the analysis a METTLER-TOLEDO DSC823 was used. Analyses through DSC were repeated three times for each polymer sample. From the obtained results no clear differences are observed between them. It's quite important to define a certain range for: glass transition temperature T_g , crystallization temperature T_c , crystallization enthalpy ΔH_C , melting point T_f , and fusion enthalpy ΔH_f . The temperature region where transition from rubbery to glassy state takes place is called the “Glass Transition” and it is characterized by a step change in C_p . The glass transition covers a wide range of temperature (10–15° C for pure, uncross linked polymers and wider for blends, filled,

and cross-linked polymers). A defined point in this temperature range is called glass-transition temperature (T_g). ΔH_C is the exothermic heat of reaction for 100% conversion, expressed as heat per mole of reacting groups (kcal/mole or kJ/mole) or per mass of material (cal/g or J/g) at time t . The fractional degree of conversion is given by

$$\alpha_1 = \frac{\Delta H_1}{\Delta H_C} \quad [6.1]$$

where α_1 is the fractional conversion or extent of reaction and ΔH_1 the heat generated up to time t_1 . Crystallization temperature is related to crystallization enthalpy, and it covers the range where phase transition takes place and usually crystallization peak is taken as reference. The enthalpy of fusion or heat of fusion ΔH_f is the change in enthalpy resulting from heating a given quantity of a substance to change its state from a solid to a liquid. The temperature at which this occurs is the melting point. The enthalpy of fusion is a latent heat, because during melting the introduction of heat cannot be observed as a temperature change, as temperature remains constant during the process. The latent heat of fusion is the enthalpy change of any amount of substance when it melts. When the heat of fusion is referred to a unit of mass, it is usually called specific heat of fusion, while molar heat of fusion refers to enthalpy change per amount of substance in moles. A temperature is related with fusion enthalpy, as well as crystallization. Melting point of a solid is the temperature at which it changes from solid state to liquid state at a given pressure. At the melting point solid and liquid phases exist in equilibrium. The procedure used for DSC analysis was the following:

- 1) heating from 0°C to 200°C;
- 2) leaving the sample at 200°C for 3 minutes,;
- 3) cooling from 200°C to 0°C;
- 4) leaving the sample at 0°C for 1 minute;
- 5) heating from 0°C to 200°C.

For all steps a cooling/heating rate of 5°C/min under a flux of 50ml/min of Nitrogen was set.

6.2.1.3 Experimental Results for experiments at Constant Temperature

For each polymer three tests were done in order to evaluate T_g , T_c , ΔH_c , T_f , ΔH_f .

-polymer A: $M/C = 1\ 500$; $ROH/C = 20$; $T=141^\circ\text{C}$; $M_w=70\ 000$

	A	b	c
T_g	82,77	79,02	76,09
T_c	76	92,44	106,3
ΔH_c [J/g]	28,3	29,71	39,97
T_f	165,73	171,61	174,65
ΔH_f [J/g]	-42,92	-45,87	-43,67

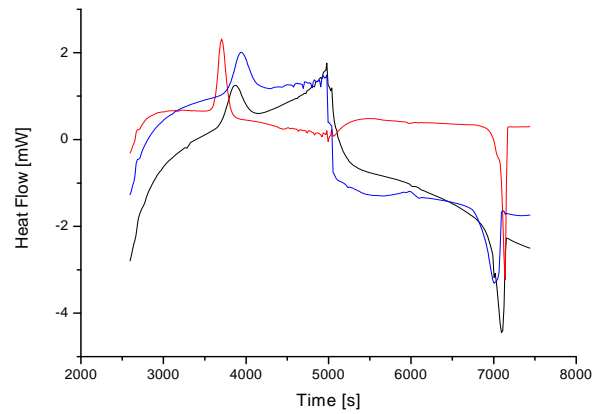


Fig. 6.2 DSC analysis of three different samples of the same polymer

-polymer B: $M/C = 1\ 500$; $ROH/C = 10$; $T=141^\circ\text{C}$; $M_w=50\ 000$

	A	b	c
T_g	53,85	54,71	51,98
T_c	103,37	103,29	102,6
ΔH_c [J/g]	46,29	49,74	51,66
T_f	173,91	174,63	173,54
ΔH_f [J/g]	-78	-74,54	-74,63

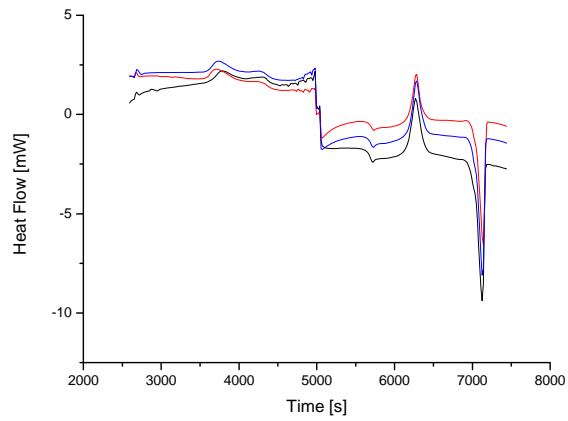


Fig. 6.3 DSC analysis of three different samples of the same polymer
-polymer C: M/C =20 000; ROH/C = 45; T=141°C Mw=68 000

	A	b	c
Tg	54,48	53,31	52,3
Tc	101,7	100,12	102,3
ΔHc [J/g]	49,31	33,86	49,08
Tf	173,82	173,25	173,79
ΔHf [J/g]	-80,2	-79,27	-77,11

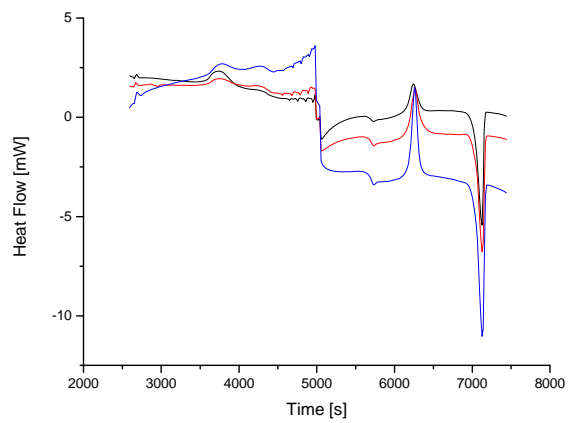


Fig. 6.4 : DSC analysis of three different samples of the same polymer

-polymer D: M/C =20 000; ROH/C = 125; T=141°C; Mw=10 000

	A	b	c
Tg	85,76	94,87	73,56
Tc	100,49	89,57	54,99
ΔHc [J/g]	64,64	53,92	43,988
Tf	152,11	146,98	133,4
ΔHf [J/g]	-61,17	-37,14	-52,55

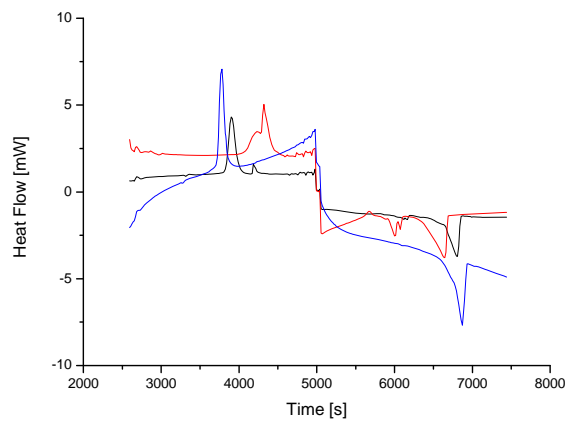


Fig. 6.5 DSC analysis of three different samples of the same polymer

6.2.1.4 Experimental Results for experiments at Constant Ratios

For each polymer two tests were done in order to evaluate T_g , T_c , ΔH_c , T_f , ΔH_f .

-polymer E: M/C =500; ROH/C = 2; T = 141°C Mw = 37 000

	A	b
Tg	46,26	90,9
Tc	102,46	104,23
ΔHc [J/g]	78,51	66,9
Tf	166,6	169,99
ΔHf [J/g]	-51,87	-39,24

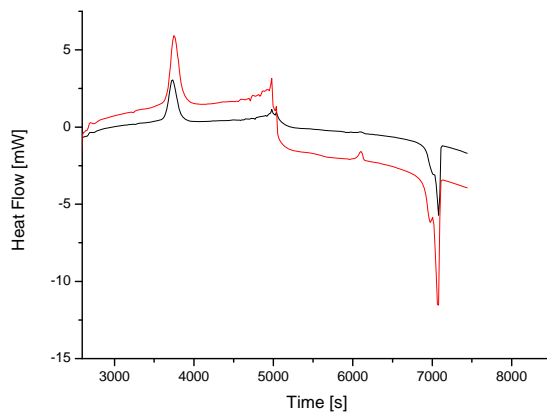


Fig. 6.6 DSC analysis of two different samples of the same polymer

-polymer F: $M/C = 500$; $ROH/C = 2$; $T = 200^{\circ}\text{C}$ $M_w = 42\ 000$

	a	b
T_g	47,57	55,44
T_c	97,55	94,16
ΔH_c [J/g]	55,67	31,12
T_f	165,07	166,93
ΔH_f [J/g]	-70,12	-68,4

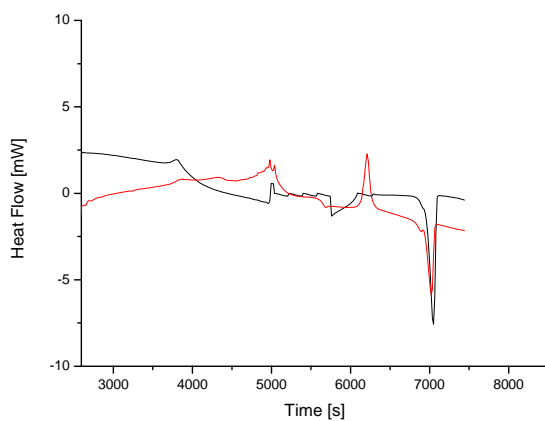


Fig. 6.7 DSC analysis of two different samples of the same polymer

-polymer G: M/C =500; ROH/C = 2; T = 173°C Mw=85 000

	a	b
Tg	80,15	65,57
Tc	103,61	103,76
ΔHc [J/g]	72,86	70,69
Tf	170,39	171,54
ΔHf [J/g]	-80,93	-75,56

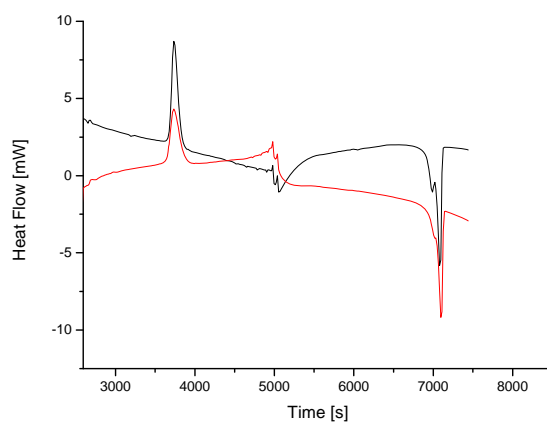


Fig. 6.8 DSC analysis of two different samples of the same polymer

-polymer H: M/C =500; ROH/C = 2; T = 162°C; Mw= 50 000

	a	b
Tg	49,48	49,76
Tc	99,08	101,39
ΔHc [J/g]	34,92	49,96
Tf	168,42	169,34
ΔHf [J/g]	-76,36	-76,52

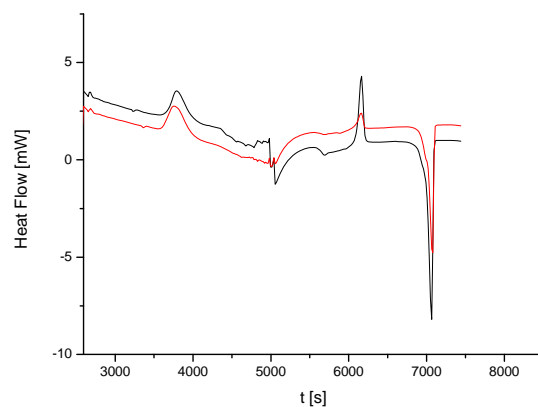


Fig. 6.9 DSC analysis of two different samples of the same polymer

-polymer I: M/C =500; ROH/C = 2; T = 185°C; Mw 75 000

	a	b
Tg	77,88	46,39
Tc	103,71	105,92
ΔHc [J/g]	71,95	76,07
Tf	170,33	170,89
ΔHf [J/g]	-80,99	-79,27

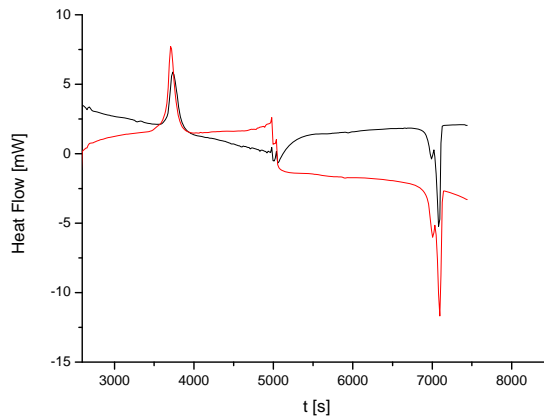


Fig. 6.10 DSC analysis of two different samples of the same polymer

All DSC analyses gave good results. From each of them it's possible to evaluate PLA physical parameters. Obtained average values are similar to the ones reported in literature [73].

	VALUE
Tg	64,35
Tc	97,37
ΔHc [J/g]	52,47
Tf	165
ΔHf [J/g]	-75,47

It can be observed from previous diagrams that in some cases crystallization peak appears in the first heating, while in other cases in the second step. The best condition should be that transition takes place in the first heating, because it should mean that all crystals are formed in the mentioned step. This condition leads to a better definition of the crystallization degree from DSC curves. By the way in Poly(L,Lactide) DSC analyses it's common to find crystallization peak in the first step, but this doesn't affect very much the final result. Generally the best situation is verified in polymer with higher molecular weight. This means that residual monomer content affects in a deep way PLA crystallization. It can be observed that the narrower fusion and crystallization peaks are, the more homogenous PLA structure is. DSC analysis of the polymer produced at 200°C

present a very disturbed profile (in particular between 5000 and 6000 s). This is due to degradation processes that took place during polymerization.

6.2.2 TGA - Thermogravimetric analysis

6.2.2.1 Introduction

The terms thermogravimetry (TG) and thermogravimetric analysis (TGA) are synonymous. Both ICTAC and International Union of Pure and Applied Chemistry (IUPAC) accept either of them. This is because of the early use and popularity of the term TGA, as well as an interest in avoiding verbal confusion with the glass transition T_g . Thermogravimetry involves the continuous recording of mass versus temperature or time when a sample is heated in a furnace with a controlled environment. The sample may be heated at a constant rate ($^{\circ}\text{C}/\text{min}$) or held at isothermal conditions. An exhaustive study on polymers thermogravimetry is reported in the works of Madorsky [70] and Jellinek [71]. The era of modern automated thermogravimetry started with the introduction of the electrobalance by Cahn and Schultz [72].

6.2.2.2 Instrumentation

Components of the instrument are: microbalance, furnace, programmer controller, and a computer or data acquisition system. Typical arrangements of the components for TGA are shown in Fig. 6.11. The sample can be connected to the balance in three different ways: (1) above the balance, (2) below the balance, and (3) beside the balance as a horizontal extension to the beam. Arrangement (1) is the most common. However, arrangement (3) is preferred because it minimizes heat effects of the furnace that may be encountered in arrangement (2) and is less influenced by the flow patterns of the gases within the balance and furnace chamber. It also increases balance lever arm, increasing sensitivity, and minimizing problem of condensation of volatiles on sample support. In order to minimize thermal expansion of the balance lever arm, quartz is frequently used as construction material for the beam. For the performed experiments a METTLER TOLEDO TGA/DSC 1 STAR system equipped with a Gas Controller GC10 was used. During experimentations temperature has been increased from 25°C to 500°C with a Nitrogen flux of $50\text{ ml}/\text{min}$.

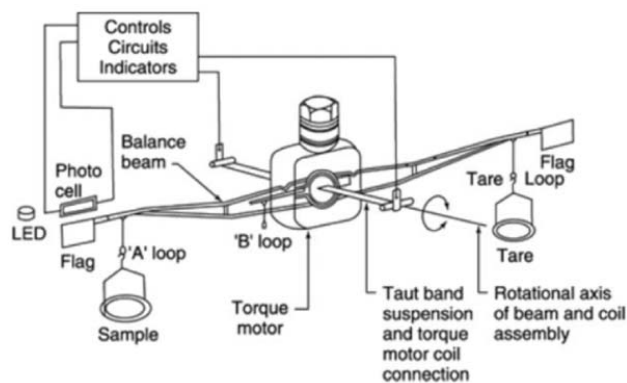
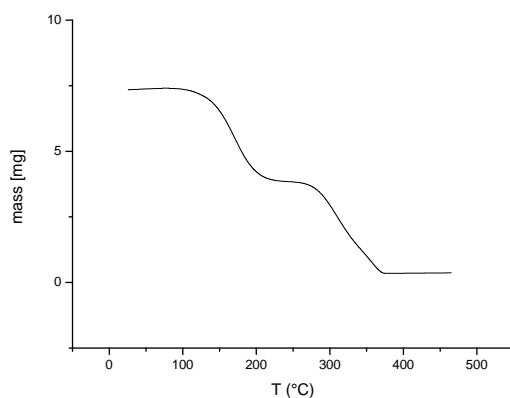


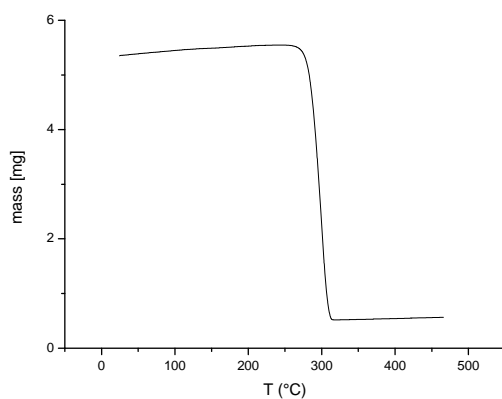
Fig. 6.11 Typical arrangements of the components for TGA

6.2.2.3 Experimental Results for experiments at Constant Temperature

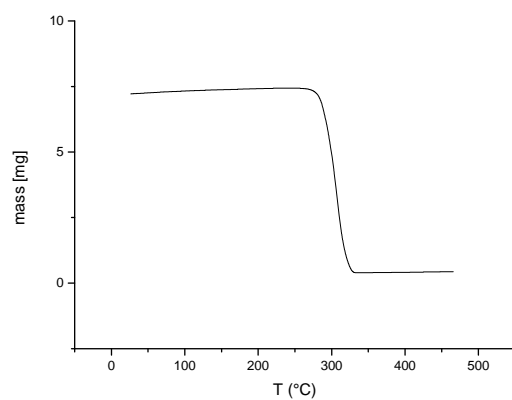
-polymer A: $M/C = 1\ 500$; $ROH/C = 20$; $T=141^{\circ}C$; $M_w=70\ 000$



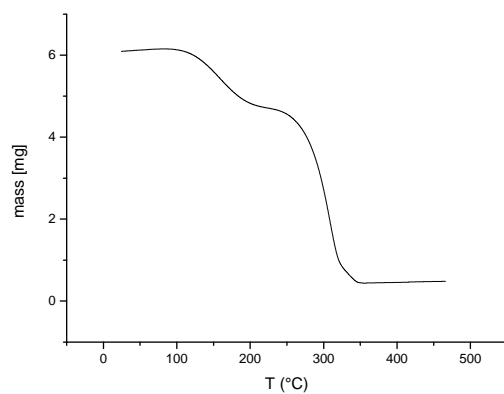
-polymer B: $M/C = 20\ 000$; $ROH/C = 45$; $T=141^{\circ}C$ $M_w=68\ 000$



-polymer C: $M/C = 20\ 000$; $ROH/C = 125$; $T = 141^\circ\text{C}$; $M_w = 10\ 000$

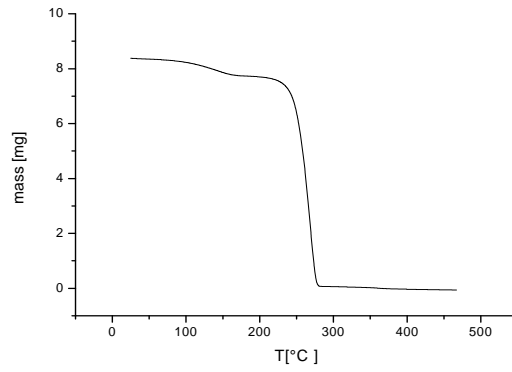


-polymer D: $M/C = 500$; $ROH/C = 2$; $T = 141^\circ\text{C}$ $M_w = 37\ 000$

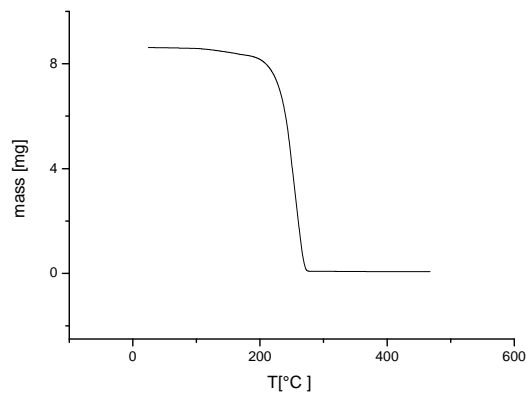


6.2.2.4 Experimental Results for experiments at Constant Ratios

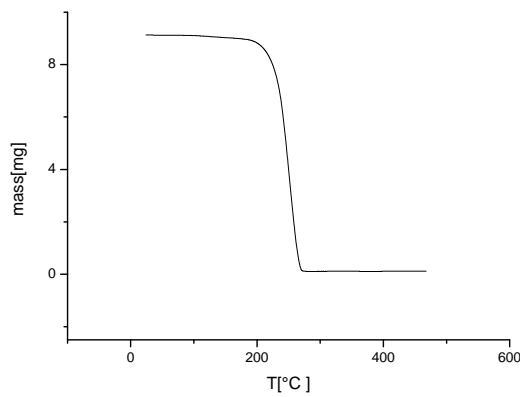
-polymer E: M/C =500; ROH/C = 2; T = 141°C Mw = 37 000



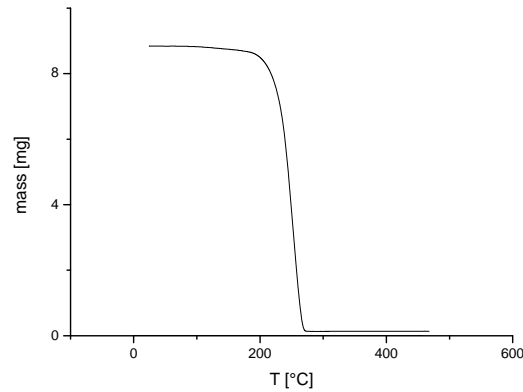
-polymer F: M/C =500; ROH/C = 2; T = 200°C Mw = 42 000



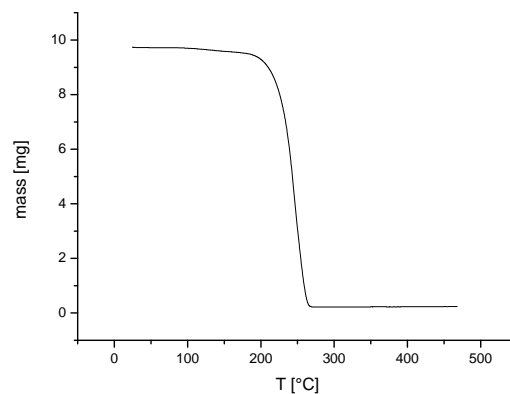
-polymer G: M/C =500; ROH/C = 2; T = 175°C Mw=85 000



-polymer H: M/C =500; ROH/C = 2; T = 165°C; Mw= 50 000



-polymer I: M/C =500; ROH/C = 2; T = 185°C; Mw 75 000



TGA analyses led to two types of profiles for polymers synthesized at constant temperature. Since for other analyses pure polymer was needed, before doing TGA analysis polymers produced in higher quantities were purified. These polymer were A and D, their behavior were similar compare to normal TGA of Poly-L,Lactide. On the other hand the two other polymers show different profile at 100°C. This is due to the presence of water. Since polymers B and C had higher monomer contents and weren't purified, the amount of monomer present, that is strongly hygroscopic, caused water absorption. Thus, weight loss at 100°C for this polymers is due to water vaporization. Another possible explication is that also monomer could devolatilized at a temperature of about 100°C, but as can be observed in Fig. 6.11 monomer's volatilization occurs at temperature higher than 100°C.

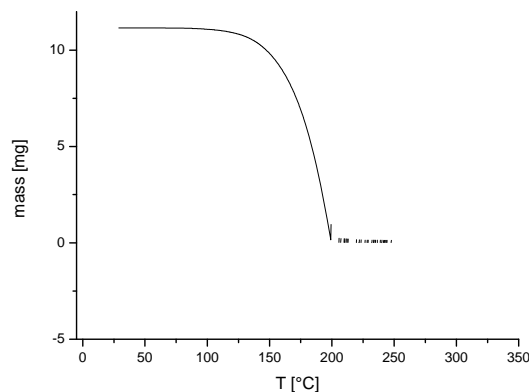


Fig. 6.11 Lactid-Acid (M) TGA analysis

For polymers synthesized at constant M/C and ROH/C ratios, the higher the molecular weight is, the narrower volatilization temperature range is. Since all these polymers have almost complete conversion it's difficult that the phenomena explained before occurs. Although, for the polymer with lower molecular weight (*-polymer E M/C = 500; ROH/C = 2; T = 141°C Mw = 37 000*) the same behavior can be slightly observed.

6.3 Spectroscopic Analysis

Spectroscopic analyses were done primarily to verify the presence of PLA in the samples, through detection of the chemical groups (e.g. carboxyl and hydroxyl groups) with FT-IR analysis. Furthermore, FT-IR analysis defines crystallinity degrees of synthesized PLAs.

6.3.1 FT-IR - Fourier transform infrared spectroscopy

6.3.1.1 Introduction

Fourier transform spectroscopy is a measurement technique whereby spectra are collected based on measurements of the coherence of a radiative source, using time-domain or space-domain measurements of the electromagnetic radiation or other types of radiation. It can be applied to a variety of types of spectroscopy including infrared spectroscopy (FTIR). Infrared spectroscopy (IR spectroscopy) is the spectroscopy that works in the infrared region of the electromagnetic spectrum. In this region radiations have longer wavelength and lower frequency than visible light. It covers a range of techniques, most of them based on absorption spectroscopy. As with all spectroscopic techniques, it can be used to identify chemical bonds of a substance. The infrared portion of the electromagnetic spectrum is usually divided into three regions; the near-, mid- and far- infrared, named for their relation to the visible spectrum. The highest-energy near-IR, approximately $14000\text{--}4000\text{ cm}^{-1}$ ($0.8\text{--}2.5\text{ }\mu\text{m}$ wave length) can

excite overtone or harmonic vibrations. The mid-infrared, approximately $4000\text{--}400\text{ cm}^{-1}$ ($2.5\text{--}25\text{ }\mu\text{m}$) may be used to study the fundamental vibrations and associated rotational-vibrational structure. The far-infrared, approximately $400\text{--}10\text{ cm}^{-1}$ ($25\text{--}1000\text{ }\mu\text{m}$), lying adjacent to the microwave region, has low energy and may be used for rotational spectroscopy. The names and classifications of these subregions are conventions, and are only loosely based on the relative molecular or electromagnetic properties. Infrared spectroscopy exploits the fact that molecules absorb specific frequencies that are characteristic of their structure. These absorptions are resonant frequencies, i.e. frequencies of the absorbed radiations matches the transition energy of the bond or group that vibrates. The energies are determined by the shape of the molecular potential energy surfaces, the masses of the atoms, and the associated vibronic coupling. The resonant frequencies are also related to the strength of the bond and the mass of the atoms at both ends of it. Thus, frequencies of vibrations are associated with a particular normal mode of motion and a particular bond type. A vibrational mode in a molecule is "IR active," if it is associated with changes in the dipole. A permanent dipole is not necessary, as the rule requires only a change in dipole moment. A molecule can vibrate in many ways (Fig. 6.12), and each way is called vibrational mode. Molecules with N atoms, have $3N - 5$ vibrational modes if they are linear, whereas nonlinear molecules have $3N - 6$ vibrational modes (also called vibrational degrees of freedom). Simple diatomic molecules have only one bond and only one vibrational band. If the molecule is symmetrical, e.g. N_2 , the band is not observed in the IR spectrum, but only in the Raman spectrum. Asymmetrical diatomic molecules, e.g. CO , absorb IR radiations. More complex molecules have many bonds, and their vibrational spectra are consequently more complex. Thus, big and complex chemical structures (such as the one of a polymer) have many peaks in their IR spectra.

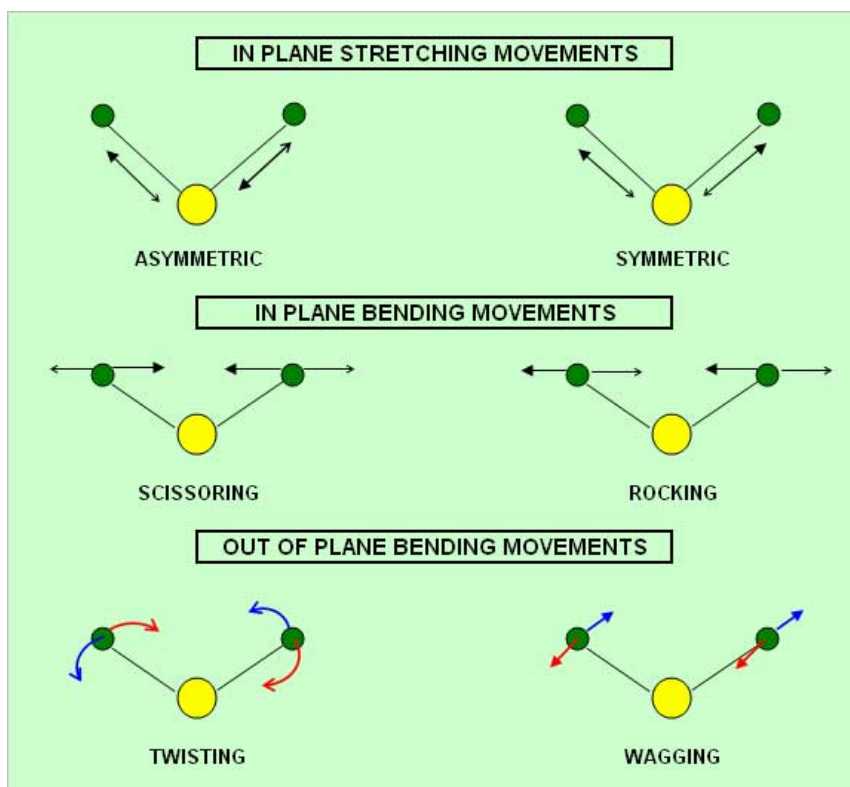


Fig. 6.12 molecule possible vibration

6.3.1.2 Instrumentation

For the FT-IR analysis a Thermo scientific Nicolett 670 was used . Depending on polymer conditions two different methods are required: for purified polymers (n° 2-3) a flaked sample was used (Fig.6.13-14), while for the ones that weren't purified (n° 1-4-5-6-7-8-9), since they were powdered, they required a particular treatment. Samples must be in tablets and to do it we mixed the polymer with KBr for the following reasons:

- If the tablet was totally made of polymer the final spectra would not show any kind of peak since the tablet absorb all the IR;
- If low polymer contents were present in the tablet a complete reflection of IR radiation occurred, since KBr doesn't absorb IR-radiations.

The tablets were produced, mixing the polymer with KBr in a ratio of 2/100 in a mortar in order to obtain a very fine paste. This mixture is inserted in a tablet mixing and then collocated in a press under 7 tons pressure for 10 minutes.



Fig. 6.13 FT-IR for purified polymers



Fig. 6.14 Particular of FT-IR analysis



Fig. 6.15 Press

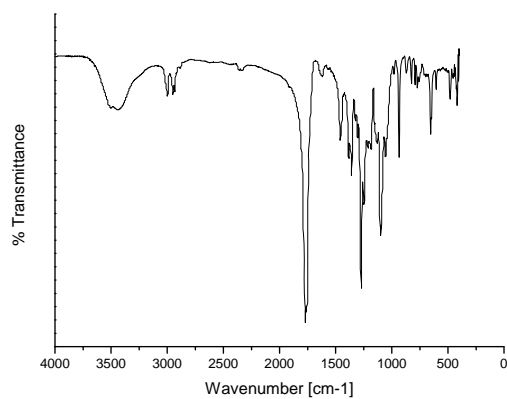
Fig. 6.16 Mixing material



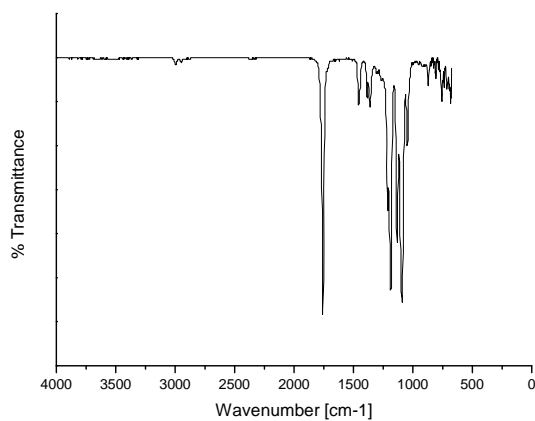
Fig. 6.17 Brake pads equipment

6.3.1.3 Experimental Results for experiments at Constant Temperature

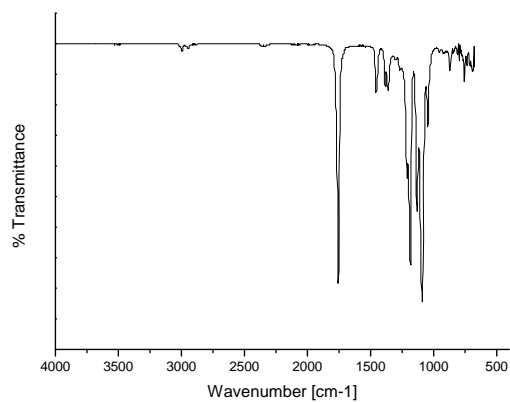
-*polymer A*: $M/C = 1\ 500$; $ROH/C = 20$; $T=140^{\circ}\text{C}$; $M_w=70\ 000$



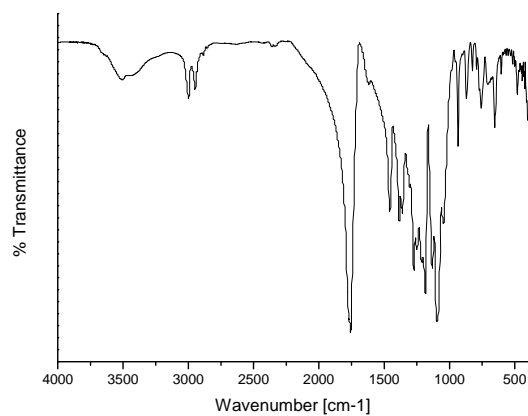
-*polymer B*: $M/C = 1\ 500$; $ROH/C = 10$; $T=140^{\circ}\text{C}$ $M_w=68\ 000$



-*polymer C*: $M/C = 20\ 000$; $ROH/C = 45$; $T=140^{\circ}\text{C}$; $M_w=10\ 000$

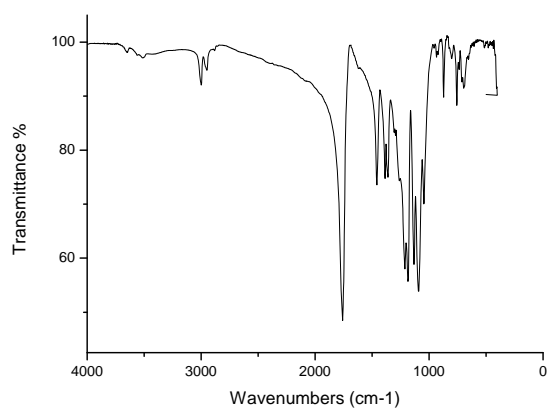


-polymer D: M/C =20 000; ROH/C = 125; T = 140°C Mw = 37 000

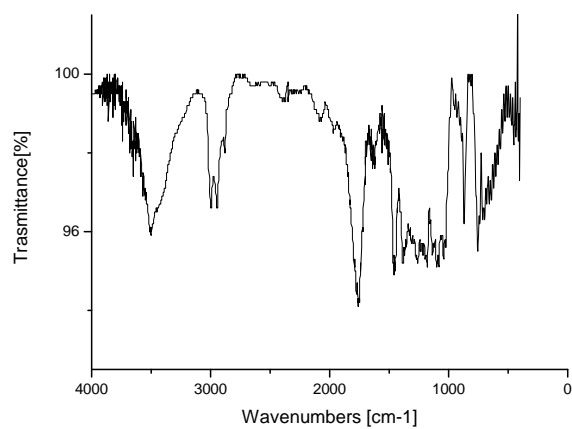


6.3.1.4 Experimental Results for experiments at Constant Ratio

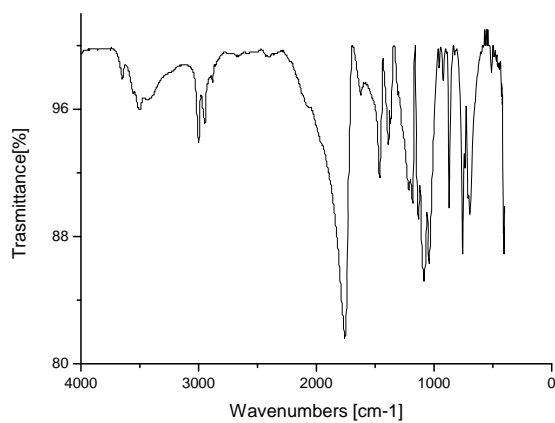
-polymer E: M/C =500; ROH/C = 2; T=140°C; Mw = 37 000



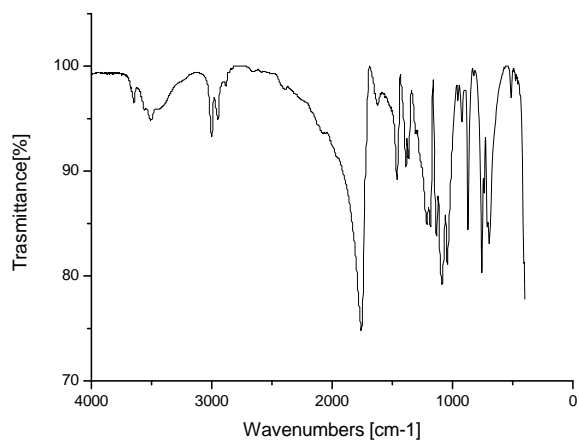
-polymer F: $M/C = 500$; $ROH/C = 2$; $T = 200^{\circ}\text{C}$; $M_w = 42\ 000$



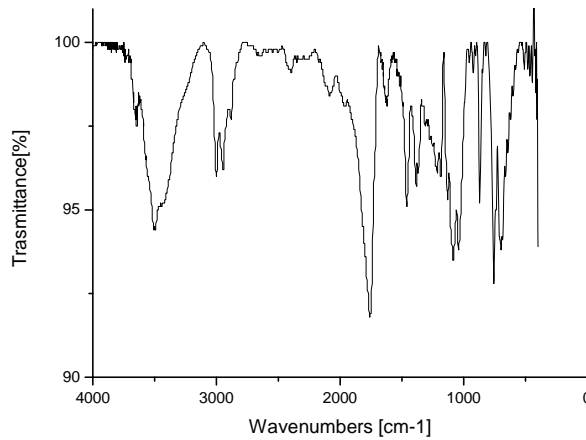
Polymer G: $M/C = 500$; $ROH/C = 2$; $T = 175^{\circ}\text{C}$; $M_w = 85\ 000$



polymer H: $M/C = 500$; $ROH/C = 2$; $T = 165^{\circ}\text{C}$; $M_w = 50\ 000$



polymer I: M/C =500; ROH/C = 2; T = 185 °C; Mw = 75 000



All FT-IR analyses show typical PLLA profile. In each diagrams it's possible to see PLLA characteristic peaks, that are reported on the diagram of Fig. 6.18. As mentioned for TGA analysis there is a clear difference between purified polymers (A,B) and not purified ones. In this case the difference is caused by both a lower quantity of subproducts like monomer, catalyst and cocatalyst, which can be revealed by detection of their characteristic chemical groups through FT-IR analysis, and by the different ways of analysis (described in section 6.3.1.2). The two methods follow the same principle, but their precision is different: the method used with not pure polymers is more accurate. The reason for the higher accuracy of the second method can be explained considering O-H group, between 3000-4000 cm^{-1} . Hydroxyl group is present for sure in the polymer, but it doesn't appear in FT-IR analysis of polymer B and C. The observed peaks of this group in other polymers assume different aspects. They can be narrow (e.g. Polymer E or reference polymer) or larger. When the peak is very large is because the O-H group of PLLA termination is added to O-H group of absorbed water. Since O-H in water has hydrogen bond its characteristic shape is wide and with a less pronounced peak is observed.

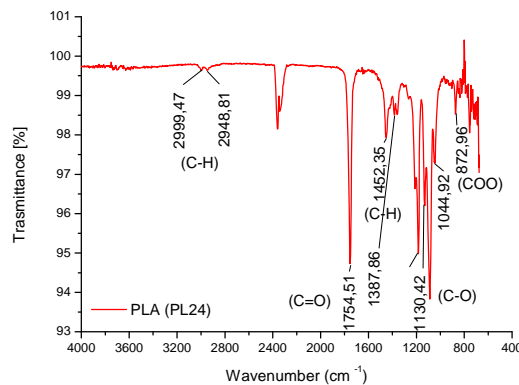
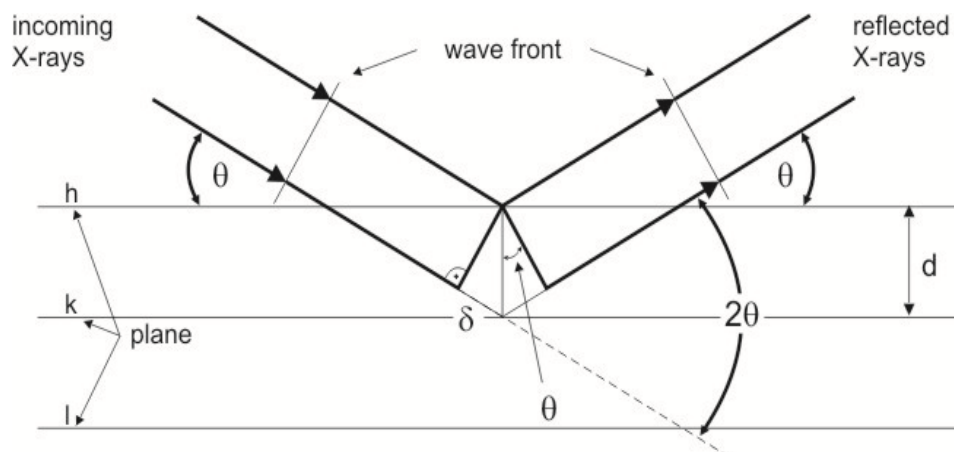


Fig. 6.18 FT-IR analysis of PLA reference

6.3.2 RDX – X-Ray Diffraction

6.3.2.1 Introduction

X-ray powder diffraction (XRD) is a rapid analytical technique primarily used for phase identification of a crystalline material and can provide information on unit cell dimensions. The analyzed material is finely ground, homogenized, and average bulk composition is determined. X-ray diffraction is now a common technique for the study of crystal structures and atomic spacing, it is based on constructive interference of monochromatic X-rays and a crystalline sample. These X-rays are generated by a cathode ray tube, which is filtered to produce monochromatic radiation. This radiation is collimated, in order to be concentrated, and directed toward the sample. The interaction of the incident rays with the sample produces constructive interference (and a diffracted ray) when conditions satisfy Bragg's Law ($n\lambda=2d \sin \theta$). This law relates the wavelength of electromagnetic radiation to the diffraction angle and the lattice spacing in a crystalline sample. These diffracted X-rays are then detected, processed and counted. By scanning the sample through a range of 2θ angles, all possible diffraction directions of the lattice should be attained due to the random orientation of the powdered material. Conversion of the diffraction peaks to d-spacings allows identification of the mineral because each mineral has a set of unique d-spacings. Typically, this is achieved by comparison of d-spacings with standard reference patterns. All diffraction methods are based on generation of X-rays in an X-ray tube. These X-rays are directed at the sample, and the diffracted rays are collected. A key component of all diffraction is the angle between incident and diffracted rays. Powder and single crystal diffraction vary in instrumentation. X-ray powder diffraction is most widely used for the identification of unknown crystalline materials (e.g. minerals, inorganic compounds). Determination of unknown solids is critical to study in geology, environmental science, material science, engineering and biology.



6.3.2 .2 Instrumentation

X-ray diffractometers consist of three basic elements: an X-ray tube, a sample holder, and an X-ray detector. X-rays are generated in a cathode ray tube by heating a filament to produce electrons. Electrons are accelerated toward a target, by applying a voltage, and these electrons hit the target material. When electrons have sufficient energy to dislodge inner shell electrons of the target material, characteristic X-ray spectra are produced. These spectra consist of several components, the most common being K_α and K_β . K_α consists, in part, of $K_{\alpha 1}$ and $K_{\alpha 2}$. $K_{\alpha 1}$ has a shorter wavelength and twice the intensity of $K_{\alpha 2}$. Specific wavelengths are characteristic of the target material (Cu, Fe, Mo, Cr). Filtering operation, carried out by foils or crystal monochrometers, is required to produce monochromatic X-rays needed for diffraction. $K_{\alpha 1}$ and $K_{\alpha 2}$ are sufficiently close in wavelength such that a weighted average of the two is used. Copper is the most common target material for single-crystal diffraction, with $\text{Cu}K_\alpha$ radiation = 1.5418 Å. These X-rays are collimated and directed onto the sample. As the sample and detector are rotated, the intensity of the reflected X-rays is recorded. When geometry of the incident X-rays impinging the sample satisfies the Bragg Equation, constructive interference occurs and a peak in intensity occurs. A detector records and processes this X-ray signal and converts the signal to a count rate which is then sent to a device, such as a printer or computer monitor. The geometry of an X-ray diffractometer is such that the sample rotates in the path of the collimated X-ray beam at an angle θ while the X-ray detector is mounted on an arm to collect the diffracted X-rays and rotates at an angle of 2θ . The instrument used to maintain the angle and rotate the sample is a *goniometer*. For the performed experiments the following equipment and conditions were used:

Equipment: X ray diffraction – XRD (Fig. 6.18 – 6.19 – 6.20)

Mark: Philips Analytical X Ray (Almelo, Netherlands)

Model: X'Pert-MPD

Radiation: Cu (K α) $\lambda = 1.54060$ Angstrom

For the samples a voltage of 40 kV, current of 40 pA, 2 Theta from 5° to 65° degrees, a step size of 0.01 degrees and a scan speed 0.0166 degrees/ second were used.

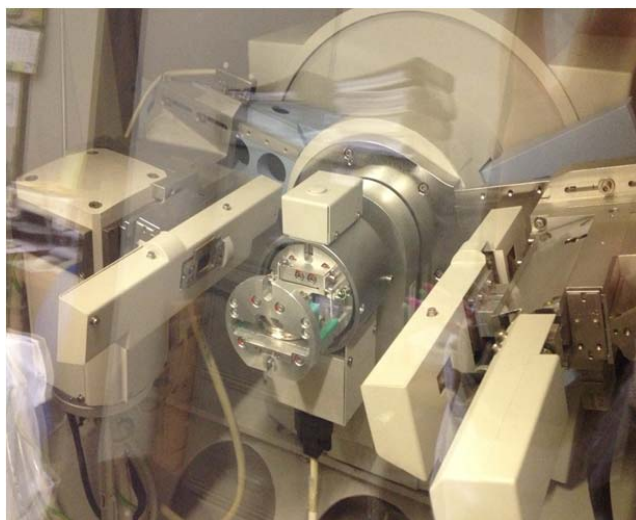


Fig 6.18 XRD machinery

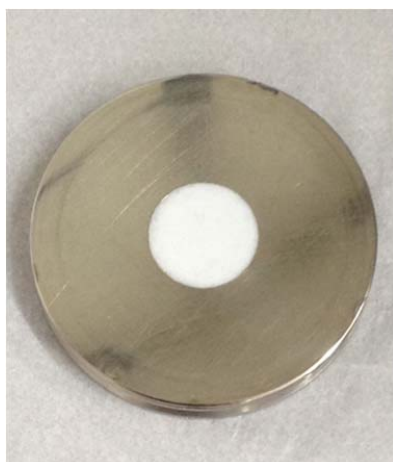


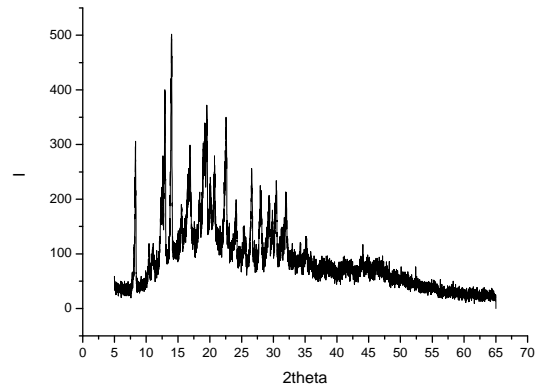
Fig. 6.17 Polymer support



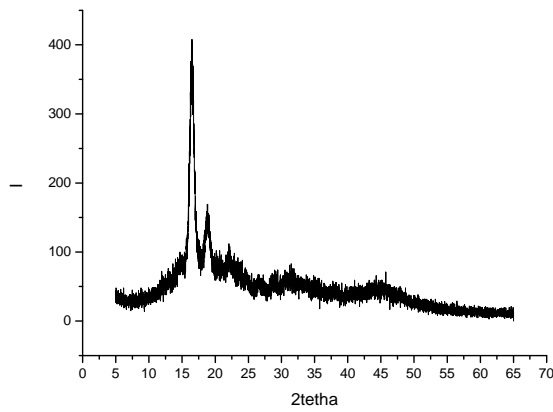
Fig. 6.18 Process data

6.3.2.3 Experimental Results for experiments at Constant Temperature

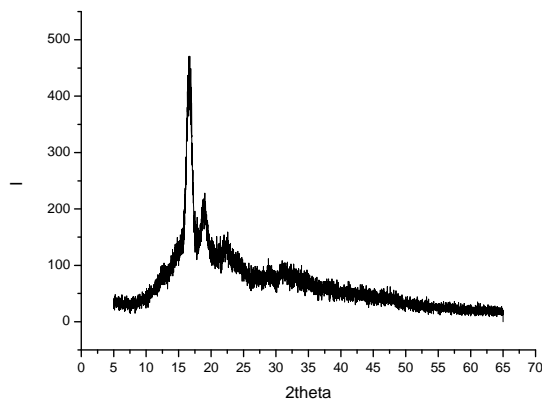
-*polymer A* : $M/C = 1\ 500$; $ROH/C = 20$; $T=140^{\circ}C$; $M_w = 70\ 000$



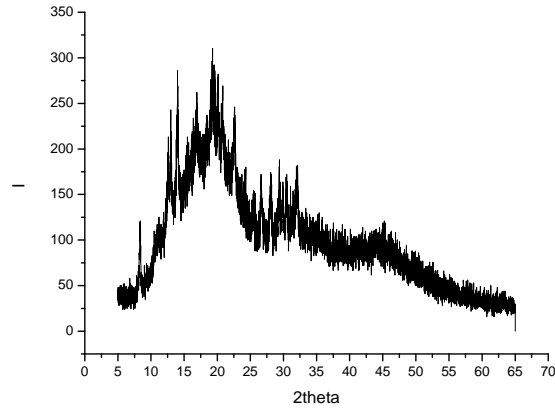
-*polymer B*: $M/C = 1\ 500$; $ROH/C = 10$; $T=141^{\circ}C$; $M_w = 50\ 000$



-*polymer C*: $M/C = 20\ 000$; $ROH/C = 125$; $T=141^{\circ}C$; $M_w = 10\ 000$

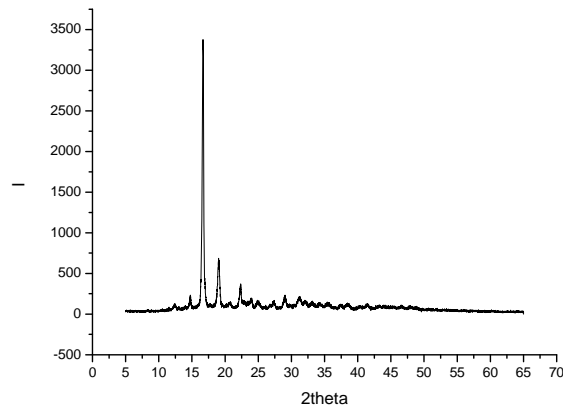


-*polymer D*: $M/C = 20\ 000$; $ROH/C = 45$; $T = 141^\circ\text{C}$; $M_w = 68\ 000$

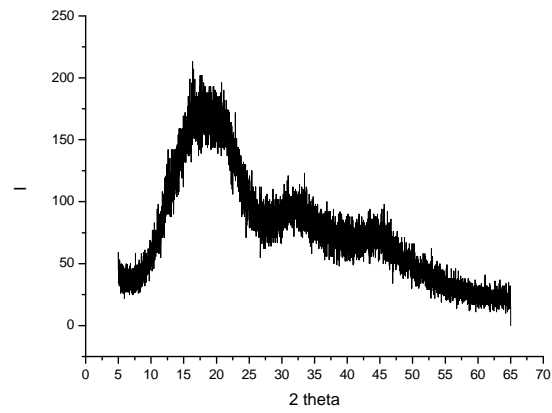


6.3.2.4 Experimental Results for experiments at Constant Ratio

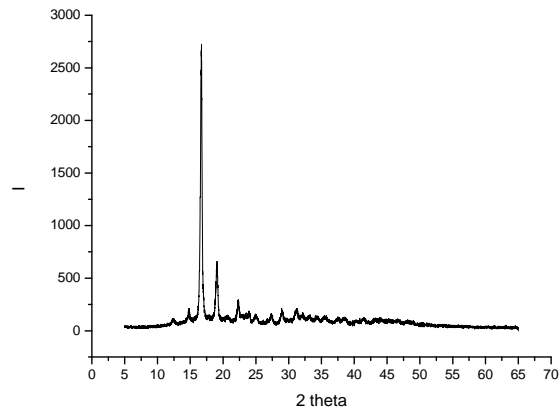
-*polymer E*: $M/C = 500$; $ROH/C = 2$; $T = 200^\circ\text{C}$; $M_w = 37\ 000$



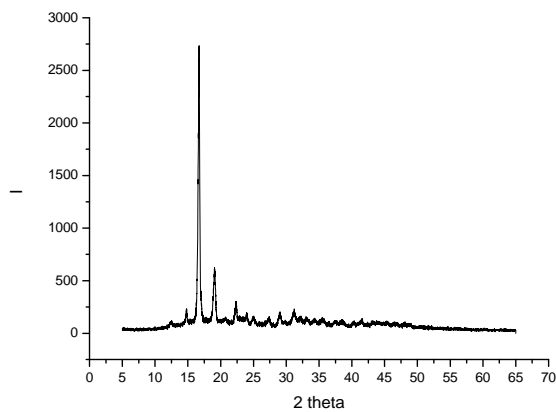
- *polymer F*: $M/C = 500$; $ROH/C = 2$; $T = 200^{\circ}C$; $M_w = 42\ 000$



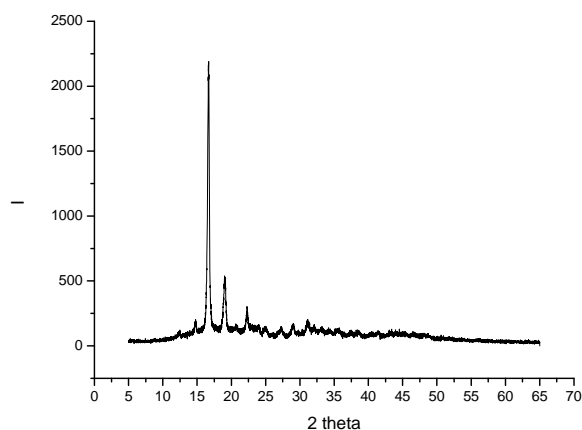
- *polymer G*: $M/C = 500$; $ROH/C = 2$; $T = 200^{\circ}C$; $M_w = 85\ 000$



polymer H: $M/C = 500$; $ROH/C = 2$; $T = 200^{\circ}C$; $M_w = 50\ 000$



- *polymer I*: $M/C = 500$; $ROH/C = 2$; $T = 200^{\circ}\text{C}$; $M_w = 75\ 000$



With XRD analysis it's possible to define crystallinity of the produced polymer. Quite good results are obtained for polymers E,G,H and I. Polymer A,B,C and D can be defined as crystal polymers even if their crystallinity degree is lower. Polymer F is completely amorphous and this is caused by the fact that it was synthesized at 200°C . Since, degradation phenomena were observed at this temperature, this could have led to a less crystalline PLA at the end of polymerization. Generally crystallinity is an important feature of PLA and it's directly correlated to mechanical strength, impact resistance, and transparency properties, which must satisfy proper requirements to find applications as material for biomedical devices. Furthermore, lactic acid, PLA monomeric unit, has chiral carbon atoms and thus it can exist in two enantiomeric forms. Both isomeric ratio between L-Lactide and D-Lactide, and PLA molecular weight influence crystallinity, so their roles must be considered during polymerization process. In fact, racemization during ROP of L-Lactide could lead to higher amounts of D-isomer in the final polymer. This polymer will show less crystallinity, due to the higher D-Lactide contents. Although, catalyst used in this work ($\text{Sn}(\text{Oct})_2$) is reported to be the one that shows less racemization (less than 1% [4]). Thus, the presence of D-Lactide in the synthesized PLLA is almost negligible.

6.4 Microscopic analysis

6.4.1 SEM/ EDS - Scanning Electron Microscopy/Energy dispersive x-ray detector

6.4.1.1 Introduction

The scanning electron microscope (SEM) is a device capable of producing images of high magnification (300,000x) and resolution. The images provided by SEM have a virtual character, because what is displayed on the screen of the device is the transcoding of the energy emitted by electrons instead of light radiations which are commonly used. The operating principle of the SEM is the emission of electron beams by a tungsten capillary (negative electrode) by applying a potential difference, which may vary from 0.5 to 30 KV. This voltage variation causes acceleration of electrons, and heating of the filament. The positive part connected to the filament microscope (positive electrode) strongly attracts the electrons generated, resulting in an acceleration toward the positive electrode. The correction of the path of the beams is accomplished by condenser lenses lining the beams toward the opening. The lens adjusts focus electron beams before they reach the sample. The EDS (energy dispersive x-ray detector, EDX or EDS) is an essential tool in the microscopic characterization of materials. When the electron beam focuses on a mineral, the outermost electrons of atoms and ions are excited and they change energy levels. Once electrons return to their initial position, they release the energy absorbed which is emitted with a wavelength in the spectrum of x-rays. A detector, installed in the vacuum chamber of the SEM, measures the energy associated with these electrons. As the electrons of a given atom have different energies, it is possible, at the point of incidence of the beam, to determine which chemical elements are present at that location. The reduced diameter of the beam allows the determination of the mineral composition in very small sample sizes (<5 μm), leading to an almost punctual analysis. Using this among with the EDX SEM is of great importance in petrographic and petrological study in geosciences. While SEM provides sharp images (although virtual, because what it' s observed on the monitor is the transcoding of the energy emitted by the particles, rather than light radiations, which are commonly used), the EDX immediate identification . Apart from mineral identification, this analysis allows to map the distribution of chemical elements for minerals, and so to generate maps of compositional elements. SEM-EDS systems provide direct observation of edges or grain boundaries, also for polished sections, and characterization of inter-and intra-granular porosity. Grain edges are concentrated where there is a large number of crystal defects. In these regions there is a huge quantity of pores and structures resulting from the action of various processes in polycrystalline aggregates. With SEM-EDS, it is possible to determine chemical composition of the mineral phases.

6.4.1.2 Instrumentation

To perform SEM/EDS analysis, the samples must be electrical conductors. For this reason, they were covered with a gold layer and then analyzed. The operative conditions are reported below:

- *Coating METAL (Fig. 6.18-6.19-6.20-6.21)*

Equipment: Sputter Coater POLARON

Pock-mark: VG Microtech Model: SC7620 (Uckfield, Inglaterra)

Calculation of Au thickness: $\text{thickness} = K.i.V.t$,

where $K=0.17 \text{ A}^\circ/\text{mA.Volt.s}$; $i=3 \text{ mA}$; $V=1 \text{ Volt}$ and $t=180 \text{ s}$. Therefore:

Thickness = 92 A° .

- *Micrographs and/or elemental microanalysis:*

Equipment: Scanning Electron Microscope with Energy Dispersive Detector X ray - SEM/EDS (Fig. 6.22 – 6.23)

Pock-mark: LEO Electron Microscopy/Oxford

Model SEM: Leo 440i

Model EDS: 6070

(Cambridge, England)

Note: Accelerating voltage of 10 kV and beam current equal to 100 pA were used to obtain micrographs, while accelerating voltage of 20 kV and beam current equal to 600 pA were used to obtain X ray spectra.



Fig. 6.18 Pads support.

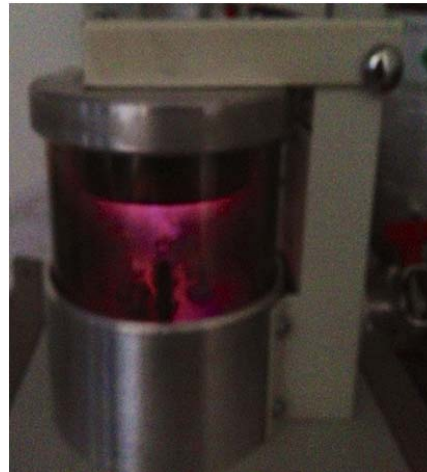
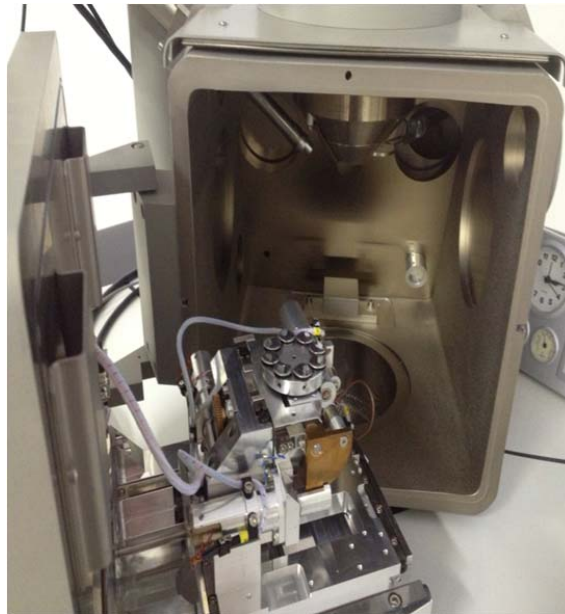


Fig. 6.19 Sputter Coater POLARON



6.20 Sputter Coater POLARON inside 6.21 Sputter Coater POLARON complete equipment



6. 22 Scanning Electron Microscope

6. 23 Scanning Electron Microscope inside particular

6.4.1.3 Results and Discussions



Fig. 6.24 half pad pressed

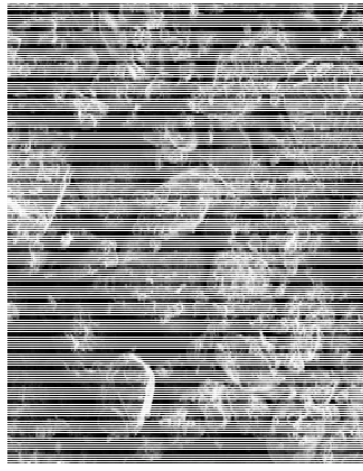


Fig. 6.25 particular of pressed pad

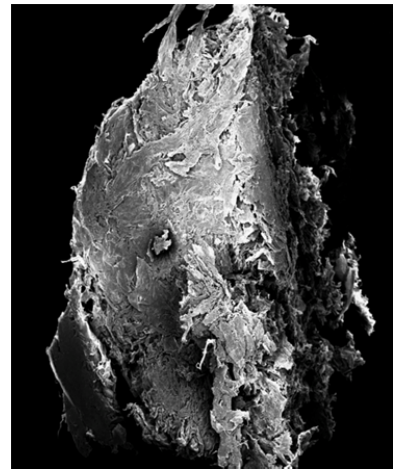


Fig. 6.26 Purified polymer

MEV analysis was applied either on pure polymer (Fig 6.25), or on pressed polymer (Fig 6.23-6.24). Poly(L-Lactide) is not a porous polymer. Porosity that can be observed in the pictures reported above is generated during pad production process. The aim of this analysis was to analyze pad porosity since the “in vitro” experiments (which were performed on synthesized PLA in order to verify its biocompatibility) need a polymer porous structure, in order to allow cell growth inside the pad.

6.5 In vitro experiments

6.5.1 Introduction

The final step of the work focused on biocompatibility of the synthesized polymer. To verify this properties “in vitro” experiments were done using animal cells. This part of the work was done in collaboration with with the medical department of Campinas University.

6.5.2 Material and methods- Adipose cells – mesenchymal tissue

Sources of mesenchymal cells

Mesenchymal cells (MSC) were obtained from human adipose tissue coming from patients undergoing liposuction surgery under total anesthesia . The procedures were referred for approval to the Ethics in Research committee at *UNICAMP*. Both Statement of Consent, and consent form specific to the specialty were applied to all patients undergoing liposuction that agree with the donation.

Extraction of cells AT- MSC

The lipoaspirate tissue was washed carefully with PBS ("phosphate -buffered saline") to remove conjunctive tissue and red blood cells . For 10 g of tissue , the proportion of substances to the digestion buffer , which was added below is : 20mg of collagenase type 1A , 200 mg of bovine serum albumin (BSA) , 20 ml of D -MEM Low Glucose and 10µl of gentamicin . The mixture was treated in a water bath at 37 ° C for 30 minutes , shaking the container every 5 minutes. After complete tissue digestion, the reaction was quenched with 10 ml of fetal bovine serum (FBS) . Then, they were centrifuged for 15 minutes at 1500rpm . The supernatant was removed and the pellet re-suspended in 10 ml D -MEM Low Glucose with 10% of FBS. After 24 hours, the culture medium was exchanged for three consecutive days and then every two days until the cells adhered to the plastic reaching a confluence of 70 to 80% of the surface of the culture flask . The cells were removed from the flask by adding a trypsin solution at 0.05% and 1 mM ethylenediaminetetraacetic acid (EDTA) and expanded until the 4th passage of culture. After the tests , the cells were removed according to rules established by the Health Surveillance.

Immunophenotyping of mesenchymal cells by flow cytometry

After purification and expansion of undifferentiated mesenchymal cells , they were phenotypically characterized by flow cytometry using a set of specific monoclonal antibodies. The antibodies to be used were CD 90 (Thy -1), CD105 (SH-2/endoglin), CD73 (SH3/SH4) and Stro -1 which correspond to surface antigens expressed by mesenchymal cells.

1.0×10^5 cells diluted in 100 µl of PBS and 5 µl of specific antibody in each reaction marking were used. This mixture was kept at 4 ° C for 30 minutes, in absence of light. The labeled cells were washed twice with PBS through centrifugation at 1500 rpm for 5 minutes and fixed in 500 µl of 1% paraformaldehyde. They were kept in the refrigerator until time of purchase.

Controls were carried out for cells' samples without marking, in order to verify auto-fluorescence of cells, while for stained cells isotype matched controls for specific labeling scan were carried out. 10,000 events were acquired from FACScalibur flow cytometer and data analysis was performed using the program CellQuest .

Confocal laser scanning microscopy

Immunophenotyping of the MS of the two sources was also analyzed by immunofluorescence . The AT- MSC and BS - MSC , in the fourth passage were grown on glass coverslips and fixed in 4% paraformaldehyde for 15 minutes and washed in PBS with 0.1 % Triton 100X and incubated for 30 minutes at room temperature in a

blocking solution (PBS, 0.1 % Triton 100X and 1 % BSA) for reduction of nonspecific reactions . Then coverslips were incubated for 18 hours at 4° C protected from light with the same CD 90 antibody (BD Pharmingen PE - Cy5) , CD73 purity (Invitrogen) and CD 105 (Invitrogen PE) (1:500) then washed with 0.1% 100X Triton in PBS 5 times. AlexaFluor™ 488 conjugate was used as secondary antibody. After the last wash in PBS , coverslips were mounted on slides using mounting medium with DAPI fluorescence . The slides were then analyzed by laser scanning on a LSM- 510 (Zeiss) mounted on an Axioplan microscope (Zeiss) using the 40X objective in oil immersion .

Mesodermal differentiation "in vitro"

To prove the obtaining of mesenchymal cells from procedures explained above, they were differentiated into bone, fat and cartilage, using protocols and specifics.

a) Differentiation chondrogenic

For differentiation into chondrocytes about 1.0×10^6 mesenchymal cells at the 4th passage of expansion were transferred to a 15ml Falcon tube with the induction medium and centrifuged at 800 rpm for 5 minutes to allow formation of the button cell. The chondrogenic differentiation inducing medium consist of low glucose DMEM without FBS, supplemented with 100ng/ml of transforming growth factor - $\beta 3$ (TGF- $\beta 3$) , 100 nM sodium pyruvate , 1mM dexamethasone , 50 nM ascorbic acid , 0.5 X insulin-transferrin - selenium - A (ITS) and 0.2 % human albumin . Half of the culture medium was exchanged every three days, with the one used for protein extraction . The time for chondrogenic differentiation varies from 14 to 25 days. During this period, cells are kept for total RNA extraction. RNA is used to perform analysis of expression of specific genes. Finally slides are arranged for morphological and cytochemical analyses which have the aim of monitoring the differentiation process.

b) Osteogenic differentiation

For differentiation into osteocytes ,about 1.0×10^5 cells/cm² in 4th passage mesenchymal expansion were placed in culture dishes containing medium inductor consisting of low- glucose DMEM supplemented with 10 % FBS , supplemented with 0.1 mM dexamethasone, 200 mM ascorbic acid and 10 mM β - glycerophosphate . Culture medium was exchanged every three days, with the one used for protein extraction. The time required for osteogenic differentiation went from 25 to 30 days. During this period, cells are kept for total RNA extraction. RNA is used to perform analysis of expression of specific genes. Finally slides are arranged for morphological and cytochemical analyses which have the aim of monitoring the differentiation process.

c) Adipogenic differentiation

For differentiation into adipocytes about 1.0×10^5 cells/cm² in mesenchymal expansion 4th passage were placed in culture dishes containing medium inductor consisting of low-glucose DMEM supplemented with 15 % FBS , supplemented with 1mM dexamethasone, 10mg/ml insulin , 0.45 mM 3 -isobutyl -methylxanthine (IBMX) and 100 mM indomethacin. Culture medium was exchanged every three days, with the one used for protein extraction. The time required for adipogenic differentiation is 14 days. During this period, cells are kept for total RNA extraction. RNA is used to perform analysis of expression of specific genes. Finally slides are arranged for morphological and cytochemical analyses which have the aim of monitoring the differentiation process.

Cytochemical Analysis of Mesenchymal Cells Differentiated

Cytochemical analysis of differentiated mesenchymal cells was performed by staining with dyes and specific cell observation by conventional optical microscopy.

During the differentiation of cells into adipocytes, samples were collected, fixed in formaldehyde solution for 30 minutes 1X and stained with Oil Red O solution at 0.3 % for 20 minutes and counterstained with hematoxylin. This staining allows visualization of intracellular lipid accumulation.

Samples of mesenchymal cells subjected to differentiation into osteoblasts were collected, fixed in 50% ethanol for 15 minutes at 4 ° C and stained with a solution of 1% Alizarin Red S. This mixture was kept under stirring for 45 minutes. After this calcification in the extracellular matrix was observed .

Cells subjected to differentiation into chondrocytes, were collected and stained with toluidine blue 1%. After the removal of the stain the cells are exposed at RT for 2 hours and fixed for 1 minute in 70% ethanol, 90% and 100% respectively. This type of marking, allows visualization of an extracellular matrix rich in proteoglycans.

Mesenchymal cells , which weren't subjected to any differentiation processes, were used as control.

Analysis of the activity of the enzyme telomerase

Test of the activity of the enzyme telomerase was performed with cells in three separate passages, 4th, 8th and 12th . The methodology adopted was in accordance with kit Trapeze ® Telomerase Detection Kit, S7700, Chemicon International, USA. Highly sensitive system was used to detect telomerase activity "in vitro". The enzyme consists of two systems, which use polymerase chain reaction (PCR) . In the first step of the reaction, telomerase adds a number of telomeric repeating unit (GGTTAG) to the 3' end

of an oligonucleotide substrate (TS). In the second step, the extended products are amplified by PCR using TS and (reverse primer) PR, generating a sequence of products with 6 bases increments from nucleotides 50 : 50, 56, 62 , 68, etc. Using a template (TSK1) for the amplification of a 36 bp internal positive standard makes possible to quantify telomerase activity more accurately and to identify false negative samples containing inhibitors of Taq polymerase.

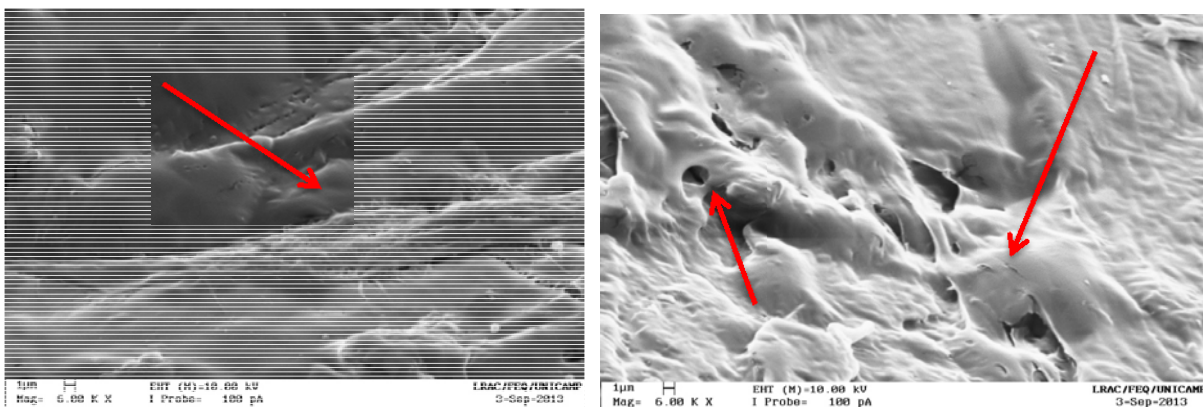
Cythyogenetics

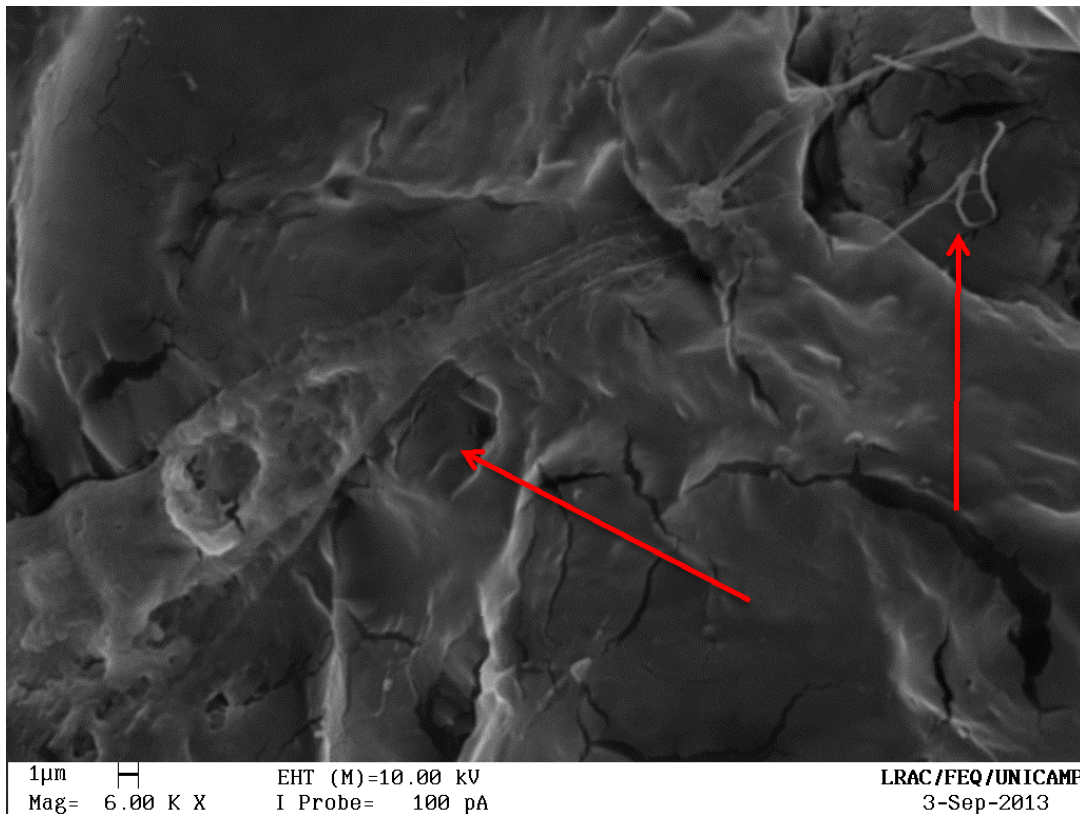
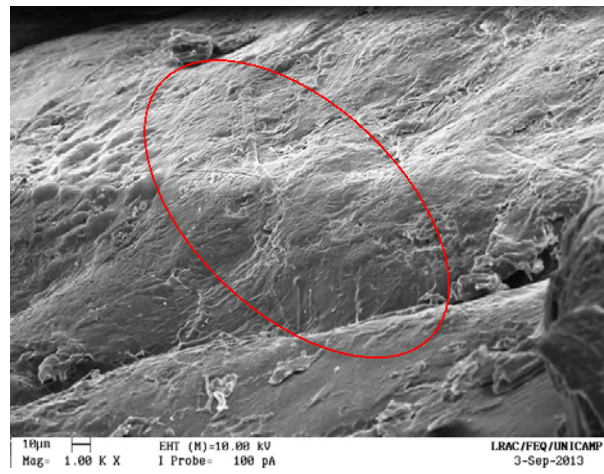
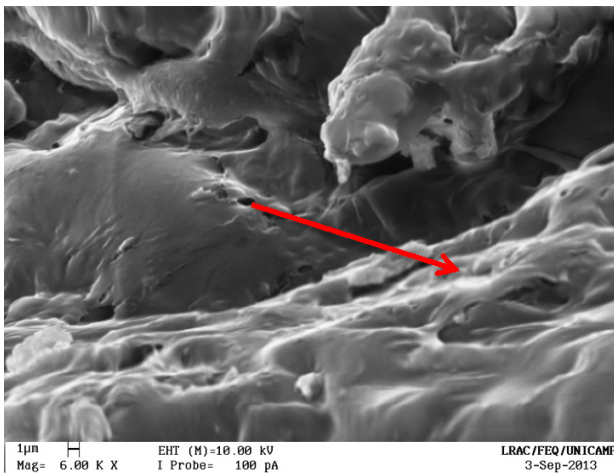
Metaphase chromosome was obtained by cells from an active cells division process originating from adipose tissue MSC for about 70 % to 80 %. They were treated with colchicine (10µg/mL) concentration 100µL/mL, added directly to the culture and incubated overnight at 37 °C. The cells were removed from the plate using trypsin solution for 3 min at 37 °C, washed with 1X PBS , collected in 15ml conical tubes and pelleted by centrifugation at 1200 g for 10 min. The supernatant was discarded and the pellet re-suspended in 5 ml of KCl 0.075 mol / L at 37 °C for 12 min. The cells were fixed with acid solution in methanol / acetic acid (3:1) and analyzed by banding G. The slides were analyzed under a light microscope at 10x objective e100x. Individual images of metaphases were karyotyped and captured using an automated imaging system cytogenetic (ASI APPLIED IMAGING SPECTRALTRAL , Printed Israel) through BAND VIEW software 5.5.

Interaction AT- MS Undifferentiated and Biomaterial

The scaffolds were placed in 96-well microplates and they had 10^4 cells/mm³ DMEM culture medium and fetal bovine serum 10%. The plates were placed in a 5% CO₂ incubator at 37 °C. Up to 7 days after incubation adherence and the cellular proliferation on PLA is monitored with MEV.

6.5.2.1 Results and Discussions





Comparing MEV analysis before and after “in vitro” experiments, it’s possible to observe that after the treatment the whole pad is covered by cells. Thus, cells were able to grow on polymer surface and meaning that synthesized PLA has chemical properties which are appropriate for cell growth. Even if further experimentations must be done (i.e. “in vivo” experiments), this is a first proof that the synthesized polymer has a good biocompatibility, which makes the material appropriate in the construction of biomedical devices (i.e. scaffolds).

CHAPTER 7

Conclusions and Outlook

7.1 Conclusions and Outlook

The first part of this thesis is focused on the modeling of a Batch reactor for PLA production through bulk melt ROP of L-Lactide. A comprehensive model which takes into account main physical phenomena, occurring during polymerization process was developed. The model was implemented in a C++ environment and solved with *BzzMath*© numerical library. Simulations of the model showed that the developed code was able to describe dynamics of PLA average properties (M_w and M_n), monomer conversion, reactor temperature and reaction volume (liquid level). This makes it a powerful tool for simulation of PLA production process and gives a better understanding of the process variables which can affect polymerization and PLA final properties (role of M/C and ROH/C ratios, role of acid impurities, role of polymerization temperature etc.). Furthermore, a temperature control was added to this model in order to have optimal process conditions for the production of a polymer with applications in biomedical area ($M_w = 100,000$ [Da] and 5% residual monomer content). Either PI or adaptive temperature controller show that polymerization time needed to achieve these targets is 2[h]. Possible future works could regard further improvements of the Batch reactor mathematical model, such as:

- Better estimation of transesterification and degradation kinetic constants;
- Evaluation of PLA density function, which takes into account variation with temperature and M_w ;

Furthermore, the model developed in this work could be the first brick for the developing of a more complex model regarding whole PLA production process, based on renewable sources. This can be carried out by:

- Modeling possible purification processes on PLA after polymerization;
- Modeling L-Lactide production from low molecular weight PLA;

- Modeling polycondensation process for low molecular weight PLA production from Lactic acid;
- Modeling fermentation process of Lactic acid from carbohydrates.

In the second part of the thesis the polymer was deeply analyzed under different aspects. Thermal analysis DSC and TGA were used to measure two important factors during PLLA molding manufacturing: crystallinity and heat resistance. DSC results showed the relationship between cooling rate during polymer molding manufacturing, and crystallization rate. Generally crystallinity is an important feature of PLA and it's directly correlated to mechanical strength, impact resistance, and transparency properties, which must satisfy proper requirements to find applications as material for biomedical devices. For this reason this parameter (crystallinity degree) is investigated also through DRX analysis. This analysis, among with FT-IR belongs to spectroscopic analysis. Cellular analysis carried out in this work, represents only the first step to assess effective application of the polymer in biomedical area. Generally, in addition to "in vitro" experiments, "in vivo" experiments must be carried out. Fat cells are used, since they are the ones, which proliferate more easily. For special applications, specific study, on the cells of interest must be carried out. Nowadays Poly(L-Lactide) isn't used pure, but as nano-composite, in order to maintain its intrinsic resistance properties and, at the same time, improving its flexibility. Finally, performed tests among with modeling and simulation of ROP of L-Lactide not only represent new elements for the analysis of this polymer, which has already been extensively studied in terms of chemical and physical properties, but also a fundamental starting point for developing further PLLA applications, with the aim of reducing applications of non-biodegradable materials (metals, ceramics and petrol-derived polymers), in biomedical area.

References

- [1] M. Savioli Lopes, A. L. Jardini, R. Maciel Filho,
Poly (lactic acid) production for tissue engineering applications
- [2] Erwin T.H. Vink, Karl R. Rábago, David A. Glassner, Patrick R. Gruber,
Applications of life cycle assessment to NatureWorksTM polylactide (PLA) production
- [3] Astrid J.R. Lasprilla, Guillermo A.R. Martinez, Betânia H. Lunelli, André L. Jardini, Rubens Maciel Filho,
Poly-lactic acid synthesis for application in biomedical devices — A review
- [4] Donald Garlotta,
A Literature Review of Poly(Lactic Acid)
- [5] Janne Kylvä,
Lactic Acid Based Poly(ester-urethane) - Modification via Copolymerization, Chain Linking and Blending
PhD dissertation submitted to Helsinki University of Technology, Department of Chemical Technology, Polymer Technology; Helsinki, Finland.
- [6] Z. F. Zhou, G. Q. Huang, W. B. Xu, F. M. Ren,
Chain extension and branching of poly(L-lactic acid) produced by reaction with a DGEBA-based epoxy resin
- [7] B. Buchholz,
U.S. Patent 5,302,694, (1994)
- [8] Chanfreau S., Mena M., Porrás-Dominguez JR, Ramírez-Gilly M., Gimeno M., Roquero P., Tecante A., Bárzana E.,
Enzymatic synthesis of poly-L-lactide and poly-L-lactide-co-glycolide in non ionic liquid
- [9] Kim KW, Woo SI.,
Synthesis of high-molecular-weight poly(L-lactic acid) by direct polycondensation

- [10] H. R. Kricheldorf, I. Kreiser ,
Die Makromolekulare Chemie **188** (1987), 1861–1873
- [11] V.W. Dittrich and R. C. Schulz,
Die Angewandte Makromolekulare Chemie **15** (1971), 109–126
- [12] W. H. Carothers, G. L. Dorough, and F. J. Van Natta,
Journal of the American Chemical Society **54** (1932), 761–772
- [13] C. E. Lowe,
U.S. Patent, 2,668,162 (1954)
- [14] Z. Jedlinski, W. Walach, P. Kurcok, and G. Adamus,
Die Makromolekulare Chemie **192(9)** (1991), 2051–2057
- [15] P. Kurcok, A. Matuszowicz, Z. Jedlinski, H. R. Kricheldorf, Ph. Dubois, R. Jerome
Macromolecular Rapid Communications **16** (1995), 513–519
- [16] H. R. Kricheldorf and I. Kreiser-Saunders,
Die Makromolekulare Chemie **191(5)** (1990), 1057–1066
- [17] H. R. Kricheldorf and A. Serra,
Polymer Bulletin **14** (1985), 497– 502
- [18] J. Kleine and H. Kleine,
Die Makromolekulare Chemie **30** (1959), 23–38
- [19] H. R. Kricheldorf and C. Boettcher,
Die Makromolekulare Chemie, Macromolecular Symposia **73** (1993), 47–64
- [20] H. R. Kricheldorf, I. Kreiser-Saunders, and N. Scharnagl,
Die Makromolekulare Chemie, Macromolecular Symposia **32** (1990), 285–298
- [21] J. Dahlman, G. Rafler, K. Fechner, and B. Mehlis,
British Polymer Journal **23(3)** (1990), 235–240
- [22] W. M. Stevels, M. J. K. Ankone, P. J. Dijkstra, and J. Feijen,
Macromolecular Chemistry and Physics **196** (1995), 3687–3694
- [23] H. R. Kricheldorf and M. Sumbel,
European Polymer Journal **25(6)** (1989), 585–591

- [24] F. E. Kohn, J.W. A. Van Den Berg, G. Van De Ridder, and J. Feijen, **Journal of Applied Polymer Science** **29(12) (1984)**, 4265–4277
- [25] G. Schwach, J. Coudane, R. Engel, and M. Vert, **Polymer Bulletin** **32 (1994)**, 617–623
- [26] Erwin T.H. Vink, Steve Davies, and Jeffrey J. Kolstad, **The eco-profile for current Ingeo® polylactide production**
- [27] *BzzMath® Numerical Library*
Copyright by Guido Buzzi-Ferraris all rights reserved
- [28] Saiful Izwan Abd Razak, Noor Fadzliana Ahmad Sharif and Wan Aizan Wan Abdul Rahman,
Biodegradable Polymers and their Bone Applications: A Review
- [29] Yingchuan Yu,
SYNTHESIS, KINETICS AND FUNCTIONALIZATION OF PLA AND PLA BASED BIOMATERIALS
PhD dissertation submitted to ETH ZURICH, Zurich, Swiss
- [30] Yingchuan Yu, Giuseppe Storti, and Massimo Morbidelli,
Kinetics of Ring-Opening Polymerization of L,L-Lactide
- [31] Yingchuan Yu, Giuseppe Storti, and Massimo Morbidelli,
Ring-Opening Polymerization of L,L-Lactide: Kinetic and Modeling Study
- [32] David R. Witzke, Ramani Narayan, and Jeffrey J. Kolstad,
Reversible Kinetics and Thermodynamics of the Homopolymerization of L-Lactide with 2-Ethylhexanoic Acid Tin(II) Salt
- [33] Kricheldorf HR, Kreiseraunders I, Boettcher C,
Polylactones .31. Sn(II)Octoate-Initiated Polymerization of L-Lactide – a Mechanistic Study, Polymer, (1995); 36: 1253-9
- [34] Kricheldorf HR, Kreiser-Saunders I, Stricker A.,
Polylactones 48. SnOct(2)-initiated polymerizations of lactide: A mechanistic study, Macromolecules, (2000), 33: 702-9

- [35] Adam Kowalski, Andrzej Duda, and Stanislaw Penczek,
Kinetics and Mechanism of Cyclic Esters Polymerization Initiated with Tin(II) Octoate. 3. Polymerization of L,L-Dilactide
- [36] Schwach G, Coudane J, Engel R, Vert M,
More about the polymerization of lactides in the presence of stannous octoate
- [37] Witzke DR.,
Introduction to Properties, Engineering, and Prospects of Polylactide Polymers
PhD dissertation submitted to Michigan State University, East Lansing, Michigan,
U.S.A
- [38] Nijenhuis AJ, Grijpma DW, Pennings AJ. Lewis,
Acid-Catalyzed Polymerization of L-Lactide- Kinetics and Mechanism of the Bulk-Polymerization, Macromolecules, (1992), 25:6419-24
- [39] Kotliar AM.,
Interchange Reactions Involving Condensation Polymers
- [40] Wachsen O, Platkowski K, Reichert KH.,
Thermal degradation of poly-L-lactide – Studies on kinetics, modelling and melt stabilization, Polymer Degradation and Stability, (1997), 57:87-94
- [41] Wachsen O, Reichert KH, Kruger RP, Much H, Schulz G.,
Thermal decomposition of biodegradable polyesters. 3. Studies on the mechanisms of thermal degradation of oligo-L-lactide using GPC, LACCC and MALDI-TOF-MS, Polymer Degradation and Stability, (1997), 55:225-31
- [42] Jacobson H, Stockmayer WH.,
Intramolecular Reaction in Polycondensations .1. The Theory of Linear Systems. J Chem Phys, (1950), 18:1600-6
- [43] Rosario Mazarro, Ignacio Gracia, Juan F. Rodríguez, Giuseppe Storti, Massimo Morbidelli,
Kinetics of the ring-opening polymerization of D,L-lactide using zinc (II) octoate as catalyst
- [44] D. Rasselet , A. Ruellan, A. Guinault, G. Miquelard-Garnier, C. Sollogoub, B. Fayolle ,
Oxidative degradation of polylactide (PLA) and its effects on physical and mechanical properties

[45] Boyd T. Safrit, George E. Schlager, and Ziang Li,
**MODELING AND SIMULATION OF POLYMERIZATION OF LACTIDE TO
POLYLACTIC ACID AND CO-POLYMERS OF POLYLACTIC ACID USING
HIGH VISCOSITY KNEADER REACTORS**

[46] Juliana Belincanta,
**HOMOPOLIMERIZAÇÃO E COPOLIMERIZAÇÃO VIA
RADICAL LIVRE CONTROLADA POR RADICAIS NITRÓXIDOS**
PhD dissertation submitted to UNICAMP, Campinas, São Paulo, Brazil

[47] Lamia Zuniga Linan, Anderson Bonon, Nádson M. N. Lima, Rubens Maciel
Filho, Flavio Manenti,
**Quality Control of Poly(Methyl Methacrylate) to Medical Purpose by Multiple
Headspace Extraction**

[48] Xichen Zhang, David A. Macdonald, Matheus A. F. Goosen, and Kim B. Mcauley,
**Mechanism of Lactide Polymerization in the presence of Stannous Octoate: The
Effect of Hydroxy and Carboxylic Acid Substances**

[49] T. G. Kulagina, B. V. Lebedev, Ye. G. Kiparisova, Ye. B. Lyudvig, and I. G.
Barskaya,
**THERMODYNAMICS OF dl-LACTIDE, POLYLACTIDE AND
POLYMERIZATION OF dl-LACTIDE IN THE RANGE OF 0-430K**

[50] Francesco Rigon,
**SVILUPPO DI UN MODELLO DI REATTORE DI POLIMERIZZAZIONE IN
SOLUZIONE DEL METILMETACRILATO**
MS dissertation submitted to Università degli Studi di Padova, Padova, Italy

[51] Fabio Codari,
Poly (Lactic Acid) Polycondensation, Degradation and Nanoparticles synthesis
PhD dissertation submitted to ETH Zurich, Zurich, Swiss

[52] Justin J. Cooper-White, Michael E. Mackay,
**Rheological Properties of Poly(lactides). Effect of Molecular Weight and
Temperature on the Viscoelasticity of Poly(l-lactic acid)**

[53] Qi Fang, Milford A. Hanna,
Rheological properties of amorphous and semicrystalline polylactic acid polymers

[54] John R. Dorgan, Jay Janzen, and Michael P. Clayton,
Melt rheology of variable L-content poly(lactic acid)

[55] P. Piyamanocha, T. Sedlacek, P. Saha,
On Pressure and Temperature Affected Shear Viscosity Behaviour of Poly(Lactid) Acid Melt

[56] DelcoTerm S DbT
OLIO DIATERMICO SINTETICO PER ALTE TEMPERATURE
D.E.L.CO srl, www.delcosrl.com

[57] Boyd T. Safrit, LIST USA, George E. Schlager, and Ziang Li,
MODELING AND SIMULATION OF POLYMERIZATION OF LACTIDE TO POLYLACTIC ACID AND CO-POLYMERS OF POLYLACTIC ACID USING HIGH VISCOSITY KNEADER REACTORS

[58] Nádson M.N. Lima, Lamia Zuniga Linan, Flavio Manenti, Rubens Maciel Filho, Marcelo Embiruçu, Maria R. Wolf Maciel,
Novel two-steps optimal control of batch polymerization reactors and application to PMMA production for the fabrication of artificial bone tissue

[59] J. Fernández, E. Meaurio, A. Chaos, A. Etxeberria, A. Alonso-Varona, J.R. Sarasua,
Synthesis and characterization of poly (L-lactide/ ϵ -caprolactone) statistical copolymers with well resolved chain microstructures

[60] Chandrasekhar R. Kothapalli, Montgomery T. Shaw, Mei Wei,
Biodegradable HA-PLA 3-D porous scaffolds: Effect of nano-sized filler content on scaffold properties

[61] Francesca Signori, Maria-Beatrice Coltelli, Simona Bronco
Thermal degradation of poly(lactic acid) (PLA) and poly(butylene adipate-co-terephthalate) (PBAT) and their blends upon melt processing

[62] Núria Ângelo Gonçalves,
Síntese e Caracterização de Nanocompósitos Compostos por Poli (L-lactídeo) e Hidróxido Duplo Lamelar
MS dissertation submitted to UNICAMP, Campinas, São Paulo, Brazil

- [63] R. C. Mackenzie, in I. M. Kolthoff, P. J. Elving, and E. B. Sandell, **Treatise on Analytical Chemistry, Vol. 12, Pt. 1**, John Wiley & Sons, Inc., New York, 1983, p. 1
- [64] J. O. Hill,
For Better Thermal Analysis and Calorimetry, ICTA, 3rd ed., CPC Repro-graphics, Portsmouth, U.K., 1991
- [65] P. K. Gallagher,
Adv. Anal. Geochem. 1, 211 (1993)
- [66] E. A. Turi,
Thermal Characterization of Polymeric Materials, 2nd ed., Academic Press, New York, 1997
- [67] E. S. Watson, M. J. O'Neill, J. Justin, and N. Brenner,
Anal. Chem. 36, 1233 (1964)
- [68] J. Boerio-Goatesand, J. E. Callananin, B. W. Rossitorand, R. C. Baetzold,
Physical Methods in Chemistry, Vol. 6, Wiley-Interscience, New York, 1992, p. 621
- [69] G. W. H. Ohne, J. Schawe, and C. Schick,
Thermochim. Acta 221, 129 (1993)
- [70] S. L. Madorsky,
Thermal Decomposition of Organic Polymers
- [71] H. H. G. Jellinek,
Aspects of Degradation and Stabilization of Polymers
- [72] L. Cahn and H. Schultz,
Anal. Chem. 35, 1729 (1963)
- [73] Hitachi High-Tech Science Corporation,
Thermal analysis of poly(lactic acid), Application Brief, TA no. 81